Technische Universiteit
Eindhoven

Faculteit der
Technische Natuurkunde

Vakgroep Deeltjesfysica, groep Plasma- en Atoomfysica

A NUMERICAL AND EXPERIMENTAL CHARACTERIZATION OF A HYDROGEN PLASMA

Report of a graduation study in the group Equilibrium and Transport in Plasmas by **J.C.A. Wevers**

Report number: VDF/NT 93 – 14

Under supervision of

dr. ir. M.C.M. van de Sanden and **ir. M.J. de Graaf**

Research leader: **prof. dr. ir. D.C. Schram**

Period: April 1992 - August 1993

Last corrected on: November 22, 2000

Contents

Contents 1

List of symbols 3

1 Introduction 4

2 Some basic concepts of plasma physics 5
2.1 An ionized gas . . . 5
2.2 Collisions, cross sections and densities . . . 5
2.3 Detailed balancing and microscopic reversibility . . . 6
2.4 The Boltzmann balance . . . 6
2.5 The Saha balance . . . 7
2.6 Resonant charge transfer . . . 7
2.7 Excitation transfer . . . 7
2.8 TE and LTE . . . 8
2.9 Deviations from (L)TE; pLTE . . . 8

3 A collisional radiative model of a hydrogen plasma 10
3.1 Introduction to collision-radiative models . . . 10
3.2 Processes in a plasma . . . 11
3.3 Calculation of the rate coefficients . . . 11
3.4 Solution methods . . . 13
3.5 Molecular reactions . . . 14
3.6 Vibrational and rotational distributions . . . 17
3.7 Extension of the model with molecular terms . . . 19

4 Results of the numerical model 22
4.1 Testing the model . . . 22
4.2 Locally simulating the plasma . . . 23

5 Extension with a flow model 31

6 The experimental setup 35
6.1 General overview . . . 35
6.2 Calibration . . . 37

7 Experimental results 41
7.1 Measurements on a hydrogen-argon plasma . . . 41
7.2 Measurements on a pure hydrogen plasma . . . 48

8 Conclusions 50
8.1 Comparison between model and experiment . . . 50
8.2 Comparison between the emission spectroscopy measurements and probe measurements . . . 51
8.3 The flow model . . . 51
8.4 Further recommendations . . . 51

A All reactions in a hydrogen plasma according to [10] 52

B The program listings **54**
B.1 Unit Atom_def . . . 54
B.2 Unit Read_H . . . 55
B.3 Unit New_Solv . . . 56
B.4 Main program . . . 63

C The listings of the flow model **66**
C.1 Runge-Kutta integration . . . 66
C.2 Discretisation error . . . 66
C.3 Unit RK4_N.INC . . . 67
C.4 HFLOW.PAS . . . 68

D The positioning system **76**
D.1 Basic setup of the positioning system . . . 76
D.2 Electrical diagram of the pressured air control . . . 76
D.3 Electrical diagram of the position measurement . . . 77
D.4 Position install program . . . 78

References **84**

Acknowledgement **85**

List of symbols

Symbol	Meaning
$T_\mathrm{e}, T_\mathrm{i}, T_\mathrm{a}, T_\mathrm{h}$	: Temperature of electrons,ions,neutrals & heavy particles.
Θ_v	: Characteristic temperature of vibration.
Θ_r	: Characteristic temperature of rotation.
$\dot{T}$	: Temperature in eV. 1 eV $\sim$ 7729 K.
$n_\mathrm{e}, n_\mathrm{i}, n_\mathrm{a}, n_\mathrm{h}$	: Density of electrons,ions,neutrals & heavy particles.
n_p, n_q	: Density of particles in state p and q.
n_1	: Density of particles in the ground state.
η	: Relative density; $\eta = n/g$.
$\dot{\eta}$	: Elementary level density.
g_p	: Statistical weight of state p.
Z	: Sum of states or partition function.
λ_B	: De Broglie wavelength.
k	: Boltzmanns constant $= 1,38066 \cdot 10^{-23}\mathrm{JK}^{-1}$.
τ_mn	: Relaxation time for momentum transfer between particles m and n.
τ^ε	: Relaxation time for energy transfer.
b_p	: Deviation from Saha-equilibrium; $b_p = n_p/n_p^\mathrm{S}$.
δb_p	: Reduced overpopulation from Saha equilibrium; $\delta b_p = b_p - 1$.
$\vec{q}$	: Heat flow.
$\vec{J}$	: Current density.
X_p	: Particle from species X in level p.
$I(y)$	: Absolute line intensity.
$\varepsilon(r)$	: Local emission coefficient.
ξ	: Biberman factor.
S_A	: Signal from particles of species A.
$\Delta\lambda$	: Width of the apparatus profile.
σ	: Cross section.
ℓ	: Mean free path between two collisions
K	: Rate coefficient; $K = \langle\sigma v\rangle$.
$\vec{w}$	: Drift velocity.
γ_t	: Transport frequency, $\gamma_\mathrm{t} n_1 = \nabla \cdot (n_1 \vec{w}_1)$.
p	: Pressure.
L	: Plasma gradient length; $L = \lvert n_\mathrm{e}/\nabla n_\mathrm{e}\rvert$.
λ_D	: Debeye length, $\lambda_\mathrm{D} = \sqrt{\varepsilon_0 kT/n_\mathrm{e} e^2}$.
Λ	: Escape factor for radiation; $0 \leq \Lambda \leq 1$.
E	: Energy.
$\mathcal{E}$	: E/kT.
E_{pq}	: Energy difference between level p and q.
$E_{p\mathrm{i}}$	: Energy difference between level p and the ion-groundlevel.
Ry	: Rydberg energy = 13.595 eV.
$\vec{E}$	: Electrical field.
$\mathbf{A}$, A	: Surface.
x	: Horizontal coordinate, relaxation factor.
y	: Vertical coordinate.
z	: Axial coordinate.
γ_H	: C_p/C_v from hydrogen atoms ($\gamma_\mathrm{H} = \frac{5}{3}$).
γ_{H_2}	: C_p/C_v from hydrogen molecules ($\gamma_{\mathrm{H}_2} = \frac{7}{5}$).

Chapter 1

Introduction

This graduation report deals with the study of the elementary processes in a hydrogen plasma. The work is divided in two parts. First, a numerical model has been implemented to deal with the kinetic and flow properties of the plasma. Second, a measurement system for position dependent emission spectroscopy was built and some measurements with it are done. It has to be noted that the numerical model was implemented for a pure hydrogen gas while the experiments were performed in a hydrogen-argon mixture.

Knowledge of the elementary reactions in such a plasma is useful for many other experiments and applications. Numerical simulations and measurements of excited atomic state densities and molecular ion densities in a hydrogen plasma were performed. In particular we consider a recombining plasmajet which results from the expansion of a thermal high density plasma in a vacuum vessel. The hydrogen plasma is generated in a cascaded arc. Characteristics of such a plasma are: high initial density emanating from the source, low electron temperature and high heavy particle and vibrational temperature. A numerical model is implemented to calculate the densities of several constituents of the plasma. The purpose of the model is to get insight in the main kinetics and processes in the plasma to support optimization of the plasma for different applications. Furthermore, basic knowledge obtained from this model can be transposed to other plasmas.

This source of hydrogen molecules, atoms and ions can be applied for several purposes:

- To create large numbers of H^- ions. These ions can be accelerated in an particle accelerator, the surplus electron can be stripped off in an gas cell, and the resulting neutral H beam can be injected into a fusion plasma for additional heating.
- The source can be used to produce H atoms. They can be used to clean archeological objects, which are often covered with a thick layer of dirt and/or are often corroded. The hydrogen treatment makes it easy to remove the dirt layer and reduces corroded metals such as iron.
- A hydrogen atom (H^0) source can be very useful for passivation of thin amorphous semiconducting layers. So called dangling bonds can be bound, which improves the lifetime of the material.
- In the research of plasma deposition of materials such as amorphous silicon, which can be used for the production of solar cells, and diamond, which can be used as a strong, friction-resistant coating, knowledge of the basic plasma properties is needed. In these applications, hydrogen kinetics play an important role.
- As a model for gas cells. These cells create H^+ ions, which can be used in particle accelerators.

Chapter 2

Some basic concepts of plasma physics

Some basic properties of plasma physics, like ionization degree, rate coefficients and reaction balances are explained.

2.1 An ionized gas

A plasma is a gas in which so many atoms and/or molecules have lost and/or gained one or more electrons that the electrical interaction between these charged particles is the dominating interaction in the gas.

An important quantity of a plasma is the *ionization degree* α, defined by:

$$\alpha = \frac{n_{\mathrm{i}}}{n_{\mathrm{a}} + n_{\mathrm{i}}} \tag{2.1}$$

where n_{i} is the ion density and n_{a} the neutral density. This normalization leads to $\alpha = 1$ in an completely ionized plasma, instead of the *ionization ratio* $n_{\mathrm{i}}/n_{\mathrm{a}}$ which goes to infinity if n_{a} goes to 0. The atomic density follows from:

$$n_{\mathrm{a}} = \frac{\alpha}{1-\alpha}\, n_{\mathrm{i}} \ . \tag{2.2}$$

If the plasma consists of molecules which can dissociate, for example hydrogen, the *dissociation degree* β is defined in a similar way:

$$\beta = \frac{n_{\mathrm{a}}}{n_{\mathrm{a}} + n_{\mathrm{mol}}} \ . \tag{2.3}$$

where n_{mol} is the molecular density. Sometimes, the dissociation degree is defined with respect to mass instead of particles. For hydrogen, this results in:

$$\beta' = \frac{n_{\mathrm{H}}}{n_{\mathrm{H}} + 2n_{\mathrm{H_2}}} \ . \tag{2.4}$$

where the factor of 2 appears because the hydrogen molecule consists of 2 atoms. This definition is not used here.

2.2 Collisions, cross sections and densities

If a test particle moves in a plasma over a distance dx, the chance that it will collide is given by [1]:

$$P = n\sigma dx \tag{2.5}$$

This equation defines the *cross section* σ. It is easily to compute in a hard-sphere approximation, but in case of electrically charged particles, and atomic or molecular systems, that is much more complicated.

The mean free path ℓ is defined as the average length over which a particle travels between two successive collisions. If it is calculated, assuming that a particle moves between other particles with a fixed position, one finds that:

$$\ell = \frac{1}{n\sigma} \ . \tag{2.6}$$

This also gives the average time between two collisions for a particle moving with speed v:

$$\tau_{\mathrm{c}} = \frac{1}{n\sigma v} \tag{2.7}$$

and the collision frequency $\nu_c = 1/\tau_c$.

The number of collisions between particles of kind 1 and kind 2 per unit of time and per unit of volume is therefore given by:

$$\text{Number of collisions} = n_1 n_2 \langle \sigma v \rangle \ [\text{m}^{-3}\text{s}^{-1}] \ , \tag{2.8}$$

where $\langle \sigma v \rangle = \int \sigma(E) v(E) f(E) dE$ is called the *rate coefficient* K. In the general case, the mean free path is given by:

$$\ell = \frac{v_1}{n \langle \sigma u \rangle} \ . \tag{2.9}$$

where $u = \sqrt{v_1^2 + v_2^2}$ is the relative speed between the particles. If the collisions are between particles of kind 1 and 2, $m_1 \ll m_2$, we have [5]:

$$\frac{u}{v_1} = \sqrt{1 + \frac{m_1}{m_2}} \ . \tag{2.10}$$

so for collisions between electrons and heavy particles, equation 2.6 holds for electrons because $m_e \ll m_h$. For collisions between heavy particles we get:

$$\ell = \frac{1}{n\sigma\sqrt{2}} \ . \tag{2.11}$$

Usually, equations 2.5–2.7 are accurate within a factor 2 if one takes the average speed $\langle v \rangle$ for v.

2.3 Detailed balancing and microscopic reversibility

The term "detailed balancing", which originates from statistical mechanics, means that in case of thermodynamic equilibrium the number of reactions going forward equals the number of reactions going backwards. This is caused by the fact that, for a microscopic collisional or radiative process, the forward and backward process have equal probability if we correct for the occupied phase space. From this principle, we can derive that for the reaction:

$$\sum_{\text{forward}} \text{X}_{\text{forward}} \ \rightleftarrows \ \sum_{\text{back}} \text{X}_{\text{back}} \tag{2.12}$$

where X are different species, holds:

$$\prod_{\text{forward}} \hat{\eta}_{\text{forward}} = \prod_{\text{back}} \hat{\eta}_{\text{back}} \tag{2.13}$$

If the velocity distribution is Maxwellian, we have:

$$\hat{\eta}_{\text{X}p} = \frac{n_{\text{X}p}}{g_{\text{X}p}} \frac{h^3}{(2\pi m_{\text{X}} kT)^{3/2}} \ \text{e}^{-E_{\text{kin},p}/kT} \tag{2.14}$$

where $E_{\text{kin},p}$ is the kinetic energy of the particles in state p, and g is the *statistical weight* of the particles. For an atomic state, g is the degeneracy from the state: $g = 2j + 1$. For electrons, $g_e = 2$ because the electron has 2 internal degrees of freedom, the two spin states. The quantity $h^3/(2\pi mkT)^{3/2} := V_e \approx \lambda_B^3$ is called the *elementary volume*. This volume can contain at most one particle. g/V_e is the number of possible quantum states for the particle.

The balances in the next sections will be derived with the help of equations 2.12 and 2.13, so they assume (L)TE.

2.4 The Boltzmann balance

This balance describes the ration between two excited states in the same ionization state, usually the neutral atom. The ground level is often taken to be as the reference. The reaction is:

$$\text{X}_p + \text{Y} \ \rightleftarrows \ \text{X}_1 + \text{Y} + (E_{1p}) \tag{2.15}$$

where Y is a intermedium, necessary to obey conservation of momentum. Because the kinetic energies of the electrons cancel out, the difference in kinetic energy equals the difference in internal energy of the atoms, and the equilibrium relation becomes:

$$\eta_p^{\mathrm{B}} = \eta_1 \exp\left(\frac{-E_1 + E_p}{kT}\right) \tag{2.16}$$

The balance is often obtained by electron collisions:

$$\mathrm{X}_p + \mathrm{e}^- \;\rightleftarrows\; \mathrm{X}_1 + \mathrm{e}^- + (E_{1p}) \tag{2.17}$$

In this example, if the temperatures of the different particles (e,i,a) are not equal (formally this contradicts the LTE assumption), the electron temperature T_e should be taken for T.

2.5 The Saha balance

This balance describes the ratio between the ground level ion state, the electron density and an excited neutral level. The balance is often maintained by electron collisions:

$$\mathrm{X}_p + \mathrm{e}^- + (E_{p\mathrm{i}}) \;\rightleftarrows\; \mathrm{X}_1^+ + 2\mathrm{e}^- \tag{2.18}$$

So that the equilibrium density is given by:

$$\eta_p^{\mathrm{S}} = \eta_1^+ \eta_\mathrm{e} \left(\frac{h^2}{2\pi\, m_\mathrm{e} kT}\right)^{3/2} \exp\left(\frac{E_{p\mathrm{i}}}{kT}\right) \tag{2.19}$$

Because the right hand side of equation 2.18 contains 3 particles and the left hand side 2, a factor g/V_e remains in the equilibrium equation. This factor causes the so called Saha jump [1], when $p \to \infty$, which implies that $E_{p\mathrm{i}} \to 0$.

2.6 Resonant charge transfer

The balance for charge transfer (CT) between an ion state of an element and the ground level of another element is given by:

$$\mathrm{X}_1 + \mathrm{Y}_r^+ \;\rightleftarrows\; \mathrm{X}_q^+ + \mathrm{Y}_1 + (E_{rq}) \tag{2.20}$$

Here Y_r^+ and X_q^+ are resonant states for charge transfer.

If we assume that the process is perfectly resonant, the exponential factors disappear. In the general case, the equilibrium condition is given by:

$$\eta^{\mathrm{CT}}(\mathrm{Y}_r^+) = \frac{\eta(\mathrm{Y}_1)}{\eta(\mathrm{X}_1)} \eta^{\mathrm{CT}}(\mathrm{X}_q^+) \exp\left(\frac{E_{rq}}{kT}\right) \tag{2.21}$$

We note here that that the cross sections for charge transfer can be large, in particular if the energy difference is relatively small. An order of magnitude is $\sigma \approx 300\,\text{Å}^{\,2}$.

2.7 Excitation transfer

The balance for excitation transfer (ET), between an excited level of one element and the ground level of the other is given by:

$$\mathrm{X}_r + \mathrm{Y}_1 \;\rightleftarrows\; \mathrm{X}_1 + \mathrm{Y}_q + (E_{rp}) \tag{2.22}$$

The equilibrium condition is given by:

$$\eta^{\mathrm{ET}}(\mathrm{X}_r) = \frac{\eta(\mathrm{X}_1)}{\eta(\mathrm{Y}_1)} \eta^{\mathrm{ET}}(\mathrm{Y}_q) \exp\left(\frac{E_{rq}}{kT}\right) \tag{2.23}$$

All the previous balances interact with each other. In (L)TE all four equations 2.16, 2.19, 2.21 and 2.23 apply. In case of deviations from (L)TE, deviations from one balance will cause deviations from the others.

2.8 TE and LTE

For a plasma in TE, Plancks law:

$$\rho_\nu d\nu = \frac{8\pi h\nu^3}{c^3(\exp(h\nu/kT)-1)}\, d\nu \ , \tag{2.24}$$

Boltzmann:

$$\frac{n_p}{n_q} = \frac{g_p}{g_q} \exp\left(\frac{-E_p + E_q}{kT}\right) \ , \tag{2.25}$$

and Saha:

$$\frac{(n_\mathrm{i}/g_\mathrm{i})(n_\mathrm{e}/g_\mathrm{e})}{n_p/g_p} = \left(\frac{2\pi\, m_\mathrm{e} kT}{h^2}\right)^{3/2} \exp\left(\frac{-E_{p\mathrm{i}}}{kT}\right) \ . \tag{2.26}$$

hold for all levels p. Furthermore, the particles have a Maxwellian velocity distribution, which is for 3 (translational) degrees of freedom given by:

$$N(E,T)dE = \frac{2\pi n\sqrt{E}}{(\pi kT)^{3/2}} \exp\left(\frac{-E}{kT}\right) dE \tag{2.27}$$

Of course, in TE, the temperature in these four equations is the same.

Almost no laboratory plasma is in TE, usually the deviations are large, especially from Planck's law. This is because the plasma state requires a large electron temperature and a large power density. Because laboratory plasmas usually have small dimensions, these plasmas have very large density- and temperature gradients and energy supply and losses. These are circumstances which are per definition alien to TE.

A plasma in TE, which consists of one kind of atoms with known energy levels, can be described by 2 independent parameters, e.g. pressure and temperature.

LTE is a special deviation from TE. If a plasma is in LTE, we assume that each volume-element can be described with TE, but the used parameters are a function of position: $n_\mathrm{e} = n_\mathrm{e}(\vec{x})$; $T_\mathrm{e} = T_\mathrm{e}(\vec{x})$, etc.. LTE occurs if the collisions between electrons are not influenced by the escape of radiation and if the gradients are relatively small.

For a plasma in LTE, the Boltzmann and Saha laws hold. So does the Maxwellian energy distribution. Planck's equation however, does not apply.

2.9 Deviations from (L)TE; pLTE

An often occurring deviation from LTE is pLTE, partial LTE. A plasma in pLTE has a Saha equilibrium between the excited levels and the ion-ground level, but the neutral ground level is not in Saha equilibrium with these levels. The deviation from Saha equilibrium is given by $b_1 = n_1/n_1^\mathrm{S}$. This parameter gives the amount of over- or under population from the neutral groundlevel with respect to (L)TE. This model is shown in figure 2.1. The Boltzmann- and Saha lines in figure 2.1 are the densities which agree with the Boltzmann density according to equation 2.16 and the Saha density according to equation 2.19. So, per definition, the Boltzmann line is coupled with the density of the neutral ground level, and the Saha line is coupled with the density of the ion ground level.

The situation for a *recombining* plasma is sketched in figure 2.1. Such a plasma is characterized by an *underpopulation* from the neutral ground level with respect to Saha density. The Saha line is positioned above the Boltzmann line. An *ionizing* plasma is characterized by an *overpopulation* with respect to Saha density. In this case, the Saha line lies below the Boltzmann line.

When the deviations from LTE become larger, we can define a whole set of over and under polulations b_p with respect to Saha density:

$$b_p := \frac{n_p}{n_p^\mathrm{S}} \tag{2.28}$$

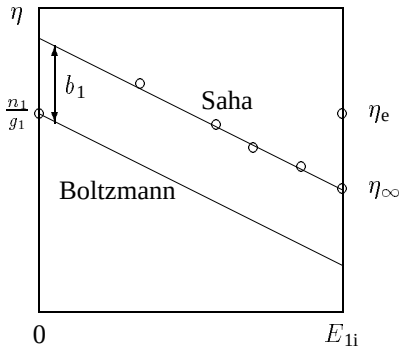

Figure 2.1: Schematical representation of a pLTE-density distribution. A case with $b_1 < 1$, a recombining plasma, is shown. $\eta_e (= \eta_i)$ and η_∞ are related to each other by the Saha equation. The slope of the lines $= 1/kT$.

It turns out that usually, the higher levels are in Saha equilibrium because the higher the level, the more collision processes become more important compared to radiation processes. So, for each plasma, there exists a level from which on the level densities are in Saha equilibrium. Therefore, pLTE is often called pLSE (partial Local Saha Equilibrium [16]).

It can be shown that for collisionally hot levels (this are high lying levels which are dominated by collision processes and radiation processes can be neglected), the deviations from Saha equilibrium are given by:

$$\delta b_p := b_p - 1 = b_0 p_{\text{eff}}^{-x} \tag{2.29}$$

where p_{eff} is the *effective main quantum number*, $p_{\text{eff}} = \sqrt{Ry/E_{ip}}$. The p_{eff}^{-x}-law holds only for certain classes of plasmas, those who are dominated by the (de)excitation-saturation balance [12]. Here, x is determined by the competition between ionization and recombination and lies between 5 and 6. For systems in ESP (Excitation Saturation Phase), where the influence of other processes than collisional (de)excitation between levels p and $p \pm 1$ is neglected, a value $x = 6$ is obtained. When a plasma is far from equilibrium, equation 2.29 is used to calculate the behaviour of the higher excited levels because they will eventually reach the ESP region, while for the lower excited levels a collisional-radiative model must be used.

Chapter 3

A collisional radiative model of a hydrogen plasma

The construction of numerical collisional-radiative models in general and for this particular hydrogen plasma is explained

3.1 Introduction to collision-radiative models

Collision-radiative models are just special balance equations for the excited levels of an excitation system.

When one wants to calculate the density of excited levels in a plasma, one can start with the continuity equation for level p:

$$\frac{\partial n_p}{\partial t} + \nabla \cdot (n_p \vec{w}) = \left(\frac{\partial n_p}{\partial t}\right)_{\text{CR}} = G - L \ , \tag{3.1}$$

where $\vec{w}$ is the drift velocity and CR notes that this term contains the collisional and radiative production and destruction rates. G stands for gain and L for loss processes of particles in state p.

We shall assume that the plasma is in a stationary condition. This means that the right-hand term, $(\partial n_p/\partial t)_{\text{CR}} = 0$. Further, we will assume that the transport in negligible for *all excited* levels, so $\nabla \cdot (n_p \vec{w}) = 0 \ \forall p \geq 2$. This is justified if the processes which populate and depopulate the levels are fast with respect to a characteristic transport time. This approach is called the *Quasi Steady State Solution* [1].

So, in general, we have to solve the following equations:

$$\left(\frac{\partial n_p}{\partial t}\right)_{\text{CR}} = 0 \quad \forall p > 1 \ , \tag{3.2}$$

$$\frac{\partial n_1}{\partial t} + \nabla \cdot (n_1 \vec{w}_1) = \left(\frac{\partial n_1}{\partial t}\right)_{\text{CR}} \ , \tag{3.3}$$

$$\frac{\partial n_{\text{i}}}{\partial t} + \nabla \cdot (n_{\text{i}} \vec{w}_{\text{i}}) = \left(\frac{\partial n_{\text{i}}}{\partial t}\right)_{\text{CR}} \ , \tag{3.4}$$

$$\tag{3.5}$$

In a stationary condition, we also have

$$\frac{\partial n_1}{\partial t} = \frac{\partial n_{\text{i}}}{\partial t} = 0 \ . \tag{3.6}$$

The solution of these equations can be written as:

$$n_p = r_p^0 n_p^{\text{S}} + r_p^1 n_p^{\text{B}} \tag{3.7}$$

$$= b_p n_p^{\text{S}} \tag{3.8}$$

$$= (1 + \delta b_p) n_p^{\text{S}} \tag{3.9}$$

Equation 3.7 gives the solution in terms of a Boltzmann and Saha distribution. Equation 3.8 gives the solution as an over ($b_p > 1$) or under ($b_p < 1$) population with respect to the Saha density, and equation 3.9 gives the solution as a deviation with respect to the Saha density.

It is necessary for the calculation to know all the relevant processes which populate and depopulate the levels. If these processes are known, one can solve equation 3.1 numerically.

To begin with, we assume that $\frac{\partial n_p}{\partial t} = \nabla \cdot (n_p \vec{w}_p) = 0 \quad \forall p \geq 2$. We note here that in some parts of the expanding plasma to be treated, this condition may not hold for $p = 2$.

3.2 Processes in a plasma

In this section, we limit ourselves to a plasma which contains only atomic constituents and singly ionized ions.

The processes relevant for our model are collisional (de)excitation to an excited level p, collisional ionization and recombination, radiative deexcitation to and from p and radiative recombination. We assume that only collisions with electrons are frequently enough to have a significant influence on the colisional-radiative behaviour of the plasma.

Thus, in a stationary condition, without transport, we have for any level p:

$$\text{Number of processes populating level } p \;=\; \text{Number of processes depopulating level } p \;,$$

So, the population density of level p follows from:

$$\underbrace{n_\mathrm{e} \sum_{q<p} n_q K_{qp}}_{\text{coll. excit.}} + \underbrace{n_\mathrm{e} \sum_{q>p} n_q K_{qp}}_{\text{coll. deexcit.}} + \underbrace{\sum_{q>p} n_q A_{qp}}_{\text{rad. deex. to}} + \underbrace{{n_\mathrm{e}}^2 n_\mathrm{i} K_{+p}}_{\text{coll. recomb.}} + \underbrace{n_\mathrm{e}\, n_\mathrm{i} \alpha_\mathrm{rad}}_{\text{rad. recomb}} =$$

$$\underbrace{n_\mathrm{e} n_p \sum_{q<p} K_{pq}}_{\text{coll. deexcit.}} + \underbrace{n_\mathrm{e} n_p \sum_{q>p} K_{pq}}_{\text{coll. excit.}} + \underbrace{n_p \sum_{q<p} A_{pq}}_{\text{rad. deex. from}} + \underbrace{n_\mathrm{e} n_p K_{p+}}_{\text{coll. ion.}} \tag{3.10}$$

As can be seen from equation 3.10, we assume that the plasma is optically thin: $\Lambda_{pq} = 1$. This is a valid assumption for the plasma which is considered; only the Lyman transitions in hydrogen $(n \geq 2 \rightarrow n = 1)$ could be trapped. (Trapping means that $\Lambda_{pq} < 1$). In this work we assume however that the plasma is also for this radiation optically thin.

The goal of the CR-model is to form a set of coupled equations like 3.10 for each level, and then solve them numerically. Some properties of the model are given in the following subsections.

To reduce computer time and to increase the reliability, a cut-off procedure for the highest levels is used [2].

A more detailed discussion about the used equations can be found in the following subsection. The program listings can be found in appendix B.

3.3 Calculation of the rate coefficients

A collisional (de)excitation process is given by:

$$\mathrm{X}_p + \mathrm{e}^- + E_{pq} \;\rightleftarrows\; \mathrm{X}_q + \mathrm{e}^- \;. \tag{3.11}$$

In equilibrium, detailed balancing exist:

$$n_\mathrm{e}\, n_p^\mathrm{B} K_{pq} \;=\; n_\mathrm{e}\, n_q^\mathrm{B} K_{qp} \tag{3.12}$$

where $^\mathrm{B}$ denotes the Boltzmann equilibrium density. Applying the Boltzmann distribution, the reverse rate coefficients can be calculated as follows:

$$\frac{K_{qp}}{K_{pq}} = \frac{g_p}{g_q} \exp\left(\frac{E_{qp}}{k\, T_\mathrm{e}}\right) \;. \tag{3.13}$$

The rate coefficients, calculated with equilibrium assumptions, also holds in non-equilibrium cases. The rate coefficients K_{pq} are calculated using the results from Vriens and Smeets [3]. These are semi-empirical formulas, assuming a hydrogenetic structure of atoms. For an element with one excited electron the hydrogenic approach becomes more accurate for higher excited states.

The rate coefficient K_{pq} in this approximation is given by [3]:

$$K_{pq} = \frac{1.6 \cdot 10^{-13}\sqrt{k\,T_{\mathrm{e}}}}{k\,T_{\mathrm{e}} + \Gamma_{pq}} \mathrm{e}^{\mathcal{E}_{pq}} \left[A_{pq} \ln\left(\frac{0.3 k\,T_{\mathrm{e}}}{Ry} + \Delta_{pq} \right) + B_{pq} \right] [\mathrm{m^3 s^{-1}}] \,, \tag{3.14}$$

where $\mathcal{E}_{pq} := E_{pq}/k\,T_{\mathrm{e}}$, $k\,T_{\mathrm{e}}$ in eV and $Ry = 13.595$ eV. We see that the transition probabilities A_{pq} are needed to calculate K_{pq}. The radiation transition probabilities are input parameters for the model, and are taken from [4]. With $s := q - p$ we have:

$$\Delta_{pq} = \exp\left(-\frac{B_{pq}}{A_{pq}} \right) + 0.06 \frac{s^2}{qp^2} \,. \tag{3.15}$$

$$\Gamma_{pq} = \frac{\left[3 + 11\frac{s^2}{p^2} \right] Ry \cdot \ln\left(1 + \frac{p^3 k\,T_{\mathrm{e}}}{Ry} \right)}{6 + 1.6qs + \frac{0.3}{s^2} + 0.8\frac{q^{1.5}}{\sqrt{s}}|s - 0.6|} \tag{3.16}$$

In these equations, p and q are the *effective quantumnumbers*, given by:

$$p = Z\sqrt{\frac{Ry}{E_{\mathrm{i}} - E_p}} \,. \tag{3.17}$$

Further, B_{pq} is given by:

$$B_{pq} = \frac{4Ry^2}{q^3} \left(\frac{1}{E_{pq}^2} + \frac{4E_{pi}}{3E_{pq}^3} + b_p \frac{E_{pi}^2}{E_{pq}^4} \right) \,, \tag{3.18}$$

where:

$$b_p = \frac{1.4\ln(p)}{p} - \frac{0.7}{p} - \frac{0.51}{p^2} + \frac{1.16}{p^3} - \frac{0.55}{p^4} \,. \tag{3.19}$$

For collisional ionization and recombination, the reaction is:

$$\mathrm{X}_p + \mathrm{e}^- \;\rightleftarrows\; \mathrm{X}^+ + 2\mathrm{e}^- \,. \tag{3.20}$$

Therefore, detailed balancing gives:

$$n_{\mathrm{e}}\, n_p^{\mathrm{S}} K_{p+} = {n_{\mathrm{e}}}^2\, {n_{\mathrm{i}}}^{\mathrm{S}} K_{+p} \,. \tag{3.21}$$

where $^{\mathrm{S}}$ denotes the Saha equilibrium density. Applying the Saha equation, the reverse rate coefficients are given by:

$$\frac{K_{+p}}{K_{p+}} = \frac{g_p}{2g_+} \left(\frac{h^2}{2\pi\, m_{\mathrm{e}} k\,T_{\mathrm{e}}} \right)^{3/2} \exp\left(\frac{E_{p+}}{k\,T_{\mathrm{e}}} \right) \,. \tag{3.22}$$

In the model we use the following equation, derived by Vriens and Smeets [3]:

$$K_{p+} = \frac{9.56 \cdot 10^{-12} (k\,T_{\mathrm{e}})^{-1.5} \mathrm{e}^{-\mathcal{E}_{p+}}}{\mathcal{E}_{p+}^{2.33} + 4.38\mathcal{E}_{p+}^{1.72} + 1.32\mathcal{E}_{p+}} \; [\mathrm{m^3 s^{-1}}] \,. \tag{3.23}$$

where $\mathcal{E}_{pi} := E_{pi}/k\,T_{\mathrm{e}}$. These equations are implemented in `unit New_Solv`.

3.4 Solution methods

With all the input parameters, a linear matrix equation is formulated. In general, this equation reads in the QSS approximation:

$$\nabla \cdot (n_p \vec{w}_p) = S(n_p) \,. \tag{3.24}$$

The source term $S(n_p)$ contains the production and destruction processes of level p. For excited levels, it is given by:

$$S(n_p) = \sum_q n_q (\underbrace{n_\mathrm{e} K_{qp}}_{\text{coll exc}} + \underbrace{A_{qp}}_{\text{rad exc.}}) - n_p \left(n_\mathrm{e} \sum_q (\underbrace{K_{pq}}_{\text{deexc}} + \underbrace{A_{pq}}_{\text{rad}}) \right) + \underbrace{{n_\mathrm{e}}^2 n_\mathrm{i} K_{+p}}_{\text{3 part rec}} - \underbrace{n_\mathrm{e} n_p K_{p+}}_{\text{ionization}} + \underbrace{n_\mathrm{e} n_\mathrm{i} \alpha_\mathrm{rad}}_{\text{2 part rec}} \tag{3.25}$$

and for ions, it is:

$$S(n_\mathrm{i}) = \underbrace{n_\mathrm{e} \sum_q K_{q+} n_q}_{\text{ionization}} - \underbrace{{n_\mathrm{e}}^2 \sum_q K_{+p}\, n_\mathrm{i}}_{\text{3 part rec}} \tag{3.26}$$

for $1 \le p \le p_{\text{cut off}}$. The QSS approximation assumes that for all excited levels $2 \le p \le p_{\text{cut off}}$ $\nabla \cdot (n_p \vec{w}_p) = 0$.

We limit the calculation to 12 excited levels. Above here, the levels are certainly in Saha equilibrium (this follows from some criteria which can be found in [2]). This results in a matrix equation:

$$\begin{pmatrix} -n_\mathrm{e} \sum_{q=1}^{+} K_{1q} & n_\mathrm{e} K_{21} & \cdots & n_\mathrm{e} K_{12,1} & {n_\mathrm{e}}^2 K_{+1} \\ n_\mathrm{e} K_{12} & -\sum_{q=1}^{+} (n_\mathrm{e} K_{2q} + A_{2q}) & \cdots & n_\mathrm{e} K_{12,2} & {n_\mathrm{e}}^2 K_{+2} \\ \vdots & \vdots & \ddots & \vdots & \vdots \\ n_\mathrm{e} K_{1,12} & n_\mathrm{e} K_{2,12} & \cdots & -\sum_{q=1}^{+} (n_\mathrm{e} K_{12,q} + A_{12,q}) & {n_\mathrm{e}}^2 K_{+,12} \\ n_\mathrm{e} K_{1+} & n_\mathrm{e} K_{2+} & \cdots & n_\mathrm{e} K_{12,+} & -{n_\mathrm{e}}^2 \sum_{q=1}^{+} K_{+q} \end{pmatrix} \cdot \begin{pmatrix} n_1 \\ n_2 \\ \vdots \\ n_{12} \\ n_\mathrm{i} \end{pmatrix} = \vec{0} \tag{3.27}$$

A solution method of this equation, which is implemented in the `procedure Calc_Stat` is obtained when we write the population of an excited level as the sum of the gain from and losses to the neutral ground state and the ion ground state. Therefore, the equations for the neutral ground state and the ion ground state can both be omitted, they are input parameters of the model:

$$\begin{pmatrix} -\sum (n_\mathrm{e} K_{2,q} + A_{2q}) & \cdots & n_\mathrm{e} K_{12,2} \\ \vdots & \ddots & \vdots \\ n_\mathrm{e} K_{2,12} & \cdots & -\sum (n_\mathrm{e} K_{12,q} + A_{12,q}) \end{pmatrix} \begin{pmatrix} n_2 \\ \vdots \\ n_{12} \end{pmatrix} =$$

$$- n_1 \begin{pmatrix} n_\mathrm{e} K_{12} \\ \vdots \\ n_\mathrm{e} K_{1,12} \end{pmatrix} - n_\mathrm{i} \begin{pmatrix} {n_\mathrm{e}}^2 K_{+2} \\ \vdots \\ {n_\mathrm{e}}^2 K_{+,12} \end{pmatrix} \tag{3.28}$$

Or, in index notation:

$$\sum_{\substack{q>1 \\ q \neq +}} c_{pq} n_q = -c_{p1} n_1 - c_{p+}\, n_\mathrm{i} \tag{3.29}$$

We can now solve the equations once for $n_\mathrm{i} = 0$ and $n_1 \neq 0$ and once for $n_1 = 0$ and $n_\mathrm{i} \neq 0$. Because of the linearity of the system, the total solution follows from adding the two partial solutions.

For $p \neq q$, c_{pq} gives the population of level p due to level q:

$$c_{qp} = n_\mathrm{e} K_{pq} + A_{pq} \tag{3.30}$$

and c_{pp} contains the destruction processes of level p:

$$c_{pp} = -n_e\left(\sum_q K_{pq} + K_{p+}\right) - \sum_q A_{pq} + J_{exc} \tag{3.31}$$

where J_{exc}, the ionization flow, exists only for the cut-off level c. For levels above a certain cut-off level, the dominant processes in the ionization flow are stepwise excitation and deexcitation. Then, the excitation flow can be calculated analytically: using the relation $\delta b_p = b_0 p_{eff}^{-6}$, which holds for highly excited states, J_{exc} can be written as a function of the effective quantum number [2]:

$$J_{exc} = n_e\left(n_c K_{c,c+1} - n_{c+1}K_{c+1,c}\right) = n_e n_c K_{c,c+1}\left(1 - \frac{p_c^6}{p_{c+1}^6}\right) . \tag{3.32}$$

The coupling coefficient with the ion ground state is given by:

$$c_{p+} = {n_e}^2 K_{+p} + n_e \alpha_{rad} . \tag{3.33}$$

3.5 Molecular reactions

The following scheme gives an overview of the most important reactions in a molecular hydrogen plasma which result in the loss of H^+ ions, one of the main scopes of this study:

$$H^+ + H_2^{v\geq 4} \longrightarrow H + H_2^+ \begin{cases} H_2^+ + e^- \longrightarrow H + H^* \\ \\ H_2^+ + H_2 \longrightarrow H + H_3^+ \;\; \{H_3^+ + e^- \longrightarrow H_2^{v\geq 4} + H \end{cases} \tag{3.34}$$

For a cold hydrogen gas, the first reaction has a low rate coefficient for $v \geq 4$, since the process is endothermic [7]. We assume that the reaction takes place in two steps: first, the molecule is vibrationally excited to $v > 4$ and then the charge exchange takes place. We assume that for this process $\sigma \approx 10^{-18}$ m^2 and $K \approx 2.5 \cdot 10^{-15}$ $m^3 s^{-1}$, typical values for charge exchange [7]. The most important reactions are given in table 3.1 [7], [8], [10], [11]. More reactions are given in A. For reaction 11, no rate coefficient was found in literature, but because the rate coefficient here is determined by the Coulomb interaction, as in reactions 7 and 9, we assume that the rate coefficient for these reaction is almost the same [11]. Some of the given rate coefficients, in particular K_2 and K_5, are still under discussion. Here, data obtained from [10] is used. It is expectable, however, that K_2 should be decreased.

Reaction mechanism	Rate coefficient [m^3/s]				ΔE
	nr.	0.3 eV	0.5 eV	1 eV	[eV]
$H_2^{v\geq 4} + H^+ \rightarrow H_2^+ + H$	$K_1 =$	$2.5 \cdot 10^{-15}$	$2.5 \cdot 10^{-15}$	$2.5 \cdot 10^{-15}$	-0.063
$H_2^{v\geq 4} + e^- \rightarrow H + H^-$	$K_2 =$	$2.8 \cdot 10^{-14}$	$2.8 \cdot 10^{-14}$	$2 \cdot 10^{-14}$	1.836
$H_2^+ + H_2 \rightarrow H_3^+ + H$	$K_3 =$	$1.1 \cdot 10^{-15}$	$1 \cdot 10^{-15}$	$2.8 \cdot 10^{-16}$	-1.92
$H_2^+ + e^- \rightarrow H^* + H$	$K_4 =$	$1.2 \cdot 10^{-13}$	$8 \cdot 10^{-14}$	$5.5 \cdot 10^{-14}$	-0.75
$H_3^+ + e^- \rightarrow H_2^{v>4} + H(2)$	$K_5 =$	$5 \cdot 10^{-14}$	$4 \cdot 10^{-14}$	$4 \cdot 10^{-14}$	3.164
$H_3^+ + e^- \rightarrow 3H$	$K_6 =$	$2 \cdot 10^{-14}$	$1.6 \cdot 10^{-14}$	$1.2 \cdot 10^{-14}$	-4.546
$H^+ + H^- \rightarrow H + H(n = 2)$	$K_7 =$	$1.3 \cdot 10^{-15}$	$1.5 \cdot 10^{-15}$	$2 \cdot 10^{-14}$	-2.649
$H^- + e^- \rightarrow H + 2e^-$	$K_8 =$	$5 \cdot 10^{-16}$	$2.5 \cdot 10^{-15}$	$1.5 \cdot 10^{-14}$	0.75
$H^+ + H^- \rightarrow H + H(n = 3)$	$K_9 =$	$4.1 \cdot 10^{-14}$	$4 \cdot 10^{-14}$	$4 \cdot 10^{-14}$	-0.761
$H^- + H \rightarrow 2H + e^-$	$K_{10} =$	$5 \cdot 10^{-16}$	$7 \cdot 10^{-16}$	$1 \cdot 10^{-15}$	0.75
$H^- + H_3^+ \rightarrow 2H_2$	$K_{11} =$	$3 \cdot 10^{-14}$	$3 \cdot 10^{-14}$	$3 \cdot 10^{-14}$	-12.784

Table 3.1: The most important reactions and their rate coefficients and energies for $0.3\,eV < T_e < 1\,eV$.

For collisions between heavy particles, one has to take into account that the time scale on which these reactions occur is larger with a factor $\approx \sqrt{m_\mathrm{i}/m_\mathrm{e}} \approx 45$. This could be of influence if transport properties become important and not all reactions get a chance to equilibrate.

For reactions between heavy particles, the target particle's energy can be important [10]. In the tables, a particle energy of 1 eV was taken for the target particle.

A possible problem arises with reaction 5. The very high energy difference results in a high rate coefficient for the backreaction. However, because with $T_\mathrm{vib} = 0.3$ eV the fraction of molecules with $v \geq 4$ is $1.56 \cdot 10^{-3}$, the effect is limited. However, if the vibration temperature becomes high, the back reaction wins relatively more in importance.

Further, many molecular ions are created in excited levels. This causes differences in the reaction energies which are not taken into account in the calculations. This plays, for example, a role in reaction 5. This reaction is very endothermic. Therefore, it is probable that H_3^+ is in an exited state, which would reduce this endothermicity.

To determine the energy difference of a reaction, we split the reaction into parts. For the first reaction equation in table 3.1 this gives:

$$\begin{array}{rcll} H_2^{v=4} & \rightarrow & H_2 & \text{Produces 1.89 eV,} \\ H_2 & \rightarrow & H_2^+ + e & \text{Requires 15.422 eV,} \\ H^+ + e & \rightarrow & H & \text{Produces 13.595 eV,} \end{array}$$

so $\Delta E = 15.422 - 1.89 - 13.595 = -0.063$ eV.

The vibrational energy differences are calculated using the equations in section 3.6. The excitation from H_2 to $H_2^{v=4}$ requires 1.89 eV. For the other energies we have the ionization energy from H_2 to $H_2^+ = 15.422$ eV, the dissociation energy for H_2 to $2H = 4.476$ eV, the dissociation energy for H^- to H+e $= 0.75$ eV and the dissociation energy of H_3^+ to H_2^+ and $H = 6.5$ eV. (All the dissociation and ionization reactions are endothermic). Then, we get for the reverse rate coefficients:

The reverse rate coefficients, which we denote with K', can be obtained by detailed balancing. We use the assumption that there is equilibrium on both a microscopic level and a macroscopic level and eliminate all quantities which are dependent on this equilibrium from the resulting equation. It must be emphasized that the rate coefficients which are obtained in this way are also usable when there are deviations from equilibrium. For the first reaction equation in table 3.1 equilibrium requires:

$$1.\text{Macroscopic}: \; n_{H_2^{v>4}} n_\mathrm{i} K_1 = n_{H_2^+} n_1 K_1' - \Delta E \; , \tag{3.35}$$

$$2.\text{Microscopic}: \; \frac{n_{H_2^{v>4}}}{g_{H_2^{v>4}}} \frac{n_\mathrm{i}}{g_\mathrm{i}} = \frac{n_{H_2^+}}{g_{H_2^+}} \frac{n_1}{g_1} \exp\left(\frac{\Delta E}{k\,T_\mathrm{h}}\right) \; . \tag{3.36}$$

where $\Delta E < 0$ if the reaction is exothermic. Now, we divide equation 3.35 by 3.36. This gives:

$$K_1 g_{H_2^{v>4}} g_\mathrm{i} = K_1' g_{H_2^+} g_1 \exp\left(-\frac{\Delta E}{k\,T_\mathrm{h}}\right) \; . \tag{3.37}$$

We use T_h here because there are no electrons involved in this reaction. So we get:

$$\frac{K_1'}{K_1} = \frac{g_{H_2^v} g_\mathrm{i}}{g_{H_2^+} g_1} \exp\left(\frac{\Delta E}{k\,T_\mathrm{h}}\right) \; . \tag{3.38}$$

$$\frac{K_1'}{K_1} = \frac{g_{H_2^{v>4}} g_\mathrm{i}}{g_{H_2^+} g_1} \, \mathrm{e}^{-0.063/\hat{T}} \; , \tag{3.39}$$

$$\frac{K_2'}{K_2} = 2\sqrt{2} \frac{g_\mathrm{e} g_{H_2}}{g_1 g_{H^-}} \left(\frac{m_\mathrm{e}}{m_1}\right)^{3/2} \mathrm{e}^{1.836/\hat{T}} \; , \tag{3.40}$$

$$\frac{K'_3}{K_3} = \frac{8}{\sqrt{27}} \frac{g_{H_2^+} g_{H_2}}{g_{H_3^+} g_1} e^{-1.92/\hat{T}} , \quad (3.41)$$

$$\frac{K'_4}{K_4} = 2\sqrt{2} \frac{g_{H_2^+} g_e}{g_2 g_1} \left(\frac{m_e}{m_1} \right)^{3/2} e^{-0.75/\hat{T}} , \quad (3.42)$$

$$\frac{K'_5}{K_5} = \frac{\sqrt{54}}{4} \frac{g_{H_3^+} g_e}{g_{H_2} g_2} \left(\frac{m_e}{m_1} \right)^{3/2} e^{3.164/\hat{T}} , \quad (3.43)$$

$$\frac{K'_6}{K_6} = \sqrt{27} \frac{g_{H_3^+} g_e}{g_1^3} \left(\frac{m_e}{m_1} \right)^{3/2} \left(\frac{h^2}{2\pi m_1 kT} \right)^{3/2} e^{-4.546/\hat{T}} , \quad (3.44)$$

$$\frac{K'_7}{K_7} = \frac{g_{H^-} g_i}{g_1 g_2} e^{-2.649/\hat{T}} , \quad (3.45)$$

$$\frac{K'_8}{K_8} = \frac{g_{H^-}}{g_1 g_e} \left(\frac{h^2}{2\pi\, m_e kT} \right)^{3/2} e^{0.75/\hat{T}} , \quad (3.46)$$

$$\frac{K'_9}{K_9} = \frac{g_{H^-} g_i}{g_1 g_3} e^{-0.761/\hat{T}} , \quad (3.47)$$

$$\frac{K'_{10}}{K_{10}} = \frac{g_{H^-}}{g_1 g_e} \left(\frac{h^2}{2\pi\, m_e kT} \right)^{3/2} e^{0.75/\hat{T}} , \quad (3.48)$$

$$\frac{K'_{11}}{K_{11}} = \frac{\sqrt{27}}{8} \frac{g_{H_3^+} g_{H^-}}{g_{H_2}^2} e^{-12.748/\hat{T}} . \quad (3.49)$$

The numerical factors arise from the different masses of the ions.

For the statistical weights, we use $g_{H^-} = 1$, $g_{H_3^+} = 1$, $g_{H_2^+} = 20$ and $g_{H_2} = 14$. For $H_2^{v \geq 4}$, we take $g = g_{H_2} - 4$ because there are 4 vibrational levels which are not used. Rotation was neglected here. We note that these values have for the molecular ions mainly an indicative value, particulary for H_3^+. For H_2, we assumed that rotational and vibrational levels had a thermal occupation with $T_{vib} = T_{rot} = 0.3$ eV. Then, g is in essence the product of the state sums Z_v and Z_r for vibration and rotation for hydrogen. They can be calculated from [17]:

$$Z_v = \sum_{v=1}^{\infty} e^{-(v+1/2)\Theta_v/T} = \frac{e^{-\Theta_v/2T}}{1 - e^{-\Theta_v/T}} \quad (3.50)$$

and

$$Z_r = \sum_{l=0}^{\infty} (2l+1) e^{-l(l+1)\Theta_r/T} \approx \int_0^{\infty} (2l+1) \exp\left(-\frac{\Theta_r}{T} l(l+1) \right) dl = \frac{T}{\Theta_r} \quad (3.51)$$

where Θ_v is the characteristic vibration temperature and Θ_r the characteristic rotation temperature. For hydrogen, $\Theta_v = 6140\,K$ and $\Theta_r = 85.5\,K$. Now, we have

$$Z_{tot} = Z_v \cdot Z_r . \quad (3.52)$$

For reactions which contain electrons, T should be set equal to T_e. For reactions which only contain heavy particles, T should be set to T_h, this is the case with K_1, K_3, K_7, K_9 and K_{11}.

A detailed list of molecular reactions in a hydrogen plasma is given in appendix A [10]. The rate coefficients are given for four electron temperatures: 0.3, 0,5, 1 and 1.5 eV. For temperatures between two of these temperatures, a linear interpolation was made. This fits well enough, as can been seen in figure 3.1.

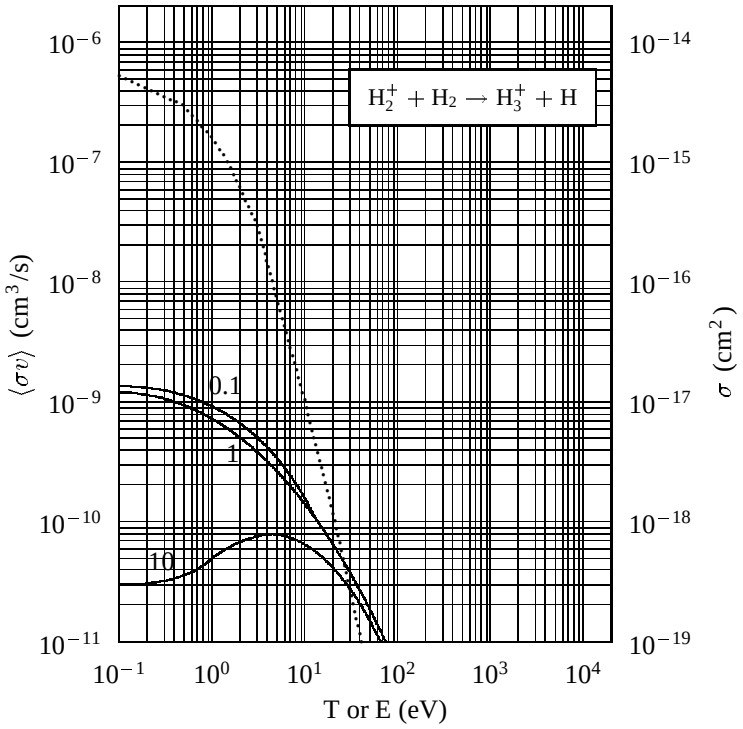

Figure 3.1: The rate coefficient for the reaction $H_2^+ + H_2 \rightarrow H_3^+ + H$ as a function of the temperature and for several values for the energy of the incoming particle according to [10]. ····· : cross section σ, —— : rate coefficient $K = \langle \sigma v \rangle$.

If we limit ourselves to the reactions given in table 3.1, the balance equations read:

For H_2^+ :

$$n_{H_2^+}[n_1 K_1' + n_{H_2} K_3 + n_e K_4] = n_i n_{H_2^{v>4}} K_1 + n_1 [n_{H_3^+} K_3' + n_{H^*} K_4'] \,, \tag{3.53}$$

For H_3^+ :

$$n_{H_3^+}[n_e (K_5 + K_6) + n_1 K_3' + n_{H^-} K_{11}] = n_{H_2^{v>4}} n_2 K_5' + n_1^3 K_6' + n_{H_2} n_{H_2^+} K_3 + n_{H_2}^2 K_{11}' \,, \tag{3.54}$$

For H^- :

$$n_{H^-}[n_1 K_2' + n_e K_8 + n_i (K_7 + K_9) + n_1 K_{10} + n_{H_3^+} K_{11}] =$$

$$n_e n_{H_2^{v\geq 4}} K_2 + n_1 n_2 K_7' + n_1 {n_e}^2 K_8' + n_1 n_3 K_9' + n_1^2 n_e K_{10}' + n_{H_2}^2 K_{11}' \,. \tag{3.55}$$

And the molecular processes which involve H^* are:

$$n_{H^*} n_H K_4' + \delta_{p2} n_2 (n_1 K_7' + n_{H_2^{v>4}} K_5') + \delta_{p3} n_1 n_3 K_9' =$$

$$n_e n_{H_2^+} K_4 + \delta_{p2} (n_i n_{H^-} K_7 + n_e n_{H_3^+} K_5) + \delta_{p3} n_i n_{H^-} K_9 \,, \tag{3.56}$$

where δ_{pq} is the Kronecker delta: $\delta_{pq} = 0$ if $p \neq q$ and $\delta_{pq} = 1$ if $p = q$.

3.6 Vibrational and rotational distributions

Because exact references on reactions which populate vibrational excited states are not present, we try to calculate the vibrational distribution of the H_2 molecules with a model with only one parameter: T_{vib}. The influence of rotational excitation is neglected.

The potential energy V of a harmonic oscillator is given by:

$$V = \tfrac{1}{2} b(r - r_0)^2 \ , \tag{3.57}$$

where r is the distance to the equilibrium position r_0. For hydrogen, $r_0 = 0.07$ nm. If, like the hydrogen molecule, the oscillator is quantized, we can calculate the possible energy levels with the Schrödinger equation. In this case, the eigenvalues of this equation are given by:

$$E = \hbar\omega_0(v + \tfrac{1}{2}) \ , \tag{3.58}$$

where v is the quantum number of vibration, which can only take integer values, and $\omega_0^2 = b/m$. For hydrogen, $\hbar\omega_0 = 8.734 \cdot 10^{-20}$ J.

Because H_2 is not a perfect harmonic oscillator, (the potential energy can be much better approximated by a Lenard-Jones potential and is not quadratic for large r), we can expand in $v + \frac{1}{2}$ for a small deviation:

$$E = \hbar\omega_e[(v + \tfrac{1}{2}) - x(v + \tfrac{1}{2})^2 + y(v + \tfrac{1}{2})^3 + ...] \ . \tag{3.59}$$

where x and $y \ll 1$, and $\omega_0 = \omega_e(1 - x + \frac{3}{4}y + ...)$. For hydrogen, $x = 57/2339 = 0.0244$ [9]. The term $\sim x$ becomes important for higher values from v. For a discrete energy distribution, the Boltzmann statistics give:

$$n(v) = g_v \frac{n_{\text{tot}}}{Z_v} \exp\left(-\frac{E(v)}{kT}\right) \ . \tag{3.60}$$

In this equation Z_v is the so called *state sum* or *partition function*:

$$Z_v = \sum_{v=0}^{v_{\max}} g(v) \mathrm{e}^{-E(v)/kT} \ . \tag{3.61}$$

$g(v)$ takes the easy form $g(v) =$ constant, so the number of molecules in each vibrational state is proportional to $\exp(-E(v)/kT) \sim \exp(-\hbar\omega_e(v - xv^2)/kT)$. [9]. The zero-point energy can be left out, since to add this to the exponent would mean only adding a factor that is constant for all the vibrational levels and would cancel out [9]. $v_{\max}$ is the value of v for which the dissociation energy is reached. For the electronic ground level of the H_2 molecule, this occurs for $v_{\max} = 14$. Now, the distribution of hydrogen over the vibrational states is given by:

$$n(v) = \frac{n_{\text{tot}} \ \exp\left(\dfrac{-\hbar\omega_e(v - xv^2)}{k\,T_{\text{vib}}}\right)}{\displaystyle\sum_{v=1}^{14} \exp\left(\frac{-\hbar\omega_e(v - xv^2)}{k\,T_{\text{vib}}}\right)} \ . \tag{3.62}$$

Even if the vibrational levels are not in equilibrium, which is to be expected, this model might give accurate results for a certain T_{vib} because in the present model the 2 reactions which need vibrationally excited molecules only molecules with $v \geq 4$ are needed. We can match T_{vib} so that it gives the actual number of molecules with $v \geq 4$. It must be noted however, that formation of H^- actually requires higher vibrational levels, up from $v = 9$ or 10. This can be understood from potential energy diagrams of these states, as can be found in [21].

The energy of a rotationally excited molecule in first order is given by:

$$E(j) = \frac{\hbar^2}{2I} j(j+1) = j(j+1)B \ , \tag{3.63}$$

where $B = 5.84 \cdot 10^{-22}$ J for hydrogen and the statistical weight of each level is:

$$g(j) = 2j + 1 \ . \tag{3.64}$$

The influence of rotationally excited molecules is unknown. The energy of a state $v = 0,\ j = 23$ is approximately the same as $v = 4,\ j = 0$. But because the statistical weight of the first state is 47 and for the second 2, it can contribute more to a reaction where the energy difference is the most important factor in the value for the rate coefficient. Hence rotational excitation can be more important than vibrational excitation if $T_{\text{rot}} \approx T_{\text{vib}}$. At this point, the present model needs to be extended in the future.

Applied to the H^+/H^- source, the creation of vibrationally and/or rotationally excited molecules on the wall of the vessel is an unknown factor. It is known that the process of associative recombination of hydrogen atoms at metals returns molecules in vibrationally excited levels.

3.7 Extension of the model with molecular terms

To use the CR model for plasmas which also contains H_2 molecules in various excited states, the following method was performed:

1. The number of free parameters of the model is increased by 2: the density of H_2 molecules and the vibrational temperature T_{vib} (see section 3.6). So, the free parameters now are $n_{\text{e}} = n_{\text{i}}$, n_1, n_{H_2}, T_{e} and T_{vib}. Initially, we used the approximation $n_{\text{e}} = n_{\text{i}}$, although the densities of $n_{\text{H}_3^+}$ and n_{H^-} can be quite large, sometimes even larger than n_{i}. This problem is solved by determining n_{i} with an iteration procedure.

2. The vibrational excitation distribution of the H_2 molecules is calculated with a vibrational temperature T_{vib}. The vibrational distribution is important because some reactions can only be initiated with vibrationally excited molecules, for example $H_2^{v\geq 4} + H^+ \rightarrow H_2^+ + H$. The influence of rotationally excited molecules is unknown, as is the influence of the wall of the vessel.

3. The initial state vector $(n_2, n_3, \ldots, n_{12})$ was expanded with states H_2^+, H_3^+ and H^- to $(n_2, n_3, \ldots, n_{12}, n_{\text{H}_2^+}, n_{\text{H}_3^+}, n_{\text{H}^-})$.

4. The most important molecular reactions were selected. They are discussed in section 3.5.

The problem, arising from the approximation $n_{\text{e}} = n_{\text{i}}$ could be solved in two ways: first, we could take n_{i} as an independent input parameter. Second, one could make the model iterative by using local charge neutrality:

$$n_{\text{i}} = n_{\text{e}} + n_{\text{H}^-} - n_{\text{H}_2^+} - n_{\text{H}_3^+} \tag{3.65}$$

and changing n_{i} in each iteration step:

$$n_{\text{i,new}} = n_{\text{e}} + n_{\text{H}^-} - n_{\text{H}_2^+} - n_{\text{H}_3^+}\ . \tag{3.66}$$

This second method is what we did in our model. The convergence is very fast, usually only a few (less then 20) iteration steps are needed to decrease the total net charge density of the plasma below 10^3 e/m^3 with e the elementary charge.

However, sometimes the iteration becomes a divergent process, resulting in unphysical negative densities. The cause of this problem lies in the sometimes high density of H_3^+ ions. This results in a too large correction on the H^+ density, which becomes negative. This problem was solved using a relaxation in the correction for n_{i}: we change the iteration relation for charge neutrality 3.66 in:

$$n_{\text{i,new}} = x \cdot \left(n_{\text{e}} + n_{\text{H}^-} - n_{\text{H}_2^+} - n_{\text{H}_3^+}\right) + (1 - x) \cdot n_{\text{i,old}}\ . \tag{3.67}$$

The relaxation parameter x can vary between 0 and 1. In the first iteration step, the program determines the maximum value of the relaxation parameter for which the ion density is higher than a certain value, usually 10^3 e/m^3. In the plasma, deviations from charge neutrality in the order of $\lambda_{\text{D}}/\tau \sim 10^{-5}$ can be expected. So 10^3 is rather small. It would be possible to use a varying relaxation factor in every iteration step, but this results in a non linear dependence of n_{i} on the iteration parameters and is therefore not done. The

value $10^3\,\mathrm{e/m^3}$ is chosen instead of 0 to increase the convergention speed: we can expect the ion density to be $> 10^3\,\mathrm{e/m^3}$ in any case.

An other problem arises when we also include collisions between heavy particles like H_3^+ and H^- in our model. This gives rise to terms quadratic in the parameters which we want to determine, and therefore, a linear matrix equation is not valid any more. This problem is solved by approximating the densities n_{H^-} and $n_{\mathrm{H}_3^+}$, which arise in reaction equation 11, by initial values $n_{\mathrm{H}^-,\mathrm{initial}}$ and $n_{\mathrm{H}_3^+,\mathrm{initial}}$; these values can be changed in the same iteration process as the charge neutrality. Because there is only one reaction (nr. 11) incorporated in our model with this problem, the effect of this non-linearity on the model is limited. An iterative model worked just fine here: the convergence is very fast for most input parameters.

Now, the extended matrix equation becomes:

$$\sum_{q\neq 1,+,\mathrm{H}_2} c_{pq} n_q = -n_1 c_{p1} - n_\mathrm{i} c_{p+} - n_{\mathrm{H}_2} c_{p,\mathrm{H}_2} \ . \tag{3.68}$$

We approximate n^* with n_2 unless an other level is explicitly given in the reaction equation (this is only the case with reaction 9). Further, we identify n_H with n_1. Then, the total matrix equation becomes:

$$\begin{pmatrix} -\sum_{q=1}^{+}(n_\mathrm{e}K_{2q}+A_{2q}) - n_1(K_4'+K_7') - n_{\mathrm{H}_2} f(v\geq 4)K_5' & \cdots & n_\mathrm{e}K_{12,2}+A_{12,2} & \cdots \\ \vdots & \ddots & \vdots & \cdots \\ n_\mathrm{e}K_{2,12} & \cdots & -\sum_{q=1}^{+}(n_\mathrm{e}K_{12,q}+A_{12,q}) & \cdots \\ n_1K_4' & \cdots & 0 & \cdots \\ n_{\mathrm{H}_2} f(v\geq 4)K_5' & \cdots & 0 & \cdots \\ n_1K_7' & \cdots & 0 & \cdots \end{pmatrix}$$

$$\begin{pmatrix} \cdots & n_\mathrm{e}K_4 & n_\mathrm{e}K_5 & n_\mathrm{i}K_7 \\ \cdots & \vdots & \vdots & \vdots \\ \cdots & 0 & 0 & 0 \\ \cdots & -n_1K_1' - n_{\mathrm{H}_2}K_3 - n_\mathrm{e}K_4 & n_1K_3' & 0 \\ \cdots & n_{\mathrm{H}_2}K_3 & \begin{cases} -n_\mathrm{e}(K_5+K_6) \\ -n_1K_3' - n_{\mathrm{H}^-}K_{11} \end{cases} & 0 \\ \cdots & 0 & 0 & \begin{cases} -n_1K_2' - n_\mathrm{e}K_8 - n_\mathrm{i}(K_7+K_9) \\ -n_1K_{10} - n_{\mathrm{H}_3^+}K_{11} \end{cases} \end{pmatrix} \cdot \begin{pmatrix} n_2 \\ \vdots \\ n_{12} \\ n_{\mathrm{H}_2^+} \\ n_{\mathrm{H}_3^+} \\ n_{\mathrm{H}^-} \end{pmatrix} =$$

$$-n_1 \begin{pmatrix} n_\mathrm{e}K_{1,2} \\ \vdots \\ n_\mathrm{e}K_{1,12} \\ 0 \\ n_1^2K_6' \\ {n_\mathrm{e}}^2K_8' + n_1 n_\mathrm{e}K_{10}' \end{pmatrix} - n_\mathrm{i} \begin{pmatrix} {n_\mathrm{e}}^2K_{+2} \\ \vdots \\ {n_\mathrm{e}}^2K_{+,12} \\ 0 \\ 0 \\ 0 \end{pmatrix} - n_{\mathrm{H}_2} \begin{pmatrix} 0 \\ \vdots \\ 0 \\ n_\mathrm{i} f(v\geq 4)K_1 \\ n_{\mathrm{H}_2}K_{12}' \\ n_\mathrm{e} f(v\geq 4)K_2 + n_{\mathrm{H}_2}K_{11}' \end{pmatrix} . \tag{3.69}$$

Here, f means the fraction H_2 molecules with a vibrational quantum number > 4. This fraction is given by:

$$f(v\geq 4) = \frac{1}{Z}\sum_{v=4}^{14} \exp\left(-\frac{\hbar\omega_e(v-xv^2)}{k\,T_\mathrm{vib}}\right) \ . \tag{3.70}$$

Equation 3.69 can be solved with same method as equation 3.29 in `unit new_solv`.

This results in the flow chart for the model given in figure 3.2.

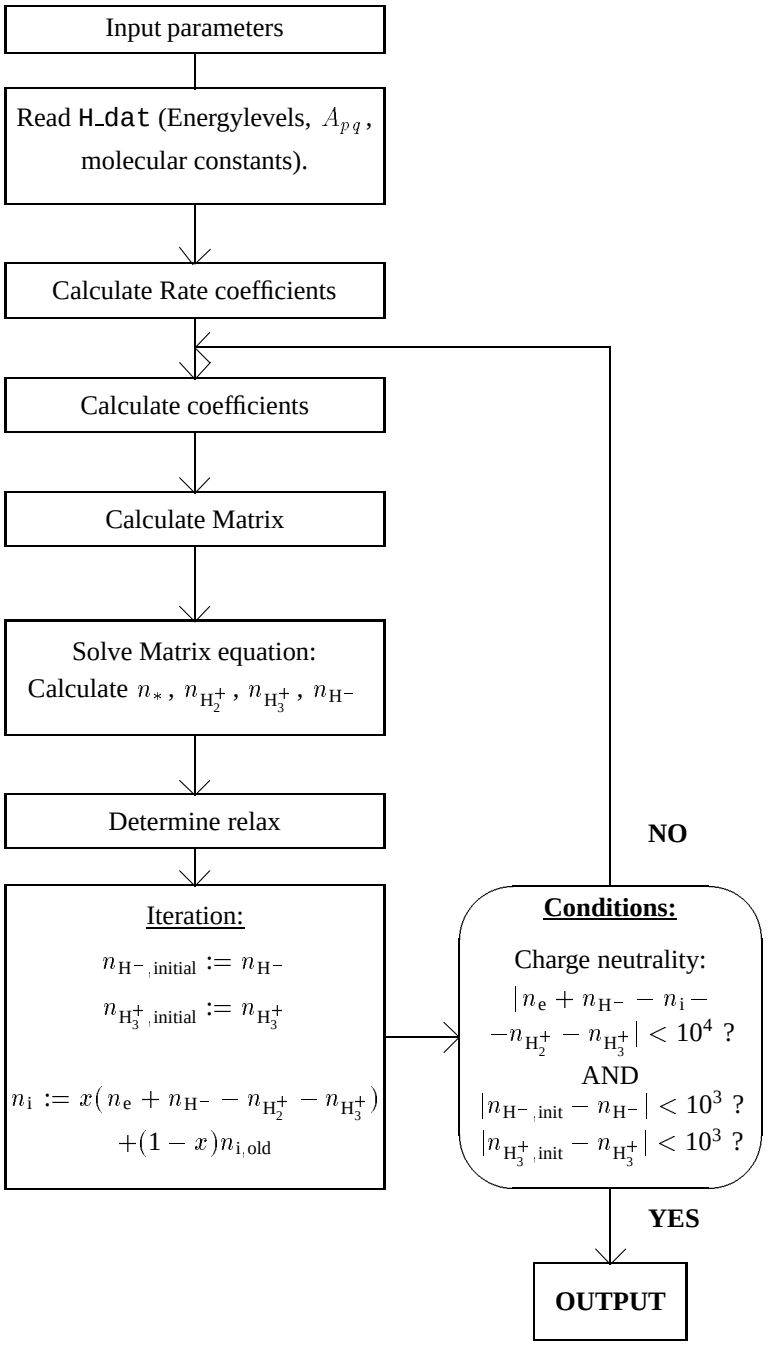

Figure 3.2: The flow chart of the numerical model including the iteration process.

Chapter 4

Results of the numerical model

The results obtained with the local model are given.

4.1 Testing the model

If the atomic part of the model is accurate, there should be no deviation from Saha equilibrium if we choose for n_1 the Saha equilibrium density, only collision processes are considered and radiation processes are neglected. This because the Saha-balance is derived only with collision processes, as can be found in chapter 2. To test this, it was tried to reproduce the Saha distribution with the model. This succeeded, the largest deviation of Saha equilibrium in cases where n_1 was taken the Saha density belonging to the given n_e was less than 10^{-15}. The conditions and results are given in table 4.1.

p_eff	b_p	$\delta b_p = b_p - 1$
1	1.0000	0
2	1.0000	0
3	1.0000	$-1.116 \cdot 10^{-16}$
4	1.0000	0
5	1.0000	$-2.522 \cdot 10^{-16}$
6	1.0000	$-1.523 \cdot 10^{-16}$
7	1.0000	0
8	1.0000	$-4.470 \cdot 10^{-16}$
9	1.0000	$-4.090 \cdot 10^{-16}$
10	1.0000	$-2.457 \cdot 10^{-16}$
11	1.0000	$-4.399 \cdot 10^{-16}$
12	1.0000	$-3.925 \cdot 10^{-16}$

Conditions		
$k\,T_\mathrm{e}$	0.3	eV
n_e	10^{19}	m^{-3}
n_i	10^{19}	m^{-3}
$n_1 = n_1^\mathrm{S}$	$9.68 \cdot 10^{30}$	m^{-3}
γ	0	s^{-1}

Table 4.1: Calculated b values without radiative transitions and without radiative recombination for each atomic level. The value $b_1 = 1$ was used for the calculation. The deviations of 0 are due to numerical errors.

The results in other conditions (higher T_e) are also good. The calculated densities are given in table 4.2, together with the theoretical Saha densities. As can be seen, the agreement is excellent.
For n_1, the Saha-equilibrium value is taken. The actual value for n_1 is much lower, $\approx 10^{20}$ m^{-3} [6]. So, according to the model, $b_1 \ll 1$. So the expanding plasma is a recombining plasma, as it is in reality.

For the molecular part, we looked to the equilibrium densities of each species H_2^+, H_3^+ and H^- belonging to each reaction for the given conditions. So, for reaction 1,

$$\mathrm{H}_2^{v\geq 4} + \mathrm{H}^+ \rightarrow \mathrm{H}_2^+ + \mathrm{H}\,, \tag{4.1}$$

we get for the equilibrium density of H_2^+:

$$n_{\mathrm{H}_2^+} = \frac{g_{\mathrm{H}_2^+} g_1}{g_\mathrm{i} g_{\mathrm{H}_2^{v\geq 4}}} \frac{n_\mathrm{i} n_{\mathrm{H}_2^{v\geq 4}}}{n_1} \exp\left(\frac{0.063}{\hat{T}}\right)\,. \tag{4.2}$$

p_{eff}	b_p	$\delta b_p = b_p - 1$
1	1.0000	0
2	1.0000	$4.913 \cdot 10^{-16}$
3	1.0000	$5.409 \cdot 10^{-16}$
4	1.0000	$7.857 \cdot 10^{-16}$
5	1.0000	$6.829 \cdot 10^{-16}$
6	1.0000	$8.398 \cdot 10^{-16}$
7	1.0000	$5.687 \cdot 10^{-16}$
8	1.0000	$5.577 \cdot 10^{-16}$
9	1.0000	$4.604 \cdot 10^{-16}$
10	1.0000	$6.418 \cdot 10^{-16}$
11	1.0000	$6.520 \cdot 10^{-16}$
12	1.0000	$7.437 \cdot 10^{-16}$

Conditions		
kT_{e}	1.0	eV
n_{e}	10^{19}	m^{-3}
n_{i}	10^{19}	m^{-3}
$n_1 = n_1^{\text{S}}$	$2.663 \cdot 10^{16}$	m^{-3}
γ	0	s^{-1}

Table 4.2: Calculated b values without radiation for each atomic level. The value $b_1 = 1$ was used for the calculation. The deviations from 0 are due to numerical errors.

When the calculated density of H_2^+ is lower than the density following from equation 4.2 with given n_{H} and n_{H_2}, there should be less destruction reactions for H_2^+ than creation reactions for H_2^+ in this balance: there is no equilibrium in reaction 4.1. When the actual calculated density of H_2^+ is higher than the density following from equation 4.2, there should be more destruction reactions for H_2^+ than creation reactions for H_2^+ in this balance.

This should hold for all reactions and all densities. This is used as a check for the model. The effect occurred also in the simulations, so the model is consistent in this view.

4.2 Locally simulating the plasma

The densities of H_2^+, H_3^+ and H^- were calculated using the model. We also added a transport frequency to the balance equations, which arises from diffusion. The total balance equation for each species becomes with diffusion:

$$\left(\frac{\partial n}{\partial t}\right)_{\text{CR}} = \nabla \cdot (n\vec{w}) \tag{4.3}$$

where $\vec{w}$ is the transport velocity (In this case we use the diffusion velocity). We assume that the approximation $\nabla(n\vec{w}) = \gamma_{\text{t}} n$ is valid, so we get [22]:

$$\left(\frac{\partial n}{\partial t}\right)_{\text{CR}} = \gamma_{\text{t}} n \ . \tag{4.4}$$

The densities of the molecular ions as a function of this transport parameter γ are given in figure 4.1. Because the thermal speed of particles is proportional with $1/\sqrt{m}$, we took $\gamma_{H_2^+} = \gamma_{H^-}/\sqrt{2}$ and $\gamma_{H_3^+} = \gamma_{H^-}/\sqrt{3}$.

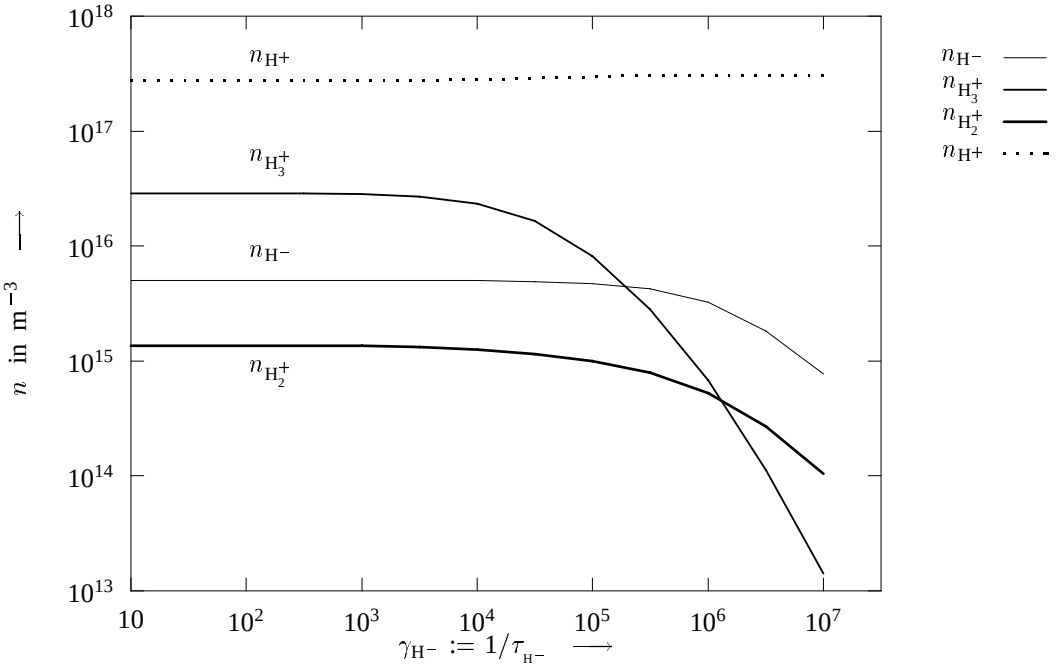

Figure 4.1: Calculated molecular ion densities for hydrogen. $T_e = 0.26$ *eV,* $n_e = 3 \cdot 10^{17}$ m^{-3}, $n_1 = 10^{20}$ m^{-3} *and* $n_{H_2} = 7 \cdot 10^{20}$ m^{-3}. $\gamma_{H_2^+} = \gamma_{H^-}/\sqrt{2}$ *and* $\gamma_{H_3^+} = \gamma_{H^-}/\sqrt{3}$.

The molecular ion densities as a function of the electron temperature are given in figure 4.2. No diffusion or transport was considered in this calculation.

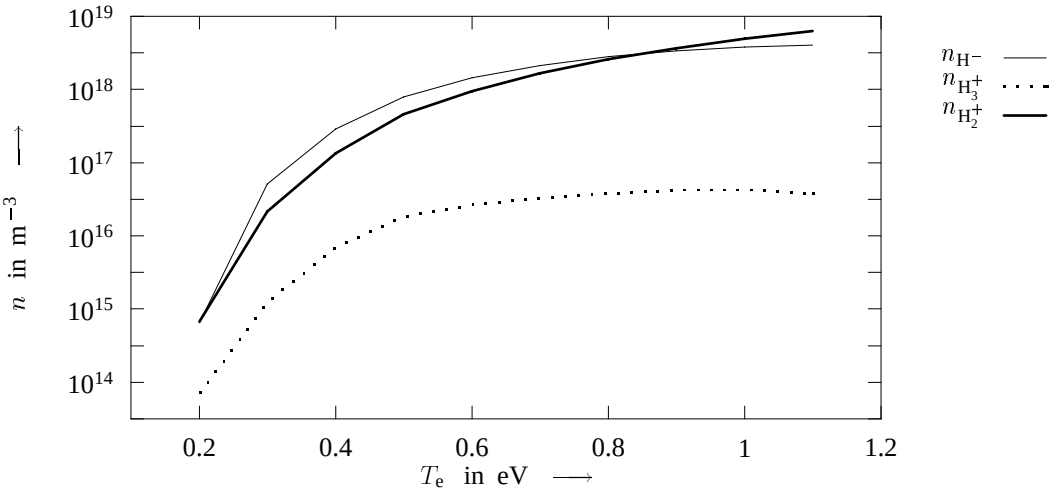

Figure 4.2: Calculated molecular ion densities for hydrogen as a function of the electron temperature. Conditions: $n_{H_2} = 7 \cdot 10^{20}$ m^{-3}, $\alpha = 0.1$, $\beta = 0.7$, $T_{vib} = T_e$ *and* $n_e = n_{i,initial} = 3 \cdot 10^{17}$.

We see here that the density of H_2^+ becomes larger than the density of H_3^+. This is caused by the large dissociation degree of 0.7 which is used in this calculation.

When we calculate the densities of the molecular ions with the more realistic parameters of $\beta = 0.125$ and $\alpha = 0.003$ we get the result of figures 4.3 and 4.4. The difference between them is, that in figure 4.3 the vibration temperature is kept constant on 0.3 eV, while in figure 4.4 the vibration temperature is kept equal to T_e.

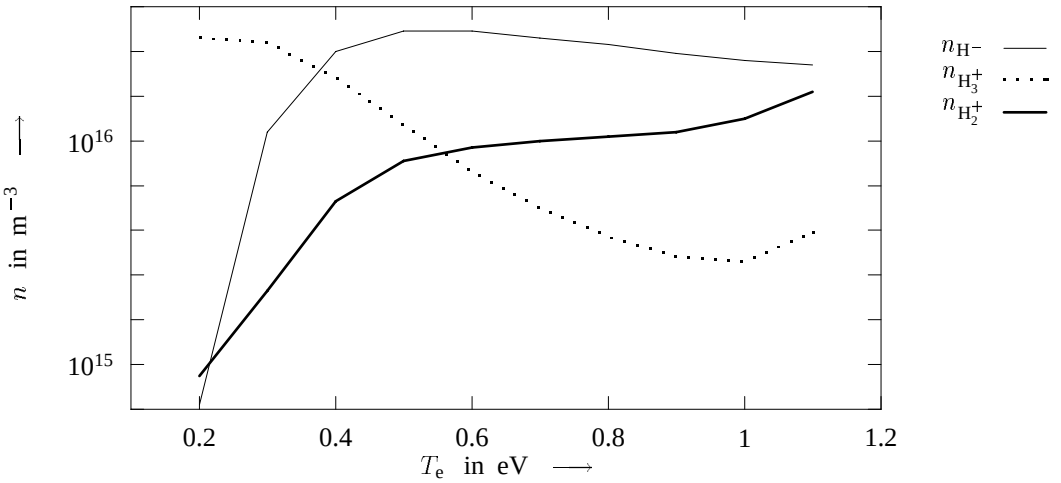

Figure 4.3: Calculated molecular ion densities for hydrogen as a function of the electron temperature. Conditions: $n_{H_2} = 7 \cdot 10^{20}\ m^{-3}$, $T_{\text{vib}} = 0.3$ *eV,* $\alpha = 0.003$, $\beta = 0.125$.

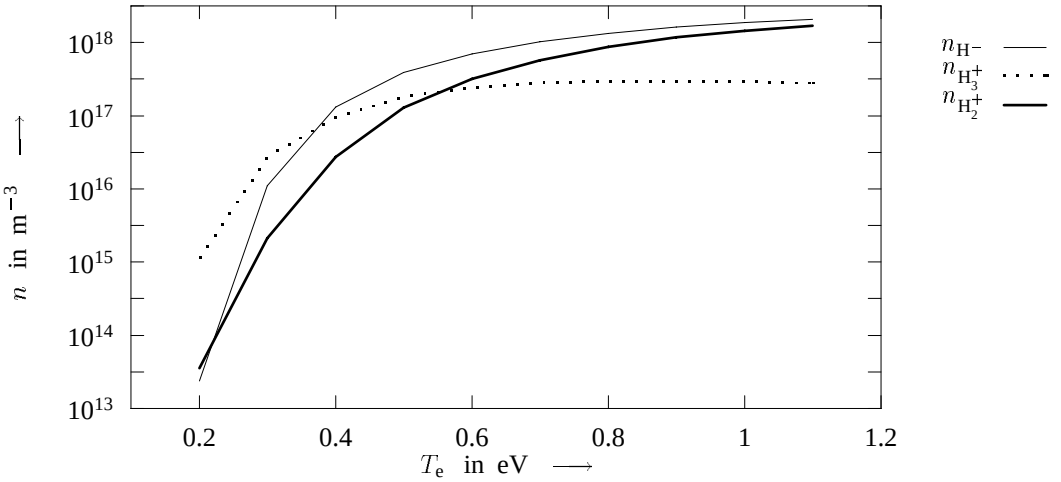

Figure 4.4: Calculated molecular ion densities for hydrogen as a function of the electron temperature. Conditions: $n_{H_2} = 7 \cdot 10^{20}\ m^{-3}$, $T_{\text{vib}} = T_{\text{e}} = T_{\text{h}}$, $\alpha = 0.003$, $\beta = 0.125$.

When we compare figures 4.3 and 4.4 with figure 4.2 we see that the effect of a very high ionization degree is that the density of H_2^+ becomes very large. The influence of the dissociation degree on the H^- density is very small, as can be seen in figure 4.5. The density depends much more on the electron temperature than on the dissociation degree, although temperature and dissociation degree can not be seen independent of each other. For H_2^+, the density depends even more emphatic on T_{e}, as can be seen in figure 4.6.

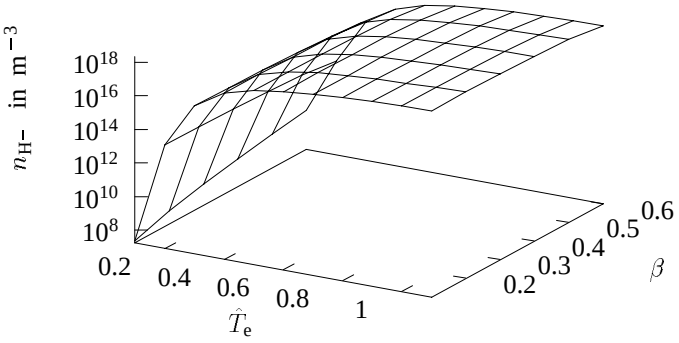

Figure 4.5: Calculated H^- densities for a pure hydrogen plasma as a function of the electron temperature and the dissociation degree. Conditions: $n_{H_2} = 7 \cdot 10^{20}\ m^{-3}$, $\alpha = 0.1$, $T_{vib} = T_e$ and $n_e = n_{i,initial} = 3 \cdot 10^{17}\ m^{-3}$.

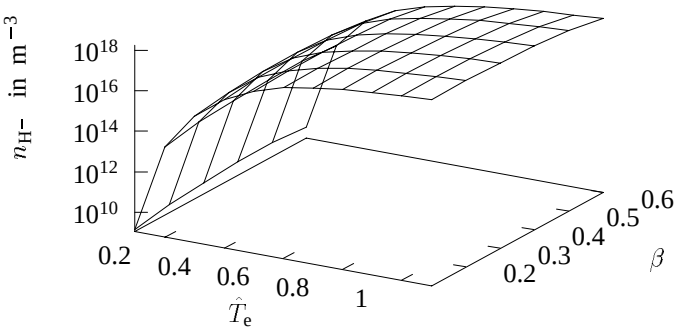

Figure 4.6: Calculated H_2^+ densities for a pure hydrogen plasma as a function of the electron temperature and the dissociation degree. Conditions: $n_{H_2} = 7 \cdot 10^{20}\ m^{-3}$, $\alpha = 0.1$, $T_{vib} = T_e$ and $n_e = n_{i,initial} = 3 \cdot 10^{17}\ m^{-3}$.

The densities of the molecular ions turned out to be very sensitive for the vibrational temperature. If T_{vib} increases, the densities of the molecular ions increase also. The results of the calculation are given in figure 4.7.
To investigate which reactions are the most important, the number of reactions per second and per m^3 are calculated. The results for some temperatures are shown in table 4.3.
The densities of the excited states of atomic hydrogen, calculated in the presence of molecular reactions, are shown in figure 4.8, the calculated values for 4 different n_e values are listed in tables 4.4 to 4.7, as are the b_p factors.

The giant overpopulation of $H(n = 3)$ for low electron densities is mainly caused because reaction 9 ($H^+ + H^- \rightleftarrows H + H(n = 3)$) gives rise to a net flow in this state.

Further, the giant underpopulation of $H(n = 1)$ with respect to the Saha equilibrium value might also cause some effects. This large non-equilibrium situation can spread out towards many excited levels. The Saha equilibrium value for the ratio $n^S_{H_2}/n^S_H$, derived from assuming equilibrium for the reaction $H_2 \rightleftarrows H + H + \Delta E$ is given by:

$$\frac{n^S_{H_2}}{n^S_H} = \frac{g_{H_2}}{g_H} n^S_{H_2} \left(\frac{h^2}{2\pi m_H e \hat{T}_h} \right)^{3/2} \exp\left(\frac{4.476}{\hat{T}_h} \right) \qquad (4.5)$$

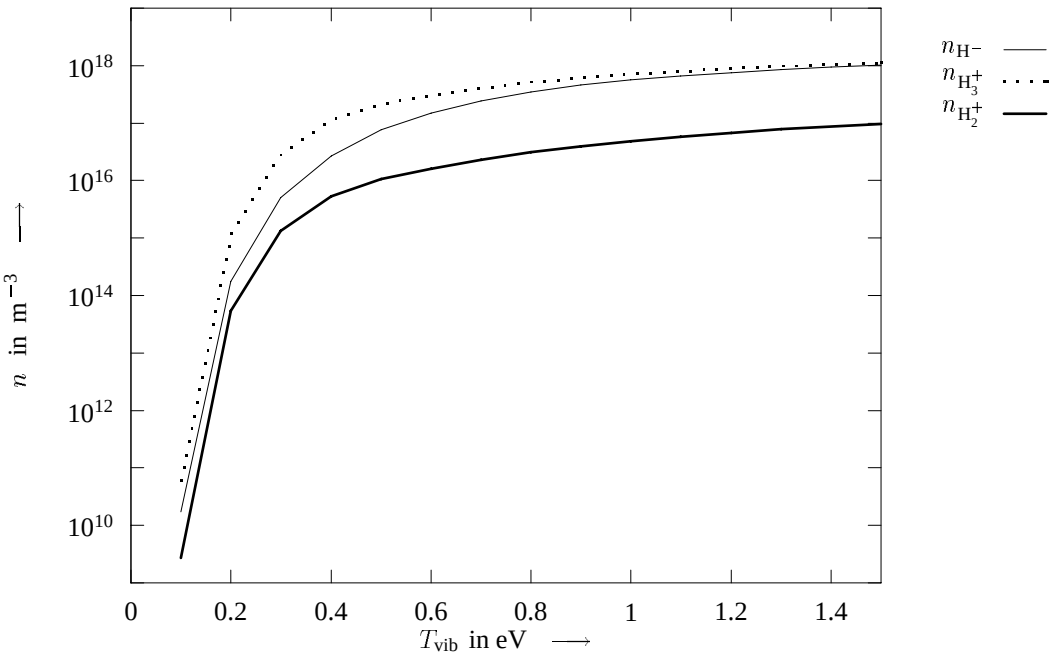

Figure 4.7: Calculated molecular ion densities for hydrogen as a function of the vibrational temperature. Conditions: $T_{\text{e}} = 0.26$ *eV,* $n_{H_2} = 7 \cdot 10^{20}\ m^{-3}$, $n_{\text{e}} = 3 \cdot 10^{17}\ m^{-3}$ *and* $n_1 = 10^{20} m^{-3}$.

reaction:	Number of reactions to the right: $\text{s}^{-1}\text{m}^{-3}$	Number of reactions to the left: $\text{s}^{-1}\text{m}^{-3}$
$H_2^{v\geq 4} + H^+ \rightleftarrows H_2^+ + H$	$7.529 \cdot 10^{20}$	$6.669 \cdot 10^{19}$
$H_2^{v\geq 4} + e^- \rightleftarrows H + H^-$	$9.205 \cdot 10^{21}$	$8.229 \cdot 10^{21}$
$H_2^+ + H_2 \rightleftarrows H_3^+ + H$	$1.066 \cdot 10^{21}$	$4.320 \cdot 10^{20}$
$H_2^+ + e^- \rightleftarrows H^* + H$	$5.221 \cdot 10^{19}$	$2.534 \cdot 10^{14}$
$H_3^+ + e^- \rightleftarrows H_2^{v>4} + H(2)$	$4.498 \cdot 10^{20}$	$1.264 \cdot 10^{16}$
$H_3^+ + e^- \rightleftarrows 3H$	$1.799 \cdot 10^{20}$	$2.780 \cdot 10^{2}$
$H^+ + H^- \rightleftarrows H + H(n=2)$	$1.734 \cdot 10^{20}$	$5.839 \cdot 10^{13}$
$H^- + e^- \rightleftarrows H + 2e^-$	$1.503 \cdot 10^{17}$	$1.006 \cdot 10^{13}$
$H^+ + H^- \rightleftarrows H + H(n=3)$	$5.671 \cdot 10^{20}$	$3.469 \cdot 10^{17}$
$H^- + H \rightleftarrows 2H + e^-$	$2.304 \cdot 10^{20}$	$1.543 \cdot 10^{16}$
$H^- + H_3^+ \rightleftarrows 2H_2$	$4.332 \cdot 10^{18}$	$2.477 \cdot 10^{4}$

Table 4.3: The number of reactions per s and per m^3 *for the molecular reactions.* $T_e = 0.26$ *eV,* $n_e = 3 \cdot 10^{17} m^{-3}$, $n_{H_2} = 7 \cdot 10^{20} m^{-3}$, $n_1 = 10^{20} m^{-3}$, $T_h = 0.26$ *eV,* $T_{vib} = 0.30$ *eV.*

For $\hat{T}_{\text{h}} = 0.3$ eV, this gives: $n^{\text{S}}_{\text{H}_2}/n^{\text{S}}_{\text{H}} = 8.6 \cdot 10^{-27} n^{\text{S}}_{\text{H}}$. For $n_{\text{H}_2} = 7 \cdot 10^{20}\ \text{m}^{-3}$, this means that $n^{\text{S}}_{\text{H}} = 2.9 \cdot 10^{23}\ \text{m}^{-3}$.

p	E	n_p/g_p	b_p
1	0.000	$5.000 \cdot 10^{19}$	$9.4747 \cdot 10^{-12}$
2	10.196	$2.465 \cdot 10^{11}$	$5.0162 \cdot 10^{-3}$
3	12.084	$3.144 \cdot 10^{11}$	9.1141
4	12.745	$6.455 \cdot 10^{8}$	0.2378
5	13.051	$3.184 \cdot 10^{8}$	0.3806
6	13.217	$2.670 \cdot 10^{8}$	0.6043
7	13.318	$2.316 \cdot 10^{8}$	0.7732
8	13.383	$2.016 \cdot 10^{8}$	0.8641
9	13.427	$1.795 \cdot 10^{8}$	0.9111
10	13.459	$1.638 \cdot 10^{8}$	0.9402
11	13.483	$1.529 \cdot 10^{8}$	0.9625
12	13.501	$1.416 \cdot 10^{8}$	0.9557
ion	13.595	$2.748 \cdot 10^{17}$	

Table 4.4: The densities of the excited levels and the deviations from equilibrium for atomic hydrogen. $T_e = 0.26$ *eV,* $T_{vib} = 0.30$ *eV,* $n_e = 3 \cdot 10^{17} m^{-3}$, $n_{H_2} = 7 \cdot 10^{20} m^{-3}$.

p	E	n_p/g_p	b_p
1	0.000	$5.000 \cdot 10^{19}$	$7.9570 \cdot 10^{-13}$
2	10.196	$1.628 \cdot 10^{12}$	$2.7834 \cdot 10^{-3}$
3	12.084	$3.079 \cdot 10^{12}$	7.4963
4	12.745	$1.858 \cdot 10^{10}$	0.5751
5	13.051	$7.190 \cdot 10^{09}$	0.7217
6	13.217	$4.466 \cdot 10^{09}$	0.8489
7	13.318	$3.281 \cdot 10^{09}$	0.9197
8	13.383	$2.649 \cdot 10^{09}$	0.9534
9	13.427	$2.275 \cdot 10^{09}$	0.9700
10	13.459	$2.032 \cdot 10^{09}$	0.9800
11	13.483	$1.867 \cdot 10^{09}$	0.9875
12	13.501	$1.739 \cdot 10^{09}$	0.9853
ion	13.595	$9.817 \cdot 10^{17}$	

Table 4.5: The densities of the excited levels and the deviations from equilibrium for atomic hydrogen. $T_e = 0.26$ *eV,* $T_{vib} = 0.30$ *eV,* $n_e = 10^{18} m^{-3}$, $n_{H_2} = 7 \cdot 10^{20} m^{-3}$.

p	E	n_p/g_p	b_p
1	0.000	$5.000 \cdot 10^{19}$	$7.7986 \cdot 10^{-15}$
2	10.196	$4.374 \cdot 10^{13}$	$7.3273 \cdot 10^{-4}$
3	12.084	$9.074 \cdot 10^{13}$	2.1653
4	12.745	$3.073 \cdot 10^{12}$	0.9318
5	13.051	$9.839 \cdot 10^{11}$	0.9681
6	13.217	$5.283 \cdot 10^{11}$	0.9843
7	13.318	$3.610 \cdot 10^{11}$	0.9919
8	13.383	$2.822 \cdot 10^{11}$	0.9954
9	13.427	$2.386 \cdot 10^{11}$	0.9971
10	13.459	$2.112 \cdot 10^{11}$	0.9981
11	13.483	$1.927 \cdot 10^{11}$	0.9988
12	13.501	$1.798 \cdot 10^{11}$	0.9986
ion	13.595	$1.002 \cdot 10^{19}$	

Table 4.6: The densities of the excited levels and the deviations from equilibrium for atomic hydrogen. $T_e = 0.26$ *eV,* $T_{vib} = 0.30$ *eV,* $n_e = 10^{19} m^{-3}$, $n_{H_2} = 7 \cdot 10^{20} m^{-3}$.

p	E	n_p/g_p	b_p
1	0.000	$5.000 \cdot 10^{19}$	$7.8088 \cdot 10^{-17}$
2	10.196	$9.537 \cdot 10^{14}$	$1.5997 \cdot 10^{-4}$
3	12.084	$1.086 \cdot 10^{15}$	0.2594
4	12.745	$1.924 \cdot 10^{14}$	0.5843
5	13.051	$8.216 \cdot 10^{13}$	0.8095
6	13.217	$4.866 \cdot 10^{13}$	0.9079
7	13.318	$3.460 \cdot 10^{13}$	0.9519
8	13.383	$2.751 \cdot 10^{13}$	0.9718
9	13.427	$2.346 \cdot 10^{13}$	0.9817
10	13.459	$2.087 \cdot 10^{13}$	0.9877
11	13.483	$1.912 \cdot 10^{13}$	0.9923
12	13.501	$1.782 \cdot 10^{13}$	0.9909
ion	13.595	$1.000 \cdot 10^{20}$	

Table 4.7: The densities of the excited levels and the deviations from equilibrium for atomic hydrogen. $T_e = 0.26$ *eV,* $T_{vib} = 0.30$ *eV,* $n_e = 10^{20} m^{-3}$, $n_{H_2} = 7 \cdot 10^{20} m^{-3}$.

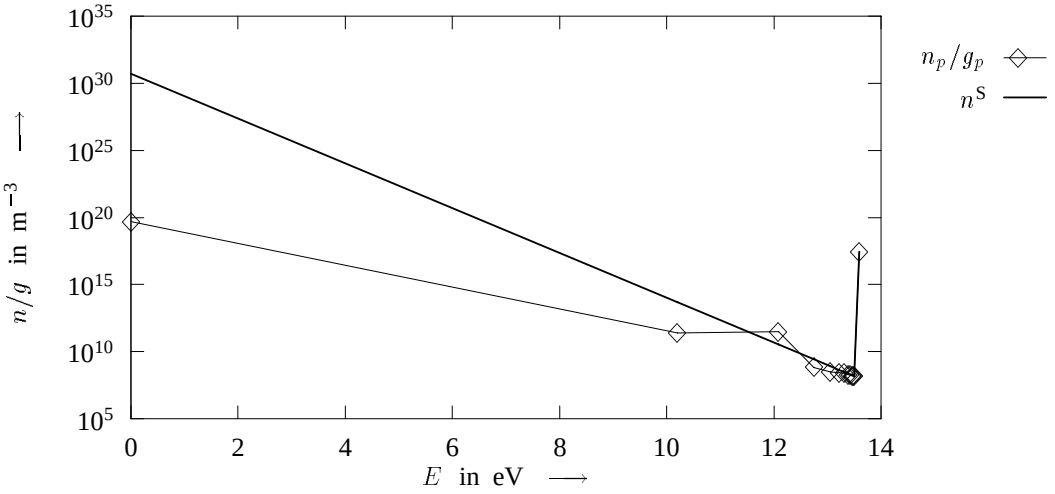

Figure 4.8: Calculated level densities (◇) for hydrogen. $T_{\mathrm{e}} = T_{\mathrm{h}} = 0.26$ *eV,* $T_{\mathrm{vib}} = 0.30$ *eV,* $n_{\mathrm{e}} = 3 \cdot 10^{17}$, $n_{\mathrm{H_2}} = 7 \cdot 10^{20}$ *The Saha density in equilibrium with the ion level is also shown. We see that the hydrogen level with* $n = 3$ *is overpopulated with respect to Saha with a factor* $\delta b = 8.1$.

Chapter 5

Extension with a flow model

To make our description of the plasma more complete, flow characteristics of the plasma are added in a more fundamental way to the completely local collision-radiative model. Here, we assume that only the flow terms for hydrogen atoms, ions and molecules, and for electrons are important because they are the main part of the plasma. The molecular ions are treated completely local, and the collision radiative model is used to calculate source terms.

We use a so called quasi-one dimensional model: we calculate the several densities only as a function of one parameter, the axial coordinate z. This approach is only valid if the axial gradients are much larger than the radial gradients. In this model, gradients are approximated with derivates to only one coordinate:

$$\vec{\nabla}\varphi = \frac{1}{A}\frac{d(A\varphi)}{dz} \; . \tag{5.1}$$

A corresponds to the surface over which the plasma parameters are averaged in the quasi one-dimensional model. This term takes into account volume effects. The expansion of the plasma is described with an expansion angle α. The surface A is given by:

$$A = \pi r^2 = \pi(r_0 + z\tan\alpha)^2 \tag{5.2}$$

so

$$\frac{1}{A}\frac{dA}{dz} = \frac{2\tan\alpha}{r_0 + z\tan\alpha} \tag{5.3}$$

where r_0 is the start radius of the plasma and α the expansion angle. The radius of the plasma is determined with the diffusion coefficient. We start with the start radius r_0. Then, we calculate the ambipolar diffusion coefficient D_{amb} with:

$$D_{\text{i}} = \frac{ekT\tau}{m_{\text{i}}e} = \frac{e\tau\hat{T}}{m_{\text{i}}} \tag{5.4}$$

and

$$D_{\text{amb}} = D_{\text{i}}\left(1 + \frac{T_{\text{e}}}{T_{\text{i}}}\right) = \frac{e\tau_{\text{i0}}}{m_{\text{i}}}(\hat{T}_{\text{e}} + \hat{T}_{\text{i}}) \; . \tag{5.5}$$

with τ_{i0} the momentum relaxation time between neutrals and ions. Then, $\tan\alpha$ is given by [6]:

$$\tan\alpha = \frac{2D}{ur} \tag{5.6}$$

and the plasma radius can be calculated with

$$r_{n+1} = r_n + d\tan\alpha \tag{5.7}$$

where d is the step size.

The general continuum equation 3.1 is given by:

$$\frac{\partial n_p}{\partial t} + \nabla\cdot(n_p\vec{u}) = \left(\frac{\partial n_p}{\partial t}\right)_{\text{CR}} \; . \tag{5.8}$$

with $\vec{u}$ the drift velocity of the plasma. This equation can, for each species, be written in the following form:

$$\frac{1}{A}\frac{d}{dz}(n_{\mathrm{H}^+}uA) = S_{\mathrm{H}^+} \ , \tag{5.9}$$

$$\frac{1}{A}\frac{d}{dz}(n_{\mathrm{H}}uA) = S_{\mathrm{H}} \ , \tag{5.10}$$

$$\frac{1}{A}\frac{d}{dz}(n_{\mathrm{H_2}}uA) = S_{\mathrm{H_2}} \ , \tag{5.11}$$

$$\frac{1}{A}\frac{d}{dz}(n_{\mathrm{e}}uA) = S_{\mathrm{e}} \ . \tag{5.12}$$

The momentum conservation equation can be written in the following form, with the density $\rho = m_{\mathrm{H}}(n_{\mathrm{H}} + n_{\mathrm{H}^+} + 2n_{\mathrm{H_2}} + 2n_{\mathrm{H_2^+}} + 3n_{\mathrm{H_3^+}} + n_{\mathrm{H}^-})$ and the pressure $p = (n_{\mathrm{H}} + n_{\mathrm{H}^+} + n_{\mathrm{H_2}} + n_{\mathrm{H_2^+}} + n_{\mathrm{H_3^+}} + n_{\mathrm{H}^-})kT_{\mathrm{h}} + n_{\mathrm{e}}kT_{\mathrm{e}}$:

$$\rho\left(\frac{\partial\vec{u}}{\partial t} + (\vec{u}\cdot\vec{\nabla})\vec{u}\right) = -\vec{\nabla}p \ . \tag{5.13}$$

Because the quasi one-dimensional model is stationary, the time derivative vanishes and this equation becomes:

$$\rho u\frac{du}{dz} = -\frac{dp}{dz} \ . \tag{5.14}$$

The general form of the energy conservation equation for one species is:

$$\frac{3}{2}\left(\frac{\partial p}{\partial t} + (\vec{u}\cdot\vec{\nabla})p\right) + \tfrac{5}{2}p\vec{\nabla}\cdot\vec{u} + \vec{\nabla}\cdot\vec{q} = Q \ . \tag{5.15}$$

We neglect the heat conductance $\vec{\nabla}\cdot\vec{q}$ so, in the one-dimensional model, the energy conservation equations for the heavy particles and the electrons read:

$$\frac{1}{A}\frac{d}{dz}((\tfrac{3}{2}n_{\mathrm{H}^+} + \tfrac{3}{2}n_{\mathrm{H}} + \tfrac{5}{2}n_{\mathrm{H_2}})kT_{\mathrm{h}}uA) + \frac{p_{\mathrm{h}}}{A}\frac{d(uA)}{dz} = Q_{\mathrm{h}} \ , \tag{5.16}$$

$$\frac{1}{A}\frac{d}{dz}(\tfrac{3}{2}n_{\mathrm{e}}kT_{\mathrm{e}}uA) + \frac{p_{\mathrm{e}}}{A}\frac{d(uA)}{dz} = Q_{\mathrm{e}} \ . \tag{5.17}$$

The source terms can be split into a molecular part and an atomic collision - radiative part. The atomic mass terms are given by:

$$\left[\frac{dn_{\mathrm{H_2}}}{dt}\right]_{\text{atomic}} = 0 \tag{5.18}$$

$$\left[\frac{dn_{\mathrm{i}}}{dt}\right]_{\text{atomic}} = n_{\mathrm{e}}\sum_q K_{q+}n_q - {n_{\mathrm{e}}}^2 n_{\mathrm{i}}\sum_q K_{+q} - n_{\mathrm{e}}\,n_{\mathrm{i}}\,\alpha_{\text{rad}} \tag{5.19}$$

$$\left[\frac{dn_{\mathrm{H}}}{dt}\right]_{\text{atomic}} = -\left[\frac{dn_{\mathrm{i}}}{dt}\right]_{\text{atomic}} \tag{5.20}$$

$$\left[\frac{dn_{\mathrm{e}}}{dt}\right]_{\text{atomic}} = \left[\frac{dn_{\mathrm{i}}}{dt}\right]_{\text{atomic}} \tag{5.21}$$

For hydrogen atoms, only ionization loss is taken into account. The molecular terms can be deduced from table 3.1:

$$\left[\frac{dn_{\mathrm{H_2}}}{dt}\right]_{\text{mol}} = n_{\mathrm{H}^-}n_{\mathrm{H_3^+}}K_{11} - n_{H_2}^2K'_{11} \tag{5.22}$$

$$\left[\frac{dn_{\mathrm{H}}}{dt}\right]_{\mathrm{mol}} = n_{\mathrm{H}_2^v}(n_{\mathrm{i}}K_1 + n_{\mathrm{e}}K_2) + n_{\mathrm{H}_2^+}(n_{\mathrm{H}_2}K_3 + n_{\mathrm{e}}K_4) + 3n_{\mathrm{H}_3^+}n_{\mathrm{e}}K_6 + n_{\mathrm{H}^-}(n_{\mathrm{i}}(K_7 + K_9) + n_{\mathrm{e}}K_8 + 2n_1K_{10}) - n_1[n_{\mathrm{H}_2^+}K_1' + n_{\mathrm{H}^-}K_2' + n_{\mathrm{H}_3^+}K_3' + n_2(K_4' + K_7') + n_1^2K_6' + {n_{\mathrm{e}}}^2K_8' + n_3K_9' + n_1n_{\mathrm{e}}K_{10}'] \quad (5.23)$$

$$\left[\frac{dn_{\mathrm{i}}}{dt}\right]_{\mathrm{mol}} = n_1(n_{\mathrm{H}_2^+}K_1' + n_2K_7' + n_3K_9') - n_{\mathrm{i}}(n_{\mathrm{H}_2^+}K_1 + n_{\mathrm{H}^-}(K_7 + K_9)) \quad (5.24)$$

$$\left[\frac{dn_{\mathrm{e}}}{dt}\right]_{\mathrm{mol}} = n_{\mathrm{H}^-}n_1K_2' + n_1n_2K_4' + n_2n_{\mathrm{H}_2^{v>4}}K_5' + n_1^3K_6' - n_{\mathrm{e}}(n_{\mathrm{H}_2^{v>4}}K_2 + n_{\mathrm{H}_2^+}K_4 + n_{\mathrm{H}_3^+}(K_5 + K_6) + n_1^2K_{10}') + n_{\mathrm{H}^-}n_{\mathrm{e}}K_8 - n_1{n_{\mathrm{e}}}^2K_8' \quad (5.25)$$

The total source term can be found by adding the atomic and molecular terms:

$$S = \left[\frac{dn}{dt}\right]_{\mathrm{atomic}} + \left[\frac{dn}{dt}\right]_{\mathrm{mol}} . \quad (5.26)$$

The energy source terms are taken from [13]. For the heavy particles, the energy source term is given by:

$$Q_{\mathrm{h}} = n_{\mathrm{e}} \sum_{\alpha=\mathrm{i,at,mol}} \left(\frac{2m_{\mathrm{e}}}{m_\alpha}\right) \tfrac{3}{2}k(T_{\mathrm{e}} - T_{\mathrm{h}})\langle\nu_{\mathrm{e}\alpha}\rangle . \quad (5.27)$$

Here $\langle\nu_{\mathrm{ei}}\rangle$ and $\langle\nu_{\mathrm{ea}}\rangle$ are the average collision frequencies for momentum transfer between electron-ion and electron-neutral collisions respectively. One should interpret this expression with care; especially when T_{e} and T_{h} differ not much. This does not imply that Q_{h} is small. It rather means that the coupling between T_{h} and T_{e} is good and therefore $\langle\nu_{ei}\rangle$ could be large.

$\langle\nu_{\mathrm{ei}}\rangle$ is given by:

$$\langle\nu_{\mathrm{ei}}\rangle = \frac{4\sqrt{2\pi}}{3}\left(\frac{e^2}{4\pi\epsilon_0 m_{\mathrm{e}}}\right)\left(\frac{m_{\mathrm{e}}}{kT_{\mathrm{e}}}\right)^{3/2} n_{\mathrm{i}}\ln(\Lambda) . \quad (5.28)$$

The interaction terms with neutral particles are neglectable compared with the one with electrons when the ionization degree $\alpha > 1\%$. For very small energies and ionization degrees, we find as an approximation [1]:

$$\nu_{\mathrm{ea}} = n_{\mathrm{a}}\sigma_{\mathrm{ea}}v_{\mathrm{e}} = 10^{-18}n_{\mathrm{a}}v_{\mathrm{e}}^{-3/5} . \quad (5.29)$$

Because equation 5.29 is not very accurate [1], one should check whether the results, obtained by using it, are acceptable.

The code to calculate the source terms is shown in appendix C. The mass source terms are a sum of differences in the number of reactions going to the left and the number of reactions going to the right. Here, `pop[plus]` = n_{i}, `pop[plus+1]` = $n_{\mathrm{H}_2^+}$, `pop[plus+2]` = $n_{\mathrm{H}_3^+}$ and `pop[plus+3]` = n_{H^-}. `deelv` is the part of H_2 molecules with a vibrational quantum number larger than 4.

This results in the following matrix equation:

$$
\begin{pmatrix}
S_{\mathrm{H^+}} - n_{\mathrm{H^+}}\, u \frac{1}{A}\frac{dA}{dz} \\
S_{\mathrm{H}} - n_{\mathrm{H}} u \frac{1}{A}\frac{dA}{dz} \\
S_{\mathrm{H_2}} - n_{\mathrm{H_2}} u \frac{1}{A}\frac{dA}{dz} \\
S_{\mathrm{e}} - n_{\mathrm{e}}\, u \frac{1}{A}\frac{dA}{dz} \\
0 \\
Q_{\mathrm{h}} - \left[\frac{\gamma_{\mathrm{H}}}{\gamma_{\mathrm{H}}-1}(n_{\mathrm{H}} + n_{\mathrm{H^+}}) + \frac{\gamma_{\mathrm{H_2}}}{\gamma_{\mathrm{H_2}}-1} n_{\mathrm{H_2}}\right] k\, T_{\mathrm{h}}\, u \frac{1}{A}\frac{dA}{dz} \\
Q_{\mathrm{e}} - \frac{\gamma_{\mathrm{H}}}{\gamma_{\mathrm{H}}-1}\, n_{\mathrm{e}}\, k\, T_{\mathrm{e}}\, u \frac{1}{A}\frac{dA}{dz}
\end{pmatrix} =
$$

$$
\begin{pmatrix}
u & 0 & 0 & 0 & n_{\mathrm{H^+}} & \cdots \\
0 & u & 0 & 0 & n_{\mathrm{H}} & \cdots \\
0 & 0 & u & 0 & n_{\mathrm{H_2}} & \cdots \\
0 & 0 & 0 & u & n_{\mathrm{e}} & \cdots \\
k\, T_{\mathrm{h}} & k\, T_{\mathrm{h}} & k\, T_{\mathrm{h}} & k\, T_{\mathrm{e}} & (2n_{\mathrm{H_2}} + n_{\mathrm{H}} + n_{\mathrm{H^+}}) m_{\mathrm{H}} u k & \cdots \\
\frac{u k\, T_{\mathrm{h}}}{\gamma_{\mathrm{H}}-1} & \frac{u k\, T_{\mathrm{h}}}{\gamma_{\mathrm{H}}-1} & \frac{u k\, T_{\mathrm{h}}}{\gamma_{\mathrm{H_2}}-1} & 0 & \left[\frac{\gamma_{\mathrm{H}}}{\gamma_{\mathrm{H}}-1}(n_{\mathrm{H}} + n_{\mathrm{H^+}}) + \frac{\gamma_{\mathrm{H_2}}}{\gamma_{\mathrm{H_2}}-1} n_{\mathrm{H_2}}\right] u k & \cdots \\
0 & 0 & 0 & \frac{u k\, T_{\mathrm{e}}}{\gamma_{\mathrm{H}}-1} & \frac{\gamma_{\mathrm{H}}}{\gamma_{\mathrm{H}}-1} k\, n_{\mathrm{e}} & \cdots
\end{pmatrix}
$$

$$
\begin{pmatrix}
\cdots & 0 & 0 \\
\cdots & 0 & 0 \\
\cdots & 0 & 0 \\
\cdots & 0 & 0 \\
\cdots & (n_{\mathrm{H}} + n_{\mathrm{H^+}} + n_{\mathrm{H_2}}) k & n_{\mathrm{e}}\, k \\
\cdots & \left[\frac{1}{\gamma_{\mathrm{H}}-1}(n_{\mathrm{H}} + n_{\mathrm{H^+}}) + \frac{1}{\gamma_{\mathrm{H_2}}-1} n_{\mathrm{H_2}}\right] u k & 0 \\
\cdots & 0 & \frac{1}{\gamma_{\mathrm{H}}-1}\, n_{\mathrm{e}}\, u k
\end{pmatrix}
\cdot
\begin{pmatrix}
dn_{\mathrm{H^+}}/dz \\
dn_{\mathrm{H}}/dz \\
dn_{\mathrm{H_2}}/dz \\
dn_{\mathrm{e}}/dz \\
du/dz \\
dT_{\mathrm{h}}/dz \\
dT_{\mathrm{e}}/dz
\end{pmatrix}
. \qquad (5.30)
$$

Here, $\gamma_{\mathrm{H}} = \frac{5}{3}$ and $\gamma_{\mathrm{H_2}} = \frac{7}{5}$ are the ratios C_p/C_v of atomic respectively molecular hydrogen.

By inverting the matrix numerically, relations for the derivates at the right-hand side of equation 5.30 appear. The properties we want to know are then achieved by Runge-Kutta integration.

Chapter 6

The experimental setup

The experimental setup is given. The main parts of the setup are discussed in more detail.

6.1 General overview

The plasma is created in a *cascaded arc* [6,8], which is shown in figure 6.1. A cascaded arc exists of a varying number of water cooled copper plates, isolated with boron nitride disks. In the middle is a small channel through which gas flows. Gas is fed in at the cathode side. In figure 6.1, the plasma flow in the arc is from left to right. There are 3 cathodes, which are screwed slanted in the arc. The large plate at the right is the anode plate. Between the cathode and the anode, a current is generated which ionizes the flowing gas and creates a plasma. Through a nozzle hole in the anode plate, the plasma can flow out. After it leaves the arc, the plasma expands supersonically into a low pressure vessel.

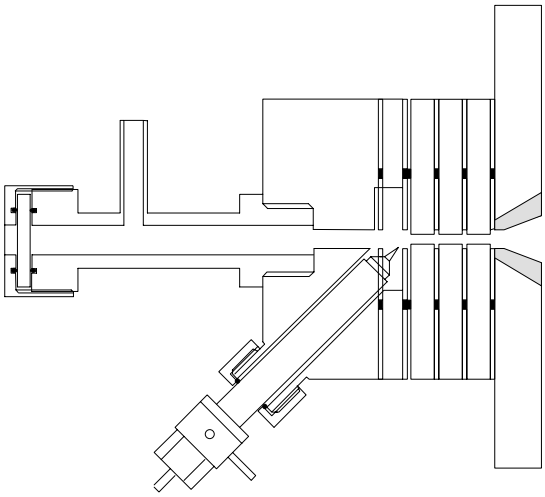

Figure 6.1: A schematical drawing of the cascaded arc with 4 plates.

The plasma emits light, which is detected with a spectroscopic setup through a quartz window in the vessel. The general overview of the spectroscopic measurement setup is shown in figure 6.2. The light which escapes from the plasma is focussed through a quartz lens on the entrance of a glass fiber with an acceptance cone angle $2a = 25°$. The fiber guides the light to a monochromator, who sends the output to a photomultiplier. From there, the signal of the photomultiplier is converted to TTL pulses and stored in a computer for further processing.

Magnetic field coils are located around the cascaded arc. The current through these coils was 250 A in the measurements which were performed. The magnetical field which was applied to the plasma is calculated numerically. It contains mainly an axial field component B_z. At 5 cm from the axis, the radial field strength B_r reaches nowhere higher values than 10% of B_z. The strength of this field on the axis is shown in figure 6.3.

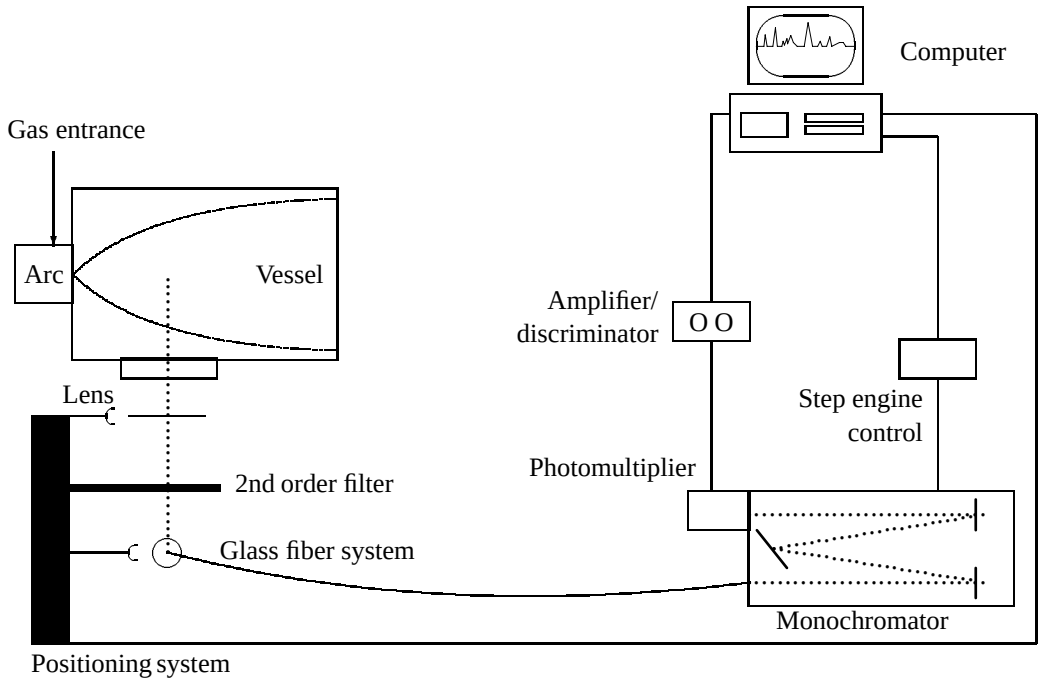

Figure 6.2: The experimental setup for spectral measurements with photon counting. The whole experiment is computerized.

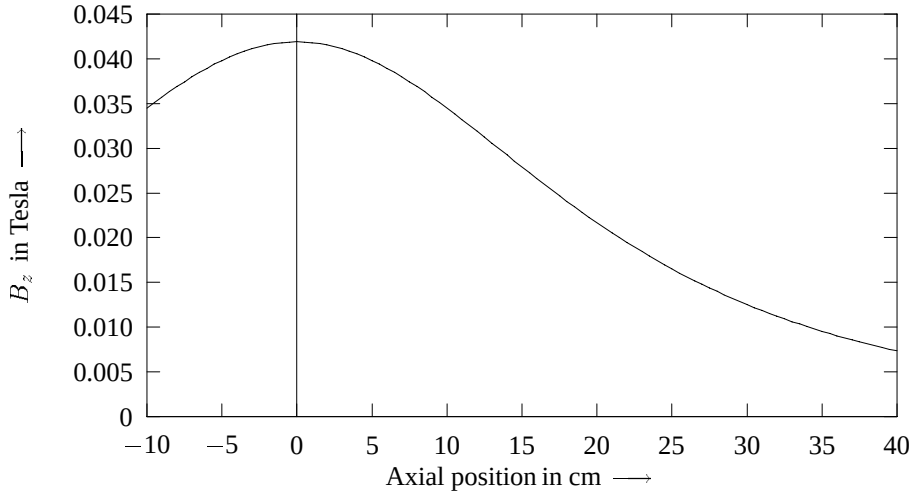

Figure 6.3: The magnetical field on the axis with $I_c = 250A$. The exit of the arc is located at $z = 0$.

The position at the plasma which is viewed can be selected with a zy-positioning system. This system contains of 2 translation rails which are controlled by pressured air and 2 linear displacement detectors which are variable resistors. This system is controlled by a computer with a PCL-718 laboratory card. The electrical schemes and the control programs for the positioning system are given in appendix D.

6.2 Calibration

The system was calibrated with an OSRAM tungsten ribbon lamp. A second order filter with a cutoff of 3500Å was used to avoid second order reflections in the monochromator. The measured signal is shown in figure 6.4. The temperature of the lamp was 2173 K by a current of 13.134 A.

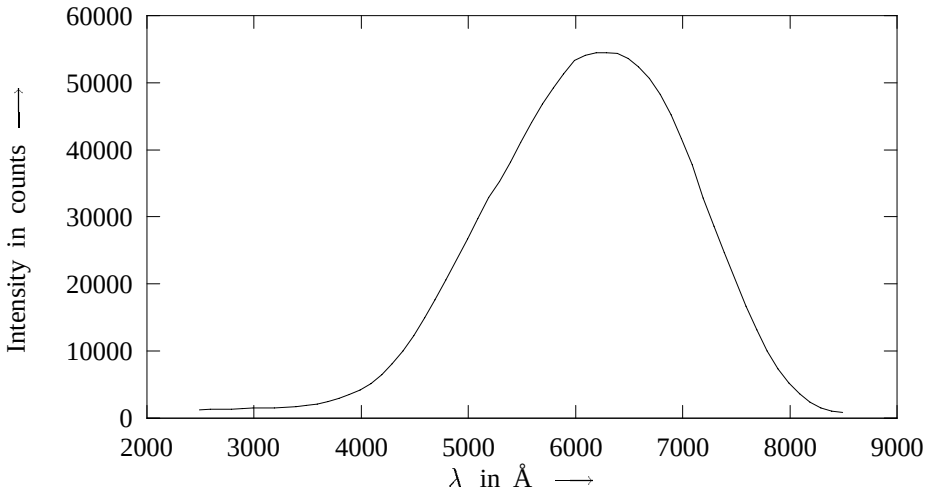

Figure 6.4: The measured signal from a tungsten ribbon lamp. The second order filter was inserted above $\lambda = 3500\ \mathring{A}$.

The transmission of the whole system as a function of the wavelength was calculated by comparing the measured signal of the Tungsten Ribbon lamp with the theoretical emission of the lamp. The transmission is shown in figure 6.5. While calibrating, we measure a photon count rate $I_{\text{exp}}^{\text{tung}}$. This count rate is connected to the system parameters by:

$$I_{\text{exp}}^{\text{tung}} = I_{\text{theor}}^{\text{tung}}(\lambda) \cdot \Delta\lambda \cdot \Delta\Omega \cdot \mathbf{A} \cdot \eta_{\text{eff}} \tag{6.1}$$

where $I_{\text{theor}}^{\text{tung}}(\lambda)$ is the theoretical emission of the tungsten lamp, **A** the surface of the detection area and η_{eff} the efficiency of the setup. $\Delta\lambda$ is the width of the apparatus profile at half height, 5Å in our case (because $\Delta\lambda$ is so small, no integration is needed), $\Delta\Omega$ is the solid angle and η_{eff} is the efficiency of the whole setup and **A** is the imaged surface of the tungsten.

A last correction should be made when determining absolute densities from the measured signal: because the quartz of the tungsten ribbon lamp gives rise to internal reflections, less signal is received from the lamp than follows from the temperature calculated with the measured current through the lamp. This results is an underestimation of the system sensitivity, which results in an overestimation for the level densities. Therefore, the measured densities should be multiplied with a factor < 1, the *De Vos factor* [19]. For the lamp used, this factor was 0.92.

An other source of errors is straylight in the monochromator. This straylight tracts attention in the very large transmission for short wavelengths. However, this is not a real transmission. The peak is caused by stray light on the monochromator grating. This straylight intensity becomes relatively more important for wavelengths where the tungsten lamp emits very little light. For more detailed information, see [14], page 92. To determine the amount of stray light, measurements with 2 filters were performed. One filter cuts at 3150Å, the other at 4350Å. The signal which is measured here is a combination of straylight and signal from the lamp. However, the band lamp emits so little light here that the contribution of the lamp is neglected. Between $\lambda = 3500\ \mathring{A}$ and $\lambda = 4000\ \mathring{A}$, signal and stray light are of the same order of magnitude. To correct for this effect, 2 measurements on the tungsten band lamp were done:

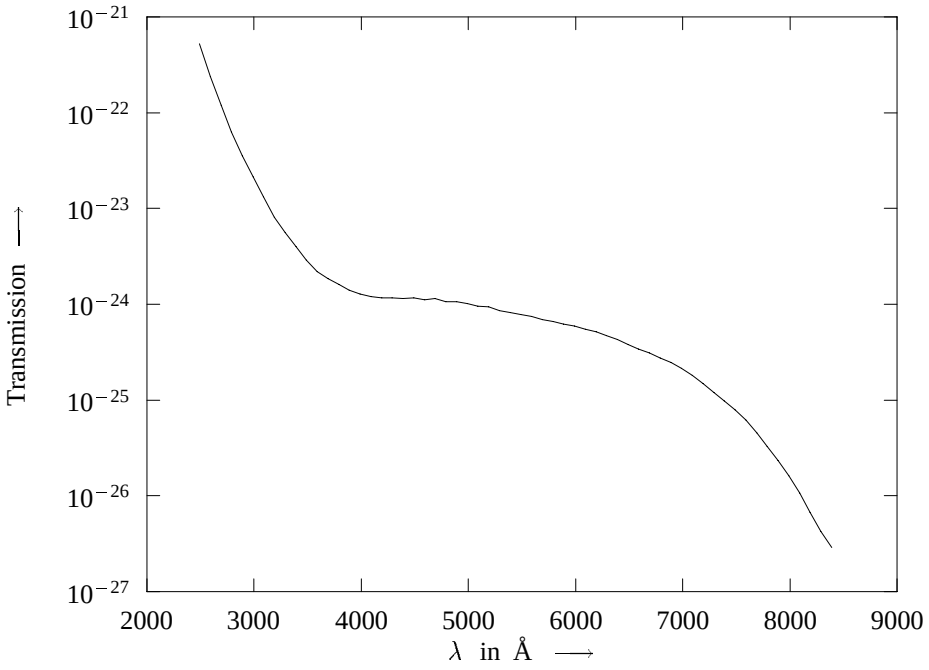

Figure 6.5: The transmission of the whole system, determined with a tungsten ribbon lamp before correction for straylight at low wavelengths.

1. A measurement with a filter that cuts at 3500 Å. Here, all signal plus straylight above 3500 Å is detected.
2. A measurement with a filter that cuts at 4350 Å. Here, all signal plus straylight above 4350 Å is detected.

The straylight intensity which occurs when using the filter which cuts at 4350Å is almost equal to the amount which occurs when using the filter which cuts at 3500Å because there is not much stray light with wavelengths between 3500 Å and 4350 Å. The difference between the detected signals in the two measurements is considered to be stray light. This assumption is valid if the amount of stray light is not very wavelength dependent. This turns out to be true: it is fairly constant at about 1620 counts/50sec (50 sec is the measurement time while calibrating), as can be seen in figure 6.6. Only for very low and high wavelengths this is not true any more because zeroth order light plays a role there, but no measurements are performed there. The straylight is substracted from the measured signal in the measurement with the filter which cuts at 3500 Å before a calibration datafile was made. The 3500 Å filter was used in all further measurements to avoid second order reflections in the monochromator.

Because zeroth order light is only important for very small wavelengths, where the system is not reliable anyway, no correction is performed for deviations caused by this effect.
This correction results in an other transmission of the system, which is shown in figure 6.8. For $\lambda < 3450\,\text{Å}$, the system is not reliable, but none of the hydrogen Balmer lines, which are measured in this study, are in this wavelengh region, so this is no problem.
The whole plasma emits light. When measurements at the plasma are performed, a part of this light is projected on the glass fiber and gives a signal. In the ideal situation, a small cylinder is projected on the fiber, but because we work only with one lens, in fact a double cone is represented on the fiber. This is shown in figure 6.9. We can approximate the measurement volume with a cylinder with radius the image of the glass fiber in the middle of the plasma: the volume is in reality a double cone, but because the light

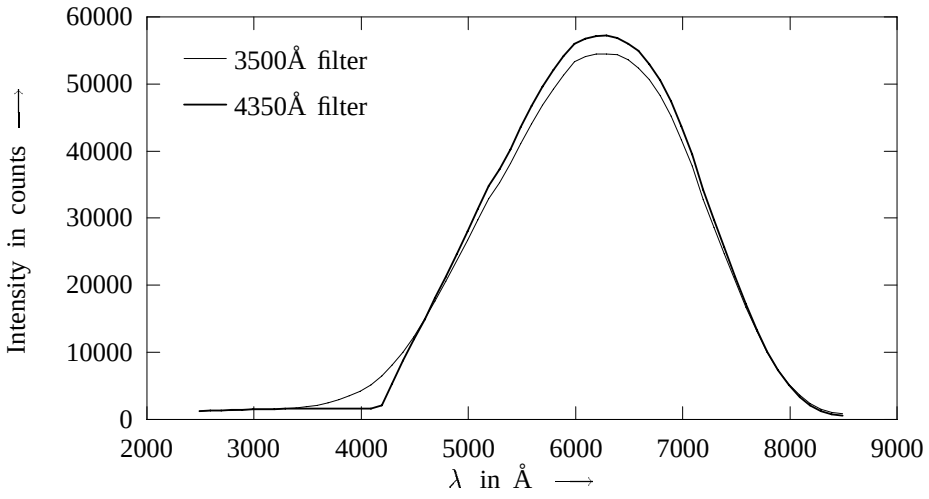

Figure 6.6: The measured signal with a filter which cuts at 3150 Å and the signal with a filter that cuts at 4350 Å.

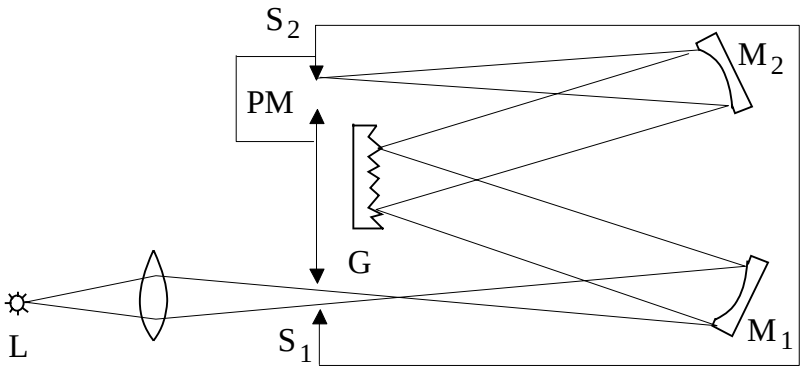

Figure 6.7: Scheme of a plane-grating monochromator. L is a source, S_1 and S_2 are the entrance and exit slits, M_1 and M_2 are the collimator and the camera mirror, G is a reflection grating and PM is a photomultiplier.

emission is smaller in the outer range of the cone, this compensates for the larger volume if the plasma properties don't change significant into this volume. Because the opening angle of the glass fiber is small, the volume is limited and this is not the case. Because the linear magnification of a lens is given by $-b/v$ were b is the distance from the lens to the image and v the distance from the lens to the object, the detection volume is given by:

$$V_{\mathrm{d}} = \frac{\pi \ell d^2}{4v^2}(a+D)^2 = 7.8 \cdot 10^{-7}\mathrm{m}^3 \,. \tag{6.2}$$

were a is the distance from the lens to the window and ℓ the distance from the window to the middle of the vessel. d Is the diameter of the glass fiber, which is 3mm in our case. D is approximately 3 cm. All light emitted in the detection volume falls within the acceptance angle of the glass fiber.
A list of all used equipment is given in table 6.1.

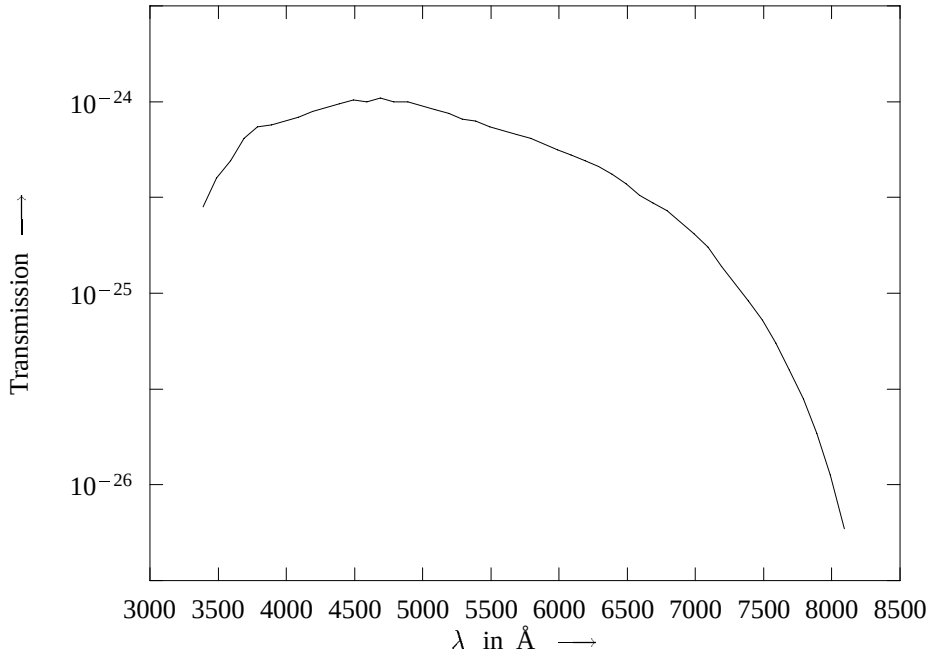

Figure 6.8: The transmission of the whole system, determined with a tungsten ribbon lamp, after the correction for zeroth order light.

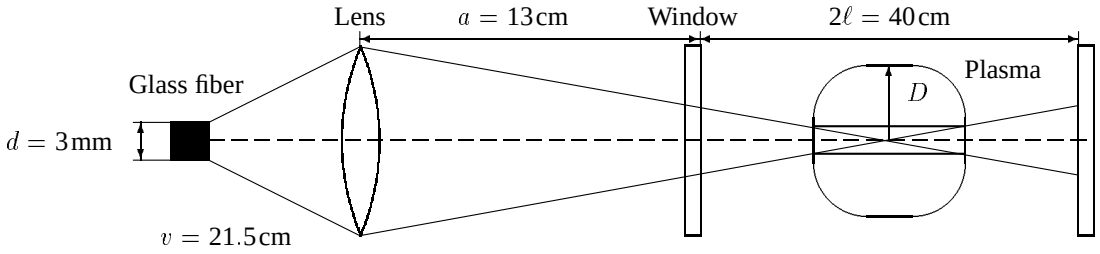

Figure 6.9: The representation of the plasma on the measurement system. The detection volume is shown with fat lines. The linear magnification is 1.53. The focal distance of the lens is 14 cm, it's diameter is 38.39 mm.

Instrument	Type
Monochromator	Jarell Ash 82-000
Photomultiplier	EMI 9698 QB
Amplifier/discriminator	EG & G PARC
3500Å filter	Schott WG335
4350Å filter	Schott GG435

Table 6.1: A list of the used equipment in the experimental setup.

Chapter 7

Experimental results

7.1 Measurements on a hydrogen-argon plasma

When we measure a spectral line in the $z-y$ plane, we measure always a line integral of the whole emission in the line of sight. To determine radial information of this measurements, the mathematical technique of *Abel inversion* was applied. This technique is explained in the following intermezzo.

Intermezzo: Abel-inversion

If one measures electromagnetical or particle emissions from a plasma, one always measures a signal which is produced by the whole line of sight, at least if the plasma is optically thin for that special radiation. This situation is drawn in figure 7.1. We measure the signal S:

$$S(y,\theta) = \int_{-a}^{a} \varepsilon(r,\theta)dx = \int_{-a}^{a} \varepsilon(r,\theta)\frac{r}{\sqrt{r^2-y^2}}dr \tag{7.1}$$

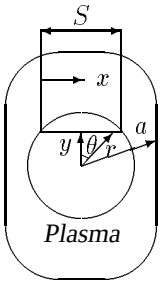

Figure 7.1: A measurement at a plasma on which Abel-inversion can be applied to achieve radial information.

As a measure of simplification, it will assumed here that $\varepsilon(r,\theta) = \varepsilon(r)$, which implies cylindrical symmetry. To calculate the radial emission $\varepsilon(r)$ from this signal, one should Abel invert the signal:

$$\varepsilon(r) = \frac{-1}{\pi}\int_{r}^{a} \frac{dS(y)}{dy}\sqrt{y^2-r^2}dy \tag{7.2}$$

$\frac{dS(y)}{dy}$ can be determined by measuring the signal on more positions in the plasma.

If equations 7.1 and 7.2 are to be solved numerically, which is the case when $S(y)$ is not known, the measured signal must be smoothed to filter out noise. This can be achieved by applying a Fourier transform on the measured signal. Then the highest frequencies, which contain most of the noise, are removed, and a smoothed profile is obtained by an inverse Fourier transform. This method is described in [15]. An other method if fitting of a function of which the Abel inverted function can be calculated analytically. For example, when the measured intensity profile $S(y)$ can be described by a Gausian:

$$S(y) = \int_{-\infty}^{\infty} \varepsilon(x,y)dx = a\exp\left(-\frac{y^2}{b^2}\right) , \tag{7.3}$$

with $a = \varepsilon(0)\, b\sqrt{\pi}$. The Abel inverted emission curve, $\varepsilon(x,y) = \varepsilon(r)$ is given by:

$$\varepsilon(r) = \frac{a}{b\sqrt{\pi}}\exp\left(-\frac{r^2}{b^2}\right) . \tag{7.4}$$

To determine the level densities from the Abel inverted intensity profiles, one has to know the relation between the level densities n and the signal strength S. We can determine this relation from the following balance: for the radiation which is emitted at the transition $p \rightarrow q$ we find [1]:

$$\begin{array}{lcl} \text{Number of spontaneous emissions /m}^3 & = & n_p A_{pq} \ , \\ \text{Number of stimulated emissions /m}^3 & = & n_p B_{pq} \rho_{\nu_{pq}} \ , \\ \text{Number of absorptions /m}^3 & = & n_q B_{qp} \rho_{\nu_{pq}} \ . \end{array} \tag{7.5}$$

here ρ_ν is the energy density of the wavelength belonging to the transition $p \rightarrow q$. The relation between the Einstein coefficients B and the transition probabilities A is given by:

$$B_{pq} = \frac{c^3 A_{pq}}{8\pi h \nu_{pq}^3} \tag{7.6}$$

and

$$\frac{B_{pq}}{B_{qp}} = \frac{g_q}{g_p} \ . \tag{7.7}$$

In the plasma under consideration, the absorption from lines from transitions $p \rightarrow q$ with $q \neq 1$ can be neglected. The level density can be determined from the Abel inverted, calibrated data, with a solid angle of 4π because the tungsten ribbon lamp is calibrated per sr:

$$n_p = C_V \frac{4\pi S_{p2}}{A_{p2}} \tag{7.8}$$

where S is the number of photons emitted by the plasma. When we assume that the whole line is covered by the openingslits of the monochromator, we measure a photon count rate of:

$$\begin{array}{rcl} I_{\text{line}}(y) & = & \dfrac{\int\limits_x (n_p(x,y) A_{qp} \mathbf{A} \cdot \Delta\Omega \cdot \eta_{\text{eff}}) dx}{4\pi C_V} \\ & = & \dfrac{\mathbf{A} \cdot \Delta\Omega \cdot \eta_{\text{eff}} \cdot A_{qp}}{4\pi C_V} \int\limits_x n_p(x,y) dx \\ & = & \dfrac{I_{\text{exp}}^{\text{tung}}}{I_{\text{theor}}^{\text{tung}}} \dfrac{A_{pq}}{\Delta\lambda \cdot 4\pi C_V} \int\limits_x n_p(x,y) dx \end{array} \tag{7.9}$$

$I_{\text{exp}}^{\text{tung}} / I_{\text{theor}}^{\text{tung}}$ is equal to the *transmission* $\mathbf{T}(\lambda)$. The *De Vos factor* C_V results from internal reflections in the tungsten lamp which was used for calibration and is 0.92 in this case. It is very weakly dependent on the wavelength. This dependence is neglected. So

$$\int\limits_x n_p(x,y) dx = \frac{I_{\text{line}} \cdot \Delta\lambda}{A_{qp} \mathbf{T}(\lambda)} \tag{7.10}$$

A two dimensional scan of the intensities of several hydrogen Balmer lines was made. Measurements for the lines from $\mathrm{H}(n = 3 \rightarrow n = 2)$ to $\mathrm{H}(n = 11 \rightarrow n = 2)$ and the lines $\mathrm{H}(n = 15 \rightarrow n = 2)$ and $\mathrm{H}(n = 17 \rightarrow n = 2)$ were performed. Because for transitions between $\mathrm{H}(n > 17 \rightarrow n = 2)$ the distance between the lines becomes smaller than 5Å, these lines can not be separated with this setup.

At the beginning of each measurement, the intensity of the H_α line was measured as a gauge: each measured intensity is multiplied with a constant which makes the intensity of the H_α line the same for each measurement. The gauge factors are shown in table 7.1.

To take the background radiation into account, a complete spectrum has been measured between $\lambda = 3640$ Å and $\lambda = 3900$ Å to determine the line/continuum ratio. This measurement is shown in figure 7.2. To correct

for the background radiation, the number of background counts for a certain wavelength is divided by the total number of counts for that wavelength. For the lines $\mathrm{H}(n = 10 \rightarrow n = 2)$, $\mathrm{H}(n = 11 \rightarrow n = 2)$ and $\mathrm{H}(n = 15 \rightarrow n = 2)$, also photons emitted by molecules at the same wavelength must be substracted, as can be seen in figure 7.2. The resulting back ground correction factors are given in table 7.1.

The background radiation is given by 2 contributions [1,14]:

1. The *free bound radiation*. This radiation originates from radiative recombination. This emission is given by:
$$\varepsilon_{fb} = \frac{C_1}{\lambda^2}\frac{z_\mathrm{i}\, n_\mathrm{i}\, n_\mathrm{e}}{\sqrt{k\, T_\mathrm{e}}}\left[1 - \exp\left(-\frac{hc}{\lambda k\, T_\mathrm{e}}\right)\right]\xi_{fb}(\lambda,\, T_\mathrm{e}) \tag{7.11}$$
were $C_1 = 1.63 \cdot 10^{-43}\mathrm{Wm^4K^{1/2}sr^{-1}}$ and ξ is the *Biberman factor*. z_i Is the charge number of the ion. In most cases, we can approximate $z_\mathrm{i}\, n_\mathrm{i}\, n_\mathrm{e}$ with ${n_\mathrm{e}}^2$.

2. The *free-free radiation*. This radiation originates from accelerations of charged particles in the electromagnetical field of other particles. The contribution of the electrons is the most important. This emission is given by:
$$\varepsilon_{ff}^{\mathrm{ei}} = \frac{C_1}{\lambda^2}\frac{z_\mathrm{i}\, n_\mathrm{i}\, n_\mathrm{e}}{\sqrt{k\, T_\mathrm{e}}}\exp\left(-\frac{hc}{\lambda k\, T_\mathrm{e}}\right)\xi_{ff}(\lambda,\, T_\mathrm{e}) \tag{7.12}$$
The Biberman factor for free-free emissivity ξ_{ff} is constant in a good approximation [20]. This emission gives significant contributions for energies which are smaller or in the order of the average thermal energy. For $T_\mathrm{e} = 0.3$ eV, this means that the free-free radiation is only significant for $\lambda > 4500\,\mathrm{\AA}$.

So, the total background emission is proportional to ${n_\mathrm{e}}^2$ and is given by:
$$\varepsilon = \frac{C_1}{\lambda^2}\frac{{n_\mathrm{e}}^2}{\sqrt{k\, T_\mathrm{e}}}\xi(\lambda,\, T_\mathrm{e})\ . \tag{7.13}$$

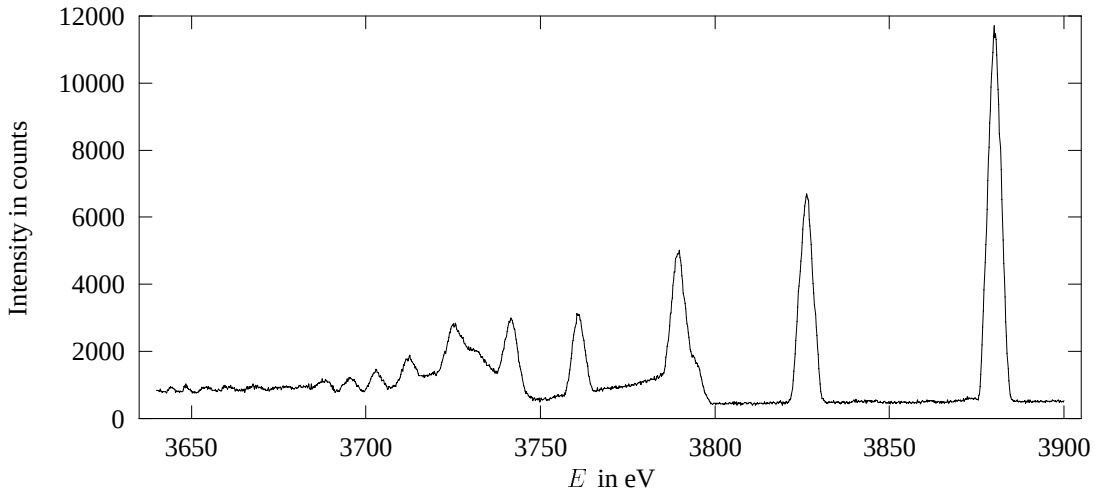

Figure 7.2: A spectrum between $\lambda = 3640\mathrm{\AA}$ and $\lambda = 3900\mathrm{\AA}$ at axial position $(z, y) = (17.2\ ,\ 7.5)$. Plasma settings: argon flow = 2.81 SLM, H_2 flow = 0.35 SLM, current through the plasma = 70 A, current through the magnetic field coils = 250 A. No calibration for the spectral sensitivity of the system is applied.

The ratio between background radiation and line radiation can be calculated. When we use $\varepsilon_{\text{line}} = n_p A_{pq} h\nu_{pq}/4\pi$, we get:

$$\frac{\varepsilon_{\text{line}}}{\varepsilon_{\text{continuum}}} = \frac{b_p\, g_p \sqrt{k\, T_{\text{e}}}\, hc^2 A_{pq}}{8\pi\, C_1\, \xi(\lambda,\, T_{\text{e}}) \cdot \Delta\lambda}\, \frac{p^2 q^2}{q^2 - p^2} Ry \cdot \exp\left(\frac{Ry}{p^2 k\, T_{\text{e}}}\right) \tag{7.14}$$

$$\sim b_p \sqrt{T_{\text{e}}} \exp\left(\frac{1}{T_{\text{e}}}\right) \tag{7.15}$$

So this ratio is independent of n_{e} if b_p is independent of n_{e}. This is only true for lines which are in Saha equilibrium.

At $(z, y) = (17.2\,,\ 7.5)$, this ratio turned out to be approximately 20 for the transition H(n = 8 → n = 2), as is to be expected from equation 7.14.

We assumed that this ratio is constant through the whole plasma. However, the Boltzmann plots of the positions of positions far from $x = 17.2$ cm, where the ratio is determined, tends towards a population inversion of the higher excited levels. This might be an indication that this assumption is not valid there any more.

Line	wavelength (Å)	Gauge factor	Background correction
$H_\alpha (n = 3 \rightarrow n = 2)$	6562.80	1.35	1
$H_\beta (n = 4 \rightarrow n = 2)$	4861.32	1.50	1
$H_\gamma (n = 5 \rightarrow n = 2)$	4340.46	1.31	1
$H_\delta (n = 6 \rightarrow n = 2)$	4101.73	1.33	1
$H_\varepsilon (n = 7 \rightarrow n = 2)$	3970.07	1.00	1
$H(n = 8 \rightarrow n = 2)$	3889.05	0.59	0.95
$H(n = 9 \rightarrow n = 2)$	3835.38	0.62	0.93
$H(n = 10 \rightarrow n = 2)$	3797.90	0.59	0.69
$H(n = 11 \rightarrow n = 2)$	3770.63	0.69	0.75
$H(n = 15 \rightarrow n = 2)$	3711.97	0.69	0.75
$H(n = 17 \rightarrow n = 2)$	3697.15	0.71	0.66

Table 7.1: The gauge factors for each measured Balmer line. The gauge factors reproduce within approximately 10%. The decay in gauge factors after the H_ε line is caused by a realignment of the optical system.

Some results are given in the figures 7.3 to 7.6. For these lines also contour plots were made. The measurement conditions were: pressure in the arc = 0.27 bar, $I_{\text{arc}} = 70$ A, argon flow = 2.81 SLM, H_2 flow = 0.35 SLM (20% hydrogen atoms when fully dissociated), background pressure = 0.167 mbar. A magnetic field was applied to confine the plasma. A magnetic field coil was placed around the arc. The current through the magnetic field coils was 250 A. This results in a magnetic field B_z that varies along the axis between 0.042 T and 0.00735 T, as is shown in figure 6.3.

Finally, all calculated densities must be multiplied with $5.6 \cdot 10^{-3}$ because the measurements were done with monochromator slits of 250μm while the calibration was done with slits of 50μm to avoid saturation of the photomultiplier.

We can say that charged particles are confined in a magnetical field if they move spiralized among the magnetical field lines. This is the case if the cyclotron radius is smaller than the mean free path between collisions. This condition is most easily fulfilled for electrons, and because the plasma obeys charge neutrality, ions will also be confined is electrons are. The ratio between the mean free path between collisions and the cyclotron radius is for electrons given by the *electron Hall parameter* [14]:

$$H_{\text{e}} = \frac{\lambda_{\text{ei}}}{\rho_{\text{e}}} = \Omega_{\text{e}} \tau_{\text{ei}} = 6.2 \cdot 10^{21} \frac{B_z \hat{T}_{\text{e}}^{3/2}}{n_{\text{e}}} \tag{7.16}$$

For $n_e = 3 \cdot 10^{17}$ m^{-3}, $T_e = 0.3$ eV and $B = 0.033$ T, we find: $H_e \approx 112$. So, the plasma is strongly magnetized. We used in the previous formula the mean free path between collisions of electrons and ions. It can be shown that this is the dominating interaction. Although the concentration of argon neutrals is much higher than the concentration of hydrogen ions, the cross section for collisions with argon neutrals is much lower than the Coulomb cross section for collisions with hydrogen ions. From [21], an estimation for the cross section for elastic $e - H_2$ scattering can be obtained of $1.5 \cdot 10^{-20}\sqrt{T_e}$ m^2, resulting in a rate of $\approx 10^{-14}\hat{T}_e$ m^3/s. With this estimate, it can be found that for $n_e/n_a > 3 \cdot 10^{-3}\hat{T}_e^{5/2} \approx 10^{-5}$ for $\hat{T}_e = 0.3$ eV, Coulomb collisions dominate.

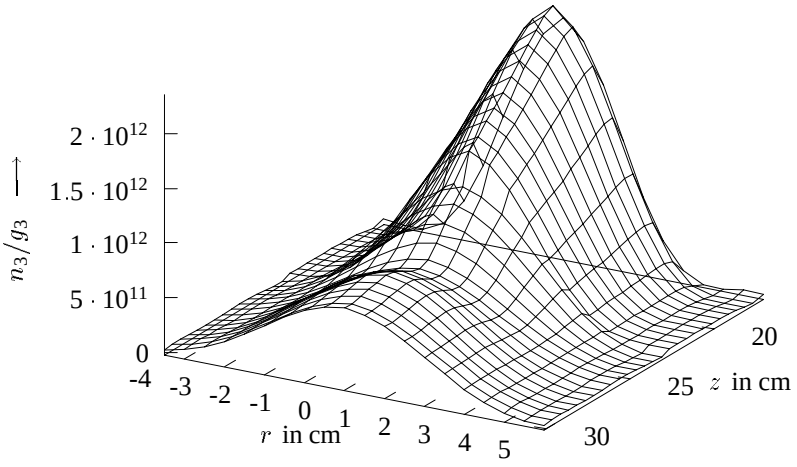

Figure 7.3: The density of H(n=3), determined from the measurement of the Abel inverted H_α line, as a function of the axial and radial position in the plasma.

The bump in the $H(n = 3)$ density tracks attention. This bump didn't appear for the other excited levels. It might be caused by flow characteristics of the plasma: if recirculation of H_2 into the vessel causes a local higher density of $H_2^{v \geq 4}$, the $H(n = 3)$ density will be more affected then the other densities. It could also be a result of the plasma flow colliding with the back wall of the vessel. If the higher excited levels ($Hn > 4$) are populated via $H(n = 2)$ and $H(n = 3)$, and T_e and n_e decrease with rising z, the intensity of the lines $H(n \geq 4 \rightarrow n = 2)$ can decrease and the intensity of H_α can increase.

Further, it tracks attention that the intensities decrease before $z = 17$ cm. This, however, is not a real decrease in intensity, but the result of a decreasing detection volume: the wall of the vessel lies in the detection volume.

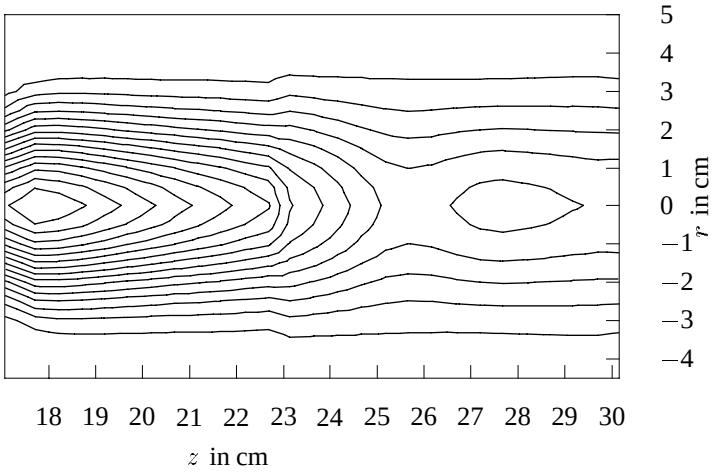

Figure 7.4: The density of H(n=3), determined from the measurement of the Abel inverted H_α line, as a function of the axial and radial position in the plasma in a contour plot. The bump after $z = 27$ cm tracks attention.

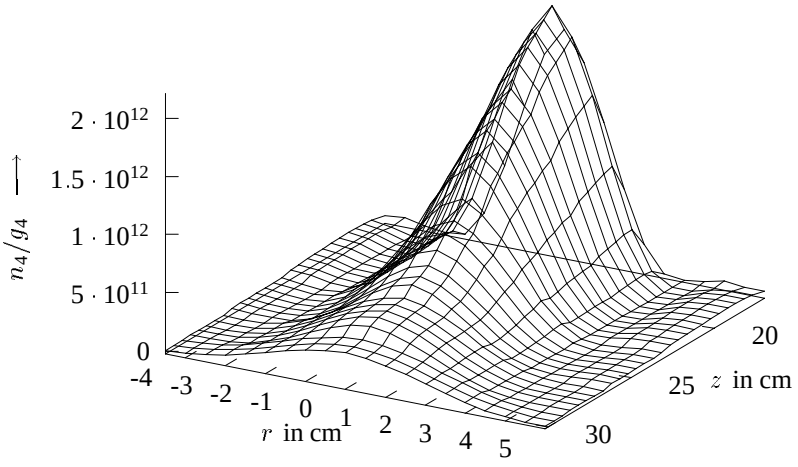

Figure 7.5: The density of H(n=4), determined from the measurement of the Abel inverted H_β line, as a function of the axial and radial position in the plasma.

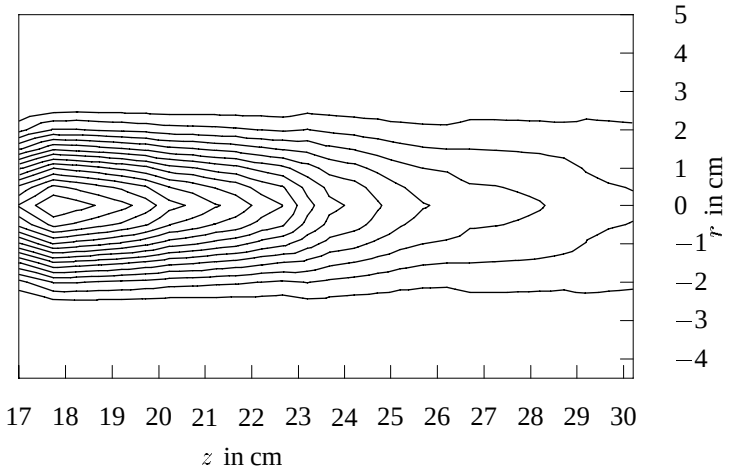

Figure 7.6: The density of H(n=4), determined from the measurement of the Abel inverted H_β line, as a function of the axial and radial position in the plasma in a contour plot.

The electron temperature can be determined from the measurements of the higher levels. We assume that, the closer a level is to ionization, the more it is in LTE, so the more accurate the Saha equation applies. Therefore, the relation between electron temperature, level density and energy for these levels is given by:

$$\ln\left[\frac{n_p}{g_p}\right] = \text{Constant} + \frac{E_i - E_p}{k\,T_\mathrm{e}} \tag{7.17}$$

with the constant equal to:

$$\text{Constant} = \ln\left[\frac{n_\mathrm{i}\,n_\mathrm{e}}{2}\right] + \frac{3}{2}\ln\left[\frac{h^2}{2\pi\,m_\mathrm{e}\,k\,T_\mathrm{e}}\right] \ . \tag{7.18}$$

If this relation holds for two levels p and q, we have:

$$T_\mathrm{e} = \frac{E_q - E_p}{k\ln\left[\frac{n_p g_q}{n_q g_p}\right]} \ . \tag{7.19}$$

This relation could in principle be used to calculate the electron temperature if the intensities of two spectral lines are known. However, determining T_e from 2 lines is a very unreliable method. A small error in the determination of a density would result in a large error in the resulting temperature. To determine the electron temperature more accurately, a *Boltzmann plot* can be made. Here, the energy of the levels is set against $^{10}\log(n_p/g_p)$. The electron temperature can be determined from the slope of a line through the upper levels, which are supposed to be in Saha equilibrium: $^{10}\log(\mathrm{e}) \cdot \text{slope} = 1/k\,T_\mathrm{e}$. An example of a Boltzmann plot is given in figure 7.7. The slope of a line which is fitted through the highest levels gives T_e.
When we assume the upper levels on the plot in Saha equilibrium, we can extrapolate the line to the ionization energy and determine the density of a fictional excited level on the ionization limit:

$$\frac{n_\infty}{g_\infty} = \frac{n_\mathrm{i}\,n_\mathrm{e}}{2}\left(\frac{h^2}{2\pi\,m_\mathrm{e}\,k\,T_\mathrm{e}}\right)^{3/2} \tag{7.20}$$

We find for $n_\infty/g_\infty \approx 10^{10.55} = 3.5\cdot 10^{10}$ m^{-3}. This results in $n_\mathrm{e}\,n_\mathrm{i} = 3.46\cdot 10^{37}$ when we use $T_\mathrm{e} = 0.3$ eV. If we assume a very low ionization degree for argon, we may approximate this with $n_\mathrm{e} = \sqrt{3.46\cdot 10^{39}} = 5.8\cdot 10^{18}$ m^{-3}. This value is too high for the plasma under consideration.

The electron temperature among the axis, determined with Boltzmann plots, is given in figure 7.8.

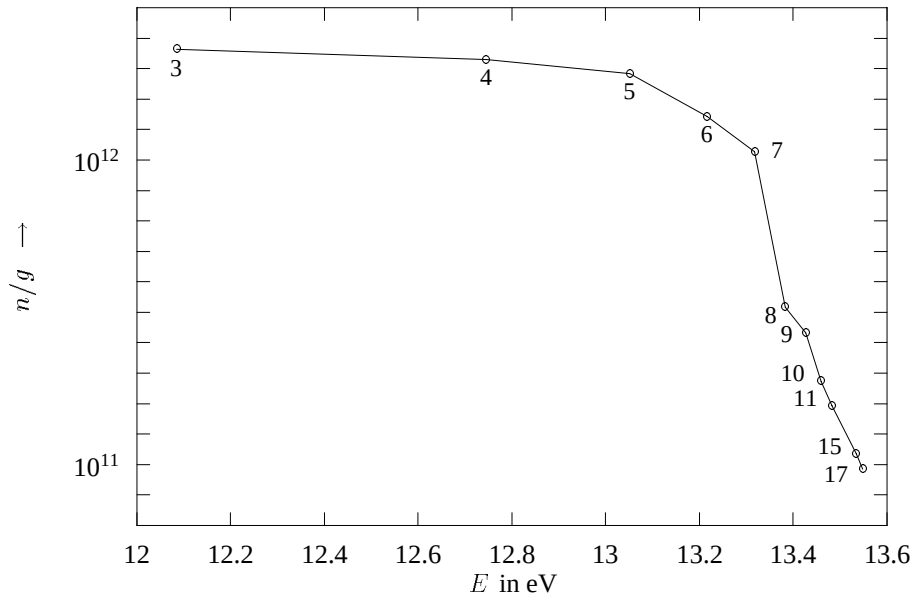

Figure 7.7: A Boltzmann plot for axial position $z = 18$ cm. The electron temperature can be derived from the slop of a line through the upper levels: ${}^{10}log(\mathrm{e}) \cdot slope := -1/k\,T_\mathrm{e}$.

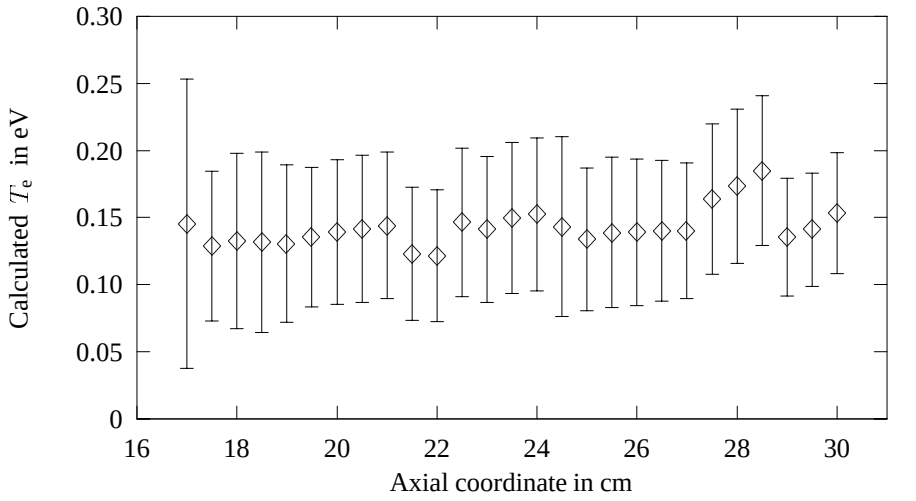

Figure 7.8: The electron temperature among the axis determined with Boltzmann plots.

7.2 Measurements on a pure hydrogen plasma

The main plasma is investigated with a magnetical field applied to the plasma. Some pictures of a pure hydrogen plasma are shown in the following figures. This plasma exists in two clearly different modes. In one mode, the spectrum of the plasma contais mostly of atomic lines, in the other mode, a fully developped molecular spectrum exists. At certain plasma conditions, depending e.g. on magnetic field and pressure, there exists a rapid transfer between these modes. One mode contains mainly molecular lines, one mode contains mainly atomic lines. An explanation of this behaviour is still unknown.

Figure 7.9: Photographs of the pink colored mode of a hydrogen plasma with a fully developed molecular spectrum.

Figure 7.10: Photographs of the red colored mode of a hydrogen plasma with mainly atomic lines.

Chapter 8

Conclusions

8.1 Comparison between model and experiment

We have implemented a kinetic model and a first attempt to a flow model has been made. Further, the spectroscopic setup is functioning and measurements are performed. The absolute calibration needs further attention. The experimental results however, are not easily comparable with the numerical results because:

1. The experiments were performed with more argon than hydrogen while the model is set up for pure hydrogen. This was nessacery because a pure hydrogen plasma emitted an undetectable amount of light in the higher Balmer lines. This can cause deviations because the flow properties of argon differ a lot from the flow properties of hydrogen. Further, some chemical reactions between argon and hydrogen might be of any influence. The possible effects of recirculation of the gas flow through the vessel are neglected. However, most reactions are so fast that a local model will be a good approximation. Further, if more than 10% H_2 is added, most ions are H^+.

2. The effects of the magnetic field are completely ignored in the program. Because magnetical fields affect the movements of all charge particles, it will be of influence on the collision and flow processes. Although the introduction of a magnetic field complicates the formulation of an adequate numerical model, it is necessary for the measurements. Without a magnetic field, the light emission of the plasma is so low that it is difficult to resolve spectral lines. Further, is no magnetical field confines the plasma, the plasma beam expands so quickly that Abel inversion becomes a serious problem because the measured profiles have a very flat intensity decay.

We see that the predicted overpopulation of $H(n = 3)$ (see figure 4.8 with respect to the Saha equilibrium density did not appear. This can be caused because the experimental conditions were rather different than the conditions used in the model or by shortcomings in the model. We can conclude that:

1. More work needs to be done, both experimentally and theoretical. The flow model needs to be improved and the kinetics of the molecular reactions needs to be studied more carefully.

2. There are 2 main differences between the numerical and the experimental results:

   I. There is no overpopulation observed for $H(n = 3)$. This might indicate that the rate coefficient for reaction 9 ($H^+ + H^- \rightarrow H + H(n = 3)$) is chosen too high, or that a larger part of the produced excited hydrogen atoms flows out to $n = 2$.

   II. The contradictions between the emission spectroscopy measurements and the Langmuir probe measurements. This is discussed in section 8.2. It could be an indication that the temperature which follows from the occupation of excited levels is not the same as T_e. If this is true, it implies input in these levels.

3. The occupation of the levels around $n = 5$ to 8 are much larger than could be expected. This could happen if there is some input to the higher levels from molecular reactions, e.g. $H^+ + H^- \rightarrow H + H(n)$, $n = 6$ or 7.

Further some of the used data about rate coefficients, originating from [10], is under discussion. In particular, the rate coefficients for reactions 2 and 5 are still a point of discussion. A lower rate coefficient for reaction 2 would decrease the H^- production. The overpopulation of $H(n = 3)$ is mainly determined by reaction 9. Reactions 4,5 and 7 result in a net flow to $H(n = 2)$. Because reaction 5 results in the largest flow and K_5 is still under discussion, this is a point that requires further attention.

8.2 Comparison between the emission spectroscopy measurements and probe measurements

Some measurements with a Langmuir probe are performed to compare them with the emission spectroscopy measurements. The results are listed in table 8.1.

Distance from the nozzle [cm]	T_e [K]	n_e [m^{-3}]
20	4000	$2.2 \cdot 10^{18}$
25.5	3530	$1.3 \cdot 10^{18}$
31	3130	$9 \cdot 10^{17}$

Table 8.1: The results of the Langmuir probe measurement.

.

We see that there is an acceptable agreement between these measurements and the results of the emission measurements. The results of Langmuir probe measurements in magnetical fields are questionable if the electron cyclotron radius becomes smaller than the diameter of the probe. However, the diameter of the probe wire is 100 μm, while the electron cyclotron radius for electrons of 0.3 eV in a field of 0.03 T is 0.06 mm. So the magnetic field does not affect this measurement seriously. The underdetermination of the electron temperature from the emission measurements could be a combined result of uncertaincies with the calibration and disturbances of a leak in the vessel. This leak shows up in the nitrogen molecular bands which appear in the spectrum in figure 7.2. Especially in the wavelength region where all the high lying hydrogen lines are the spectrum is polluted due to the vacuum leak. Further, some reactions that give input in the higher excited states are gouverned by the (lower?) heavy particle temperature T_h.

8.3 The flow model

The flow model was numerically unstable. Probably the easiest way to avoid this is to make the equations dimensionless.

8.4 Further recommendations

An extension of the model with states Ar, Ar^+ and ArH^+ is needed. Further, the properties of the magnetic field could be implemented. This extended model would more agree with the experimental conditions.

On the experimental side, the background radiation could be measured as a function of the position. After Abel inversion, a determination of n_e is possible.

Appendix A

All reactions in a hydrogen plasma according to [10]

1. Electron collisions with H_2, H_2^+ and H_3^+

Reaction mechanism			Rate coefficient [m^3/s]			
			0.3 eV	0.5 eV	1 eV	1.5 eV
$e + H_2$	$\rightarrow$	$e + 2H(1s)$	$< 10^{-17}$	$< 10^{-17}$	$< 10^{-17}$	$1.5 \cdot 10^{-15}$
$e + H_2$	$\rightarrow$	$e + H(1s) + H(2s)$	$< 10^{-17}$	$< 10^{-17}$	$< 10^{-17}$	$2 \cdot 10^{-16}$
$e + H_2$	$\rightarrow$	$e + H(2p) + H(2s)$	$< 10^{-17}$	$< 10^{-17}$	$< 10^{-17}$	10^{-17}
$e + H_2$	$\rightarrow$	$e + H(1s) + H(n = 3)$	$< 10^{-17}$	$< 10^{-17}$	$< 10^{-17}$	10^{-17}
$e + H_2$	$\rightarrow$	$2e + H_2^+$	$< 10^{-17}$	$< 10^{-17}$	$< 10^{-17}$	$8 \cdot 10^{-16}$
$e + H_2$	$\rightarrow$	$2e + H^+ + H(1s)$	$< 10^{-17}$	$< 10^{-17}$	$< 10^{-17}$	10^{-17}
$e + H_2^+$	$\rightarrow$	$2e + 2H^+$	$< 10^{-17}$	$< 10^{-17}$	$< 10^{-17}$	$6 \cdot 10^{-17}$
$e + H_2^{+(0 \leq v \leq 9)}$	$\rightarrow$	$e + H^+ + H(1s)$	$6 \cdot 10^{-17}$	$2 \cdot 10^{-15}$	$2 \cdot 10^{-14}$	10^{-13}
$e + H_2^+$	$\rightarrow$	$e + H^+ + H(n = 2)$	$< 10^{-17}$	$< 10^{-17}$	$< 10^{-17}$	10^{-14}
$e + H_2^{+(v)}$	$\rightarrow$	$H(1s) + H(n \geq 2)$	$1.2 \cdot 10^{-13}$	$8 \cdot 10^{-14}$	$5.5 \cdot 10^{-14}$	$2 \cdot 10^{-14}$
$e + H_3^+$	$\rightarrow$	$3H$	$2 \cdot 10^{-14}$	$1.6 \cdot 10^{-14}$	$1.2 \cdot 10^{-14}$	$2 \cdot 10^{-14}$
$e + H_3^+$	$\rightarrow$	$H_2(v > 5) + H(n = 2)$	$7 \cdot 10^{-14}$	$5.5 \cdot 10^{-14}$	$4 \cdot 10^{-14}$	$2 \cdot 10^{-14}$
$e + H_3^+$	$\rightarrow$	$e + 2H + H^+$	$< 10^{-17}$	$< 10^{-17}$	$< 10^{-17}$	10^{-14}
$e + H_2^{(v \geq 4)}$	$\rightarrow$	H^- +H	$2.8 \cdot 10^{-14}$	$2.8 \cdot 10^{-14}$	$2 \cdot 10^{-14}$	$4 \cdot 10^{-15}$

2. Proton collisions with H_2 and H_2^+

Reaction mechanism			Rate coefficient [m^3/s]			
			0.3 eV	0.5 eV	1 eV	1.5 eV
$H^+ + H_2^{(j=0)}$	$\rightarrow$	$H^+ + H_2(j')$ $(j' \geq 2)$	$3.5 \cdot 10^{-15}$	$3.8 \cdot 10^{-15}$	$4 \cdot 10^{-15}$	$4 \cdot 10^{-15}$
$H^+ + H_2^{(j=1)}$	$\rightarrow$	$H^+ + H_2(j')$ $(j' \geq 3)$	$1.8 \cdot 10^{-15}$	$2 \cdot 10^{-15}$	$2.8 \cdot 10^{-15}$	$3.9 \cdot 10^{-15}$
$H^+ + H_2^{(v=0)}$	$\rightarrow$	$H^+ + H_2(j')$ $(v > 0)$	$< 10^{-17}$	$2 \cdot 10^{-17}$	$8 \cdot 10^{-17}$	$1.8 \cdot 10^{-15}$
$H^+ + H_2$	$\rightarrow$	$H(1s) + H_2^+$	$< 10^{-17}$	10^{-17}	$3.8 \cdot 10^{-17}$	$9 \cdot 10^{-17}$
$H^+ + H_2$	$\rightarrow$	$H^+ + H_2(v \leq 9) + e$	$< 10^{-17}$	$< 10^{-17}$	$< 10^{-17}$	$< 10^{-17}$
$H^+ + H_2^+$	$\rightarrow$	$H(1s) + 2H^+$	$< 10^{-17}$	$< 10^{-17}$	$< 10^{-17}$	$< 10^{-17}$
$H_2^+ + H(1s)$	$\rightarrow$	H^+ +H+H(1s)	$< 10^{-17}$	$< 10^{-17}$	$< 10^{-17}$	$< 10^{-17}$
$H_2^+ + H_2$	$\rightarrow$	$2H_2^+$ +e	$< 10^{-17}$	$< 10^{-17}$	$< 10^{-17}$	$< 10^{-17}$
$H_2^+ + H_2$	$\rightarrow$	H_3^+ +H	$1.1 \cdot 10^{-15}$	10^{-15}	$8 \cdot 10^{-16}$	$2.8 \cdot 10^{-16}$

3. Collisions with H^-

Reaction mechanism			Rate coefficient [m^3/s]			
			0.3 eV	0.5 eV	1 eV	1.5 eV
$e + H^-$	$\rightarrow$	2e+H(1s)	$5 \cdot 10^{-16}$	$2.5 \cdot 10^{-15}$	$1.5 \cdot 10^{-14}$	$3.3 \cdot 10^{-13}$
$e + H^-$	$\rightarrow$	3e+H^+	$< 10^{-17}$	$< 10^{-17}$	$< 10^{-17}$	$1.5 \cdot 10^{-16}$
$H^+ + H^-$	$\rightarrow$	e+H+H^+	$< 10^{-17}$	$< 10^{-17}$	$< 10^{-17}$	$< 10^{-17}$
$H^+ + H^-$	$\rightarrow$	H(n=2)+H(1s)	$1.3 \cdot 10^{-15}$	$1.5 \cdot 10^{-15}$	$2 \cdot 10^{-15}$	$5 \cdot 10^{-15}$
$H^+ + H^-$	$\rightarrow$	H(n=3)+H(1s)	$4.1 \cdot 10^{-14}$	$4 \cdot 10^{-14}$	$4 \cdot 10^{-14}$	$3.7 \cdot 10^{-14}$
$H + H^-$	$\rightarrow$	2H+e	$5 \cdot 10^{-16}$	$7 \cdot 10^{-16}$	10^{-15}	$3 \cdot 10^{-15}$
$H + H^-$	$\rightarrow$	H_2 +e	$1.8 \cdot 10^{-15}$	$1.8 \cdot 10^{-15}$	$1.8 \cdot 10^{-15}$	$2.4 \cdot 10^{-15}$

4. Collisions between H^+ and H

Reaction mechanism	Rate coefficient [m^3/s]			
	0.3 eV	0.5 eV	1 eV	1.5 eV
$H^+ + H(1s) \rightarrow H^+ + H(2p)$	$< 10^{-17}$	$< 10^{-17}$	$< 10^{-17}$	$< 10^{-17}$
$H^+ + H(1s) \rightarrow H^+ + H(2s)$	$< 10^{-17}$	$< 10^{-17}$	$< 10^{-17}$	$< 10^{-17}$
$H^+ + H(2s) \rightarrow H^+ + H(2p)$	$1.8 \cdot 10^{-11}$	$2.8 \cdot 10^{-11}$	$4.5 \cdot 10^{-11}$	10^{-10}
$H^+ + H(1s) \rightarrow H^+ + H(n \geq 3)$				
$H^+ + H(n \geq 2) \rightarrow H^+ + H(m \geq n)$				
$H^+ + H(1s) \rightarrow 2H^+ + e$	$< 10^{-17}$	$< 10^{-17}$	$< 10^{-17}$	$< 10^{-17}$
$H^+ + H(n \geq 2) \rightarrow 2H^+ + e$				

We see that there is a strong collisional coupling between the H(2s) and the H(2p) level. Because the transition $H(2s) \rightarrow H(1s)$ is not permitted in first order, this means that the decay from H(2s) to H(1s) is still possible via $H(2s) \xrightarrow{e} H(2p) \xrightarrow{h\nu} H(1s)$.

Appendix B

The program listings

B.1 Unit Atom_def

```
Unit Atom_def;

Interface

Const
  ion_factor=1;
  Max_Levels=20;
  Max_Transitions=100;
  N_cond=10;
  N_K=11;
  h=6.6262e-34;
  kB=1.381e-23;
  ee=1.6022e-19;
  me=9.11e-31;
  m1=1.673e-27;

Type
  float = double;
  int_level_arr= array[1..Max_Levels] of integer;
  condition_arr= array[1..N_cond] of float;
  float_level_arr = array[1..Max_Levels] of float;
  float_level_arr_2dim = array[1..Max_Levels,1..Max_Levels] of float;
  int_transition_arr = array[1..Max_Transitions] of integer;
  arr_col = array[1..Max_Transitions] of float ;

Type atomic_data = record
       n,plus,m,z,mu,N_rad_trans,N_Vriens_transitions,
       N_cut_off_levels,N_cut_off_connections       : integer;
       g,g_cut_off                                  : int_level_arr;
       init_rad_lev,final_rad_lev,init_Vr_lev,final_Vr_lev,
       g_Vr_sub_tot,init_cut_off_conn_lev,
       final_cut_off_conn_lev,g_cut_off_conn_sub_tot: int_transition_arr;
       E,E_cut_off                      : float_level_arr;
       A_val,A_Vriens                   : arr_col;
       Kmol                             : array[1..N_K,1..3] of float;
  end;

Implementation
end.
```

B.2 Unit Read_H

```
Unit Read_H;

Interface

Uses Crt,Atom_def;

Procedure read_atomic_data(var element_data :atomic_data);

Implementation

Procedure read_atomic_data(var element_data :atomic_data);

Var p: integer;
    f: text;

begin
with element_data do
begin;
assign(f,'h.dat');
reset(f);
readln(f,n);      write('  Aantal atomaire niveaus: ',n);
readln(f,plus); writeln('  Ion niveau: ',plus);
readln(f,m);      write('  Aantal moleculaire toestanden: ',m);
readln(f,z);    writeln('  Ladingsgetal: ',z);
writeln;
readln(f);
for p:=1 to n do readln(f,E[p]);
readln(f,E[plus]);
readln(f);
for p:=1 to (plus+m) do readln(f,g[p]);
readln(f);
readln(f,N_Rad_Trans);
writeln('N_Rad_Trans: ',N_Rad_Trans);

for p:=1 to N_Rad_Trans do
  begin
    readln(f,init_rad_lev[p],final_rad_lev[p],A_val[p]);
  end;
readln(f);
readln(f,N_Vriens_Transitions);

writeln('N_Vriens_Transitions: ',N_Vriens_Transitions);

for p:=1 to N_Vriens_Transitions do
readln(f,Init_vr_lev[p],final_vr_lev[p],A_Vriens[p],g_vr_sub_tot[p]);
readln(f);

for p:=1 to N_K do readln(f,Kmol[p,1],Kmol[p,2],Kmol[p,3]);
readln(f);

readln(f,N_cut_off_levels);
for p:=1 to N_cut_off_levels do readln(f,E_cut_off[p],g_cut_off[p]);
```

```
readln(f,N_cut_off_connections);
for p:=1 to N_cut_off_connections do
readln(f,init_cut_off_conn_lev[p],final_cut_off_conn_lev[p],
        g_cut_off_conn_sub_tot[p]);
mu:= 1;       { mass units }
close(f);
end;
end;
end.
```

B.3 Unit New_Solv

```
Unit New_Solv;

Interface
Uses Atom_def, Matrix, Crt;

Procedure Calc_Stat_cond(n,plus       :integer;
                         gamma        :float;
                         Total_Matrix : float_level_arr_2dim;
                     Var pop:float_level_arr);

Procedure Calc_Stat(n,m,plus            : integer;
                    Total_Matrix        : float_level_arr_2dim;
                Var pop,n_plus,n_1,n_H2 : float_level_arr;
                Var alfa_CR,S_CR        : float;
                    nH2,n1,Nplus,ne     : float);

Function power(a,b :float): float;

Function Saha_dens(g_p,g_ion: integer; E_ion,E_p,Te,ne,ni: float): float;

Procedure svevriens(Var excit,deexcit: float;
                    E_ion,E_p,E_q: float;
                    gsubt,g_p,g_q: integer; Te,A_val:float);


Procedure Calc_Matrix(element_data : atomic_data;
                      ne,nplus,n1,nH2,Te,Th,Tvib:float;
                  Var deelv: float;
                  Var Total_Matrix,K_rate,A_mat : float_level_arr_2dim;
                  Var K_mol,K_mol_rev : K_arr;
                  Var exponent,nHmin,nH3plus,
                      gamma1,gamma2,gamma3:float);

implementation

{ Berekening van gehele en gebroken machten }
Function power(a,b :float): float;
Var c,d    : float;
    i,macht: integer;
begin
  if a=0 then power:=1
```

```
  else if (b-round(b))= 0 then
  begin
    c:=a;
    d:=a;
    macht:=round(b)-1;
    for i:=1 to macht do d:=d*c;
    power:=d;
    end
  else power:=exp(b*ln(a));
end;

function Saha_dens(g_p,g_ion: integer; E_ion,E_p,Te,ne,ni: float): float;
begin
Saha_dens:=(ni*g_p/(2*g_ion)*3.32E-28*ne/power(Te,1.5))
               *exp((E_ion-E_p)/Te);
end;

{SE FORMULAE OF VRIENS AND SMEETS FOR THE CALCULATION OF RATECOEFFICIENTS}
Procedure svevriens(Var excit,deexcit :float ;
                    E_ion,E_p,E_q : float;
                    gsubt,g_p,g_q : integer ; Te,A_val:float);
Var  p,q,Y,K_pY,b_p,B_pq,f_pq,A_pq,Delta_pq,Gamma_pq,dE,dummy :float;
begin
p:=sqrt(13.6/(E_ion-E_p));
q:=sqrt(13.6/(E_ion-E_q));
dE:=E_q-E_p;
b_p:=(1.4*ln(p)-0.7-0.51/p+1.16/sqr(p)-0.55/power(p,3))/p;
B_pq:=(739.84*g_q*(1+ (4*(E_ion-E_p))/(3*dE)+
      (b_p*sqr(E_ion-E_p))/sqr(dE)))/(gsubt*power(q,3)*sqr(dE));

{calculate oscillator strenght; in case the A_val given to the procedure}
{equal zero, take a hydrogen approximation                              }
if A_val<>0 then
  f_pq:=(2.306E-8*A_val*g_q)/(g_p*sqr(dE))
else
  begin
  Y:=abs(dE/(E_ion-E_p));
  if p<=1.5 then K_pY:=     1.133  - 0.4059/Y + 0.07014/sqr(Y)
     else if p<3 then K_pY:=1.0785 - 0.2319/Y + 0.02947/sqr(Y)
       else {p>=3} K_pY:=0.9935+0.2328/p-0.1296/sqr(p)
         - (0.6282-0.5598/p+0.5299/sqr(p))/(p*Y)
         + (0.3887-1.181/p+1.470/sqr(p))/sqr(p*Y);
  f_pq:=1.960*K_pY/(power(p,5)*power(q,3)*power((1/sqr(p)-1/sqr(q)),3));
  if (f_pq>1) then f_pq:=1;
  end;

A_pq:=(27.2/dE)*f_pq;

dummy:=B_pq/A_pq;
if dummy > 69 then Delta_pq:=0 else Delta_pq:=exp(-dummy);
Delta_pq:=Delta_pq + 0.06*sqr(q-p)/(q*sqr(p));

Gamma_pq:=13.6*ln(1+power(p,3)*Te/13.6)*(3+11*sqr((q-p)/p))/
 (6+1.6*q*(q-p)+0.3/sqr(q-p)+0.8*power(q,1.5)*abs(q-p-0.6)/sqrt(abs(q-p)));
```

```
Excit:=1.6E-13*sqrt(Te)*exp(-dE/Te)*A_pq*
               (ln(0.3*Te/13.6+Delta_pq)+dummy)/(Te+Gamma_pq);
Deexcit:=excit*g_p/g_q*exp(dE/Te);
end {procedure svevriens};


Procedure Calc_Matrix(element_data : atomic_data;
                      ne,nplus,n1,nH2,Te,Th,Tvib:float;
                  Var deelv: float;
                  Var Total_Matrix,K_rate,A_mat : float_level_arr_2dim;
                  Var K_mol,K_mol_rev : K_arr;
                  Var exponent,nHmin,nH3plus,gamma1,gamma2,gamma3:float);

Var
   p,q,ii,v                              : integer;
   pef,eps,beta,excit,deexcit,som,mm,ZZ : float;
   K_N_Nplus1                            : float_level_arr_2dim;

{* Approximation of exponential integral. This function *}
{* is used for the calculation of radiation combination *}

Function meimx(E_lower,E_upper,Te:real):real;
Var
   x2,dummy : real;
begin
  x2:= (E_upper-E_lower)/Te;
  if x2 < 2.5 then
  begin
    dummy:=-ln(x2)-0.57721566+0.99999193*x2-0.24991055*sqr(x2);
    dummy:=dummy+0.05519968*power(x2,3)-0.00976004*power(x2,4);
    meimx:=dummy+0.00107857*power(x2,5)
  end
  else meimx:=exp(-x2)/x2*(1-1/x2+2/sqr(x2));
end {function meimx};

begin
with element_data do begin
{*********************************************************}
{*    Determination of Excitation - Deexcitation         *}
{*          Rate Coefficients  K_rate[p,q]               *}
{*********************************************************}
  for p:=1 to plus do for q:=1 to plus do K_rate[p,q]:=0;
  for ii:=1 to N_Vriens_transitions do
  begin
    p:=init_Vr_lev[ii]; q:=final_Vr_lev[ii];
    svevriens(K_rate[p,q],K_rate[q,p],E[plus],E[p],E[q],g_Vr_sub_tot[ii],
        g[p],g[q],Te,A_Vriens[ii]);
  end;
{*****************************************************************}
{Determination of Ionization Rate Coefficients ebi[i] : Ionization of}
{the Groundlevel : Straight Line for the Excited Levels we use :     }
{Vriens & Smeets : Phys Rev A vol 22 no 3 sept.1980.                 }
{*****************************************************************}
```

```
for p:=1 to n do
begin
  eps:=(E[plus]-E[p])/Te;
  K_rate[p,plus]:=((9.56E-12/power(Te,1.5)*exp(-eps))/(power(eps,2.33)
             +4.38*power(eps,1.72)+1.32*eps));
end;

{Cut-off Procedure for the Highest Levels; PHD J.A.M. van der Mullen}
for p:=1 to plus do for q:=1 to plus do K_N_Nplus1[q,p] := 0;
for ii:=1 to N_cut_off_connections do
  begin
  pef:=sqrt((13.6*sqr(z+1))/(E[plus]-E[init_cut_off_conn_lev[ii]]));
  beta:=1-power(pef/(pef+1),exponent);
  svevriens(excit,deexcit,e[plus],E[init_cut_off_conn_lev[ii]],
      E_cut_off[final_cut_off_conn_lev[ii]],
      g_cut_off[final_cut_off_conn_lev[ii]],
      g[init_cut_off_conn_lev[ii]],
      g_cut_off[final_cut_off_conn_lev[ii]],Te,10);
  K_N_Nplus1[init_cut_off_conn_lev[ii],final_cut_off_conn_lev[ii]]:=
      excit*beta;
  end;
  for ii := 1 to N_cut_off_connections do
  begin
  K_rate[init_cut_off_conn_lev[ii],plus]:=
      k_rate[init_cut_off_conn_lev[ii],plus] +
     K_N_Nplus1[init_cut_off_conn_lev[ii],final_cut_off_conn_lev[ii]];
  end;

{** Three Particle Recombination Determined with Detailed Balance ***}
{******** be aware that K_rate[p,+]*n[p]= n[+]*K_rate[+,p]  *********}
for p:=1 to n do
K_rate[plus,p]:=Saha_dens(g[p],g[plus],E[plus],E[p],Te,ne,1)*K_rate[p,plus];

{********************** Radiation recombination *******************}
 for p:=1 to n do
   K_rate[plus,p]:=K_rate[plus,p]+
   1.31E-18*g[p]/g[plus]*{gam[i]}3*exp((E[plus]-E[p])/Te)*
   power(((E[plus]-E[p])/13.6),2.5)/power(Te,1.5)*meimx(E[p],E[plus],Te);

{*********** Determination of Molecular Rate Coefficients ***********}
if (Te < 0.3) then
begin
  writeln('Te < 0.3 eV. Extrapolating from 0.3 eV values.');
  for p:=1 to N_K do K_mol[p]:=Kmol[p,1]-5*(Kmol[p,1]-Kmol[p,2])*(Te-0.3);
  for p:=1 to N_K do if K_mol[p]<0 then K_mol[p]:=0;
end;
if (Te > 1) then
begin
  writeln('Te > 1 eV. Extrapolating from 1 eV values.');
  for p:=1 to N_K do K_mol[p]:=Kmol[p,2]-2*(Kmol[p,2]-Kmol[p,3])*(Te-0.5);
  for p:=1 to N_K do if K_mol[p]<0 then K_mol[p]:=0;
end;

if ((0.3 <= Te) and (Te < 0.5)) then
```

```
begin
  for p:=1 to N_K do K_mol[p]:=Kmol[p,1]-5*(Kmol[p,1]-Kmol[p,2])*(Te-0.3);
end;
if ((0.5 <= Te) and  (Te <= 1)) then
begin
  for p:=1 to N_K do K_mol[p]:=Kmol[p,2]-2*(Kmol[p,2]-Kmol[p,3])*(Te-0.5);
end;

{********** Determination of Vibrational Distribution ***************}
ZZ:=0;    { State sum }
deelv:=0; { fraction of H_2 molecules with v\geq4 }
for v:=0 to 14 do ZZ:=ZZ+exp(-0.545*(v-0.0244*v*v)/Tvib);
for v:=4 to 14 do deelv:=deelv+exp(-0.545*(v-0.0244*v*v)/Tvib);
deelv:=deelv/ZZ;

{******** Determination of Reverse Molecular Rate Coefficients ********}
mm:=exp(1.5*ln(me/m1));
K_mol_rev[1]:=K_mol[1]*(g[plus]*(g[plus+4]-4)/(g[1]*g[plus+1]))
                      *exp(-0.063/Th);
K_mol_rev[2]:=K_mol[2]*(g[plus+4]/g[plus+3])*mm*2*sqrt(2)*exp(1.836/Th);
K_mol_rev[3]:=K_mol[3]*(4/sqrt(27))*(g[plus+1]*g[plus+4]/g[plus+2])
                      *exp(-1.92/Th);
K_mol_rev[4]:=K_mol[4]*(g[plus+1]/2*sqrt(2))*mm*exp(-0.75/Te);
K_mol_rev[5]:=K_mol[5]*(sqrt(54)/16)*(g[plus+2]/(g[plus+4]-4))*mm
                      *exp(3.164/Th);
K_mol_rev[6]:=K_mol[6]*(sqrt(27)/4)*g[plus+2]*mm
                      *power(((h*h)/(2*pi*m1*ee*Th)),1.5)*exp(-4.546/Th);
K_mol_rev[7]:=K_mol[7]*(g[plus+3]/16)*exp(-2.649/Th);
K_mol_rev[8]:=K_mol[8]*0.25*g[plus+3]*power(((h*h)/(2*pi*me*ee*Te)),1.5)
                                    *exp(0.75/Te);
K_mol_rev[9]:=K_mol[9]*(g[plus+3]/36)*exp(-0.761/Th);
K_mol_rev[10]:=K_mol[10]*0.25*g[plus+3]*power(((h*h)/(2*pi*me*ee*Te)),1.5)
                                      *exp(0.75/Te);
K_mol_rev[11]:=K_mol[11]*(sqrt(27)/8)
               *(g[plus+2]*g[plus+3]/(g[plus+4]*g[plus+4]))*exp(-12.748/Th);

{***************** Preparation of Radiation Matrix *****************}
for p:=1 to plus do for q:=1 to plus do A_mat[p,q]:=0;
for ii:=1 to N_rad_trans do
  A_mat[init_rad_lev[ii],final_rad_lev[ii]]:=A_val[ii];

{*************************************************************}
{*                  Construction of Linear System and          *}
{*                    Extension with Molecular Terms.          *}
{*************************************************************}
{* Atomic terms *}
for p:=1 to (plus+m) do for q:=1 to (plus+m) do Total_Matrix[p,q]:=0;
for p:=1 to plus do
begin
for q:=1 to plus do
if p<>q then
begin
  Total_Matrix[p,p]:=Total_Matrix[p,p]-ne*K_rate[p,q]-A_mat[p,q];
  Total_Matrix[p,q]:=ne*K_rate[q,p]+A_mat[q,p];
```

```
end;
end;

{* Addition of moleculair terms          *}
{* They include the assumption n^* = n_2 *}

{* Terms at the right-hand side *}
Total_Matrix[plus+2,1]:=n1*n1*K_mol_rev[6];
Total_Matrix[plus+3,1]:=ne*ne*K_mol_rev[8]+n1*ne*K_mol_rev[10];
Total_Matrix[plus+1,plus+m]:=nplus*deelv*K_mol[1];
Total_Matrix[plus+2,plus+m]:=nH2*K_mol_rev[11];
Total_Matrix[plus+3,plus+m]:=ne*deelv*K_mol[2]+nH2*K_mol_rev[11];

{* terms at the left-hand side *}
Total_Matrix[2,2]:=Total_Matrix[2,2]-n1*(K_mol_rev[4]+K_mol_rev[7])-nH2
                  *deelv*K_mol_rev[5];
Total_Matrix[3,3]:=Total_Matrix[3,3]-n1*K_mol_rev[9];
Total_Matrix[plus+1,2]:=n1*K_mol_rev[4];
Total_Matrix[plus+2,2]:=nH2*deelv*K_mol_rev[5];
Total_Matrix[plus+3,2]:=n1*K_mol_rev[7];
Total_Matrix[2,plus+1]:=ne*K_mol[4];
Total_Matrix[2,plus+2]:=ne*K_mol[5];
Total_Matrix[2,plus+3]:=nplus*K_mol[7];
Total_Matrix[3,plus+3]:=nplus*K_mol[9];
Total_Matrix[plus+1,plus+1]:=-n1*K_mol_rev[1]-nH2*K_mol[3]-ne*K_mol[4]
                             -gamma1;
Total_Matrix[plus+2,plus+1]:=nH2*K_mol[3];
Total_Matrix[plus+1,plus+2]:=n1*K_mol_rev[3];
Total_Matrix[plus+2,plus+2]:=-n1*K_mol_rev[3]-ne*(K_mol[5]+K_mol[6])-
                              nHmin*K_mol[11]-gamma2;
Total_Matrix[plus+3,plus+3]:=-n1*K_mol_rev[2]-ne*K_mol[8]
                             -nplus*(K_mol[7]+K_mol[9])
                             -n1*K_mol[10]-nH3plus*K_mol[11]-gamma3;
end;
end; {procedure calc_matrix}

Procedure Calc_Stat_cond(n,plus      : integer;
                         gamma       : float;
                         Total_Matrix: float_level_arr_2dim;
                              Var pop: float_level_arr);
{procedure Calc_Stat_cond berekend de stationaire conditie voor gegeven}
{CR-matrix (Total_Matrix) en gegeven \gamma_t^+                         }
{de totale dichtheid wordt genormeerd op 1                              }
Var p,q     : integer;
    som     : float;
    data,inv: TNmatrix;
    Error   : byte;
begin
{* bepaal de inverse van Total_Matrix *}
for p:=1 to plus do for q:=1 to plus do data[p,q]:=Total_Matrix[p,q];
for q:=1 to n do data[plus,q]:=0;
data[plus,plus]:=1;
data[1,plus]:=data[1,plus]+gamma;
Inverse(plus,Data,inv,Error);
```

```
som:=0;
for p:=1 to plus do begin pop[p]:=inv[p,plus]; som:=som + pop[p]; end;
for p:=1 to plus do pop[p]:=pop[p]/som;
end {procedure calc_stat_cond};

Procedure Calc_Stat(n,m,plus           : integer;
                    Total_Matrix       : float_level_arr_2dim;
                Var pop,n_plus,n_1,n_H2: float_level_arr;
                Var alfa_CR,S_CR       : float;
                    nH2,n1,Nplus,ne    : float);
Var p,q     : integer;
    data,inv:TNmatrix;
    error   :byte;
begin
{Calc_stat berekend de dichtheden van de aangeslagen niveaus bij gegeven}
{n_1 en n_+ en CR-matrix; gamma_tˆ+ hoeft dus niet meegegeven te worden }
{bovendien worden S_CR en alfa_CR bepaald                               }

{******* bepaal inverse van Total_Matrix bij gegeven n_1, n_+ en nH2. **}
for p:=1 to (plus+m) do for q:=1 to (plus+m) do
                                  data[p,q]:=Total_Matrix[p,q];
for q:=2 to (plus+m) do data[1,q]:=0;      data[1,1]:=1;
for q:=1 to (plus+m) do data[plus,q]:=0;   data[plus,plus]:=1;
for q:=1 to (plus+m) do data[plus+m,q]:=0; data[plus+m,plus+m]:=1;
Inverse(plus+m,Data,inv,Error);

{*********** Calculation pop[p], n_plus[p], n_1[p] en n_H2[p] **********}
pop[1]:=n1;
pop[plus]:=nplus;
pop[plus+m]:=nH2;
for p:=2 to (plus+m) do
begin
  n_1[p]:=inv[p,1]*pop[1];
  n_plus[p]:=inv[p,plus]*pop[plus];
  n_H2[p]:=inv[p,plus+m]*pop[plus+m];
  pop[p]:=n_1[p]+n_plus[p]+n_H2[p];
end;

{******** Calculation alfa_CR en S_CR ******************}
alfa_CR:=0;S_CR:=0;
for p:=2 to n do
begin
  alfa_CR:=alfa_CR + n_plus[p]*Total_Matrix[1,p];
  S_CR:=S_CR - n_1[p]*Total_Matrix[1,p];
end;
if pop[plus]>0 then
  alfa_CR:=(pop[plus]*Total_Matrix[1,plus] + alfa_CR)/(ne*pop[plus])
  else alfa_CR:=0;;
if pop[1]>0 then
  S_CR:= - Total_Matrix[1,1]/ne + S_CR/(ne*pop[1])
  else S_CR:=0;
end {procedure calc_stat};

end.
```

```
end.
```

B.4 Main program

```
Program H1;
{$IFDEF CPU87} {$N+} {$ELSE} {$N-} {$ENDIF}
Uses Atom_def, Read_H, New_Solv, Crt;

Var
H_dat                                : atomic_data;
ne,ni,exponent,Te,Th,Tvib,gamma0,gamma1,gamma2,gamma3,n1,
nplus,nH2,alfa_CR,S_CR,sum,deelv,nHmin,nH3plus: float;
f                                    : text;
pop,n_plus,n_1,n_H2,nS               : float_level_arr;
K_rate,Total_Matrix,A_mat            : float_level_arr_2dim;
K_mol,K_mol_rev                      : K_arr;
l                                    : integer;

Procedure Calculation;
begin
with H_dat do
begin
  writeln(' Calculating CR matrix.');
  Calc_Matrix(H_dat,ne,nplus,n1,nH2,Te,Th,Tvib,deelv,Total_Matrix,K_rate,
      A_mat,K_mol,K_mol_rev,exponent,nHmin,nH3plus,gamma1,gamma2,gamma3);
  writeln(' Calculating stationary condition densities.');
  Calc_stat(n,m,plus,Total_Matrix,pop,n_plus,n_1,n_H2,alfa_CR,S_CR,
                                                  nH2,n1,nplus,ne);
end;
end; {Calculation}

Procedure Iteration;
Var relax,test: float;
    s         : integer;
begin
with H_dat do
begin
  relax:=1;
  test:=relax*(ne+pop[plus+3]-pop[plus+1]-pop[plus+2])+(1-relax)*nplus;
  while test < 1e3 do
  begin
    test:=relax*(ne+pop[plus+3]-pop[plus+1]-pop[plus+2])+(1-relax)*nplus;
    relax:=relax/2;
    writeln('Decreasing relaxation factor; relax = ',relax);
  end;
  write('Relaxatiefactor = ',relax:2:6,'       ');
  s:=0;
  repeat
    writeln;
    s:=s+1; writeln(s,'th iteration step. ');
    nHmin:=pop[plus+3];
    nH3plus:=pop[plus+2];
    nplus:=relax*(ne+pop[plus+3]-pop[plus+1]-pop[plus+2])+(1-relax)*nplus;
```

```
    Calculation;
  until (Abs(nplus+pop[plus+1]+pop[plus+2]-ne-pop[plus+3])<1e4) and
        (Abs(nHmin-pop[plus+3])<1e3) and
        (Abs(nH3plus-pop[plus+2])<1e3) or (s>100);
end;
writeln(s,' iteration steps used.');
end; {Iteration}


begin {main}
  ClrScr;
  gamma0:=0;              { /s }
  gamma3:=0;              { /s }
  gamma1:=gamma3/sqrt(2); { /s }
  gamma2:=gamma3/sqrt(3); { /s }
  Te:=0.26;               { kTe in eV }
  Th:=Te;                 { eV }
  Tvib:=0.3;              { eV }
  ne:=3e17;               { m^-3 }
  n1:=1e20;               { m^-3 }
  nH2:=3e21;              { m^-3 }
  nplus:=ne;              { m^-3 }
  exponent:=6;  { factor in schaalwet r_1(p)=b_0 p_eff^(-exponent) }
  nH3plus:=1e16;          { m^-3 }
  nHmin:=1e16;            { m^-3 }

write(' Reading Hydrogen data.....');
read_atomic_data(H_dat);
writeln(' Ready.');

Calculation;
Iteration;

writeln('Calculation completed. Writing data in file res.dat.');
assign(f,'res.dat'); rewrite(f);
with H_dat do
begin
writeln(f,'Te = ',Te:0:2,' eV,  ne =',ne:10,' nH2 = ',nH2:10);
writeln(f,'Th = ',Th:0:2,' eV,  n1 =',n1:10);
writeln(f);
writeln(f,'f(v\geq4) = ',deelv);
writeln(f);
for l:=1 to (plus-1) do
writeln(f,'n_',l:2,'/g_',l:2,' =',pop[l]/g[l]:12,' n_',l:2,' =',pop[l]:12);

writeln(f,'n_+ /g_+  =',nplus/g[plus]:12,'  n_ + =',nplus:12);
writeln(f);
writeln(f,'n_H_2^+/g =',pop[plus+1]/g[plus+1]:12,' n_H_2^+=',pop[plus+1]:12);
writeln(f,'n_H_3^+/g =',pop[plus+2]/g[plus+2]:12,' n_H_3^+=',pop[plus+2]:12);
writeln(f,'n_H^-/g   =',pop[plus+3]/g[plus+3]:12,' n_H^-  =',pop[plus+3]:12);
writeln(f,'n_H_2/g   =',nH2/g[plus+4]:12,'         n_H_2  =',nH2:12);
writeln(f);
sum:=0;
for l:=1 to (plus+m) do sum:=sum+pop[l];
```

```
writeln(f,'The total particle density sum(n) is: ',sum:12);
writeln(f,'The total charge density is: '
          ,nplus+pop[plus+1]+pop[plus+2]-ne-pop[plus+3]:12,' e');
writeln(f);
writeln(f,'Recombination coefficient: a_CR = ',alfa_CR:12,'m^-3 s^-1');
writeln(f,'Ionisation coefficient:    S_CR = ',S_CR:12,'m^-3 s^-1');
writeln(f);
writeln(f,'Theoretical Saha-jump:',(2/ne)*3E27*exp(1.5*ln(Te)));
writeln(f,'Calculated Saha-jump:',(pop[plus]/g[plus])/(pop[plus-1]/g[plus-1]));
writeln(f);
for l:=1 to N_K do writeln(f,'K_[',l:2,'] =',K_mol[l]:12,'  K_rev[',l:2,'] ='
                           ,K_mol_rev[l]:12);
writeln(f);
writeln(f,'Aantal reacties A_[k]:');
writeln(f,'A_[ 1] =',deelv*pop[plus+m]*pop[plus]*K_mol[1]:12,
          ';  A_rev[ 1] =',pop[plus+1]*n1*K_mol_rev[1]:12);
writeln(f,'A_[ 2] =',deelv*pop[plus+m]*ne*K_mol[2]:12,
          ';  A_rev[ 2] =',pop[plus+3]*n1*K_mol_rev[2]:12);
writeln(f,'A_[ 3] =',pop[plus+1]*pop[plus+m]*K_mol[3]:12,
          ';  A_rev[ 3] =',n1*pop[plus+2]*K_mol_rev[3]:12);
writeln(f,'A_[ 4] =',pop[plus+1]*ne*K_mol[4]:12,
          ';  A_rev[ 4] =',pop[2]*n1*K_mol_rev[4]:12);
writeln(f,'A_[ 5] =',pop[plus+2]*ne*K_mol[5]:12,
          ';  A_rev[ 5] =',deelv*pop[plus+m]*pop[2]*K_mol_rev[5]:12);
writeln(f,'A_[ 6] =',pop[plus+2]*ne*K_mol[6]:12,
          ';  A_rev[ 6] =',n1*n1*n1*K_mol_rev[6]:12);
writeln(f,'A_[ 7] =',pop[plus]*pop[plus+3]*K_mol[7]:12,
          ';  A_rev[ 7] =',n1*pop[2]*K_mol_rev[7]:12);
writeln(f,'A_[ 8] =',pop[plus+3]*ne*K_mol[8]:12,
          ';  A_rev[ 8] =',n1*ne*ne*K_mol_rev[8]:12);
writeln(f,'A_[ 9] =',pop[plus]*pop[plus+3]*K_m
          ';  A_rev[ 9] =',n1*pop[3]*K_mol_rev[9]:12);
writeln(f,'A_[10] =',pop[plus+3]*n1*K_mol[10]:12,
          ';  A_rev[10] =',n1*n1*ne*K_mol_rev[10]:12);
writeln(f,'A_[11] =',pop[plus+3]*pop[plus+2]*K_mol[11]:12,
          ';  A_rev[11] =',pop[plus+m]*pop[plus+m]*K_mol_rev[11]:12);
writeln(f);

{ Calculation of the coeficients b=n/n^S and \delta b=b-1. }
{ array nS[p] will be filled with the calculated Saha densities. }

for l:=1 to plus-1 do
nS[l]:=saha_dens(g[l],g[plus],E[plus],E[l],Te,ne,nplus);

for l:=1 to plus-1 do
writeln(f,'b_',l:2,' = ',pop[l]/nS[l],' db_',l:2,' = ',pop[l]/nS[l]-1);

end;
  close(f);
  writeln;
  writeln('Ready.');
end.
```

Appendix C

The listings of the flow model

C.1 Runge-Kutta integration

This is the program that contains a fourth order Runge-Kutta integration. We start with a differential equation

$$\frac{dy}{dx} = f(x, y) \text{ with } y(x_0) = y_0 \tag{C.1}$$

with y_0 the start value. y_{n+1} follows from:

$$y_{n+1} = y_n + hf(\xi_n, y(\xi_n)) \ . \tag{C.2}$$

where h is the step size and $\xi_n \in \{x_n, x_{n+1}\}$. The problem is that both ξ_n and $y(\xi_n)$ are unknown. Now, we take some "measurements" with various ξ's from $\{x_n, x_{n+1}\}$. With the resulting value of y_{n+1}'s we calculate the final value of y_{n+1}. With a 4th order Runge-Kutta method this becomes:

$$y_{n+1} = y_n + \tfrac{1}{6}k_1 + \tfrac{1}{3}k_2 + \tfrac{1}{3}k_3 + \tfrac{1}{6}k_4 + \mathcal{O}(h^5) \ . \tag{C.3}$$

with

$$k_1 = hf(x_n, y_n) \tag{C.4}$$
$$k_2 = hf(x_n + \tfrac{1}{2}h, y_n + \tfrac{1}{2}k_1) \tag{C.5}$$
$$k_3 = hf(x_n + \tfrac{1}{2}h, y_n + \tfrac{1}{2}k_2) \tag{C.6}$$
$$k_4 = hf(x_n + h, y_n + k_3) \tag{C.7}$$

with h the internal step size.

C.2 Discretisation error

When we discretize a quantity F with the previous method, the following equation holds [18]:

$$F = G(h) + R(h) \ . \tag{C.8}$$

Here, $G(h)$ is the approximation for F with step size h. $R(h)$ is the discretization error, and can be represented with the following power series:

$$R(h) = \sum_{m=1}^{\infty} c_m h^m \ . \tag{C.9}$$

If the discretization error is of order p, then we have $c_m = 0 \forall m < p$, $c_p \neq 0$, so $R(h) = \sum_{m=p}^{\infty} c_m h^m$.

If we halve the step size, we have

$$F = G(h) + R(h) = G(\tfrac{1}{2}h) + R(\tfrac{1}{2}h) \ . \tag{C.10}$$

If $|c_{p+1}| \ll |c_p|$ it can approximately be said that $R(h) = 2^p R(\frac{1}{2}h)$. When we substitute this in equation C.10, we receive

$$R(\tfrac{1}{2}h) = \frac{1}{2^p - 1}(G(\tfrac{1}{2}h) - G(h)) \ . \tag{C.11}$$

Now, we can estimate the error in G. This requires, however, that $|c_{p+1}| \ll |c_p|$. Consider quotient of the following differentiations:

$$\frac{G(\frac{1}{2}h) - G(h)}{G(\frac{1}{4}h) - G(\frac{1}{2}h)} = \frac{R(h) - R(\frac{1}{2}h)}{R(\frac{1}{2}h) - R(\frac{1}{4}h)} = 2^p \frac{c_p + c^*_{p+1}h + \cdots}{c_p + \frac{1}{2}c^*_{p+1}h + \cdots} \tag{C.12}$$

with

$$c^*_{p+1} = \frac{2^{p+1}}{2(2^p - 1)} c_{p+1}$$

so c^*_{p+1} has the same order of magnitude as c_{p+1}. If the left-hand side of equation C.12 is close to 2^p, then the condition $|c_{p+1}| \ll |c_p|$ holds and equation C.11 is a good estimation of the discretization error.

It turned out, however, that the model was numerically unstable. The reason of this instabillity in unknown.

C.3 Unit RK4_N.INC

This is the unit in which the 4th order Runge-Kutta integration is implemented.

```
Procedure rk4_n(n:integer; Var x:float; Var y:TNvector;
                d:float;   Var h:float);

{The function to be integrated is rechterlid(x,y,i)}

Var v, k1, k2, k3, k4  : TNvector;
    H2, U              : float;
    i,j, internal_steps: integer;

begin
  internal_steps:=round(abs(d/h)); {number of internal steps}
  for j:=1 to internal_steps do
  begin
    gotoXY(whereX,18);
    write(chr(205))
  end;
  gotoXY(1,18);
  U:=x;
  H2:=h/2;
  for j:=1 to internal_steps do
  begin
    gotoXY(whereX,18); write(chr(254));
    for i:=1 to N do
    begin
      v[i]:=y[i];
      k1[i]:=h*rechterlid(x,y,i);
    end;
    x:=x+H2;
    for i:=1 to n do y[i]:=v[i]+k1[i]/2;
    for i:=1 to n do k2[i]:=h*rechterlid(x,y,i);
    for i:=1 to n do y[i]:=v[i]+k2[i]/2;
    for i:=1 to n do k3[i]:=h*rechterlid(x,y,i);
    x:=x+H2;
    for i:=1 to n do y[i]:=v[i]+k3[i]/2;
    for i:=1 to n do k4[i]:=h*rechterlid(x,y,i);
    for i:=1 to n do y[i]:=v[i]+(k1[i]+2*(k2[i]+k3[i])+k4[i])/6;
```

```
    x:=U+j*h;
  end;
end;
```

C.4 HFLOW.PAS

```
Program HFLOW(Input,Output);
{$M 65520,0,655360}
{$N+,E-}

{*****************************************************************}
{    Model van een expanderend, chemisch actief cascadeboogplasma  }
{    bestaande uit puur waterstof. De vergelijkingen zijn eerste   }
{    orde differentiaalvergelijkingen (totaal zeven).              }
{    # dnHplus/dz                                                  }
{    # dnH/dz                                                      }
{    # dnH2/dz                                                     }
{    # dne/dz                                                      }
{    # du/dz                                                       }
{    # dTh/dz                                                      }
{    # dTe/dz                                                      }
{    De variabelen zijn:                                          }
{    nHplus : de waterstof ion dichtheid                          }
{    nH     : de atomaire waterstof dichtheid                     }
{    nH2    : de moleculaire waterstof dichtheid                  }
{    ne     : de electronendichtheid                              }
{    u      : de snelheid van het plasma                          }
{    Th     : de zware deeltjes temperatuur in eV                 }
{    Te     : de electronen temperatuur in eV                     }
{    De brontermen van de vergelijkingen zijn:                    }
{    SHplus de bronterm voor Hplus produktie-destruktie           }
{    SH     ,,    ,,     ,,  H     ,,        ,,                  }
{    SH2    ,,    ,,     ,,  H2    ,,        ,,                  }
{    Se     ,,    ,,     ,,  e     ,,        ,,                  }
{    Qh     ,, energie bronterm voor de zware deeltjes           }
{    Qe     ,,    ,,      ,,     ,,  ,, electronen               }
{                                                                 }
{    vergelijkingen:  - massabalans electronen                    }
{                     - massbalansen H, Hplus, H2                 }
{                     - energiebalans electronen                  }
{                     - energiebalans zware deeltjes              }
{                     - totale opgetelde impulsbalans             }
{    de vgl worden numeriek opgelost (m.b.v. Runge Kutta)         }
{                                                                 }
{    Opmerking: stroomgeneratie en warmtegeleiding worden         }
{    verwaarloosd                                                 }
{*****************************************************************}

Uses Crt, Matrix, Atom_def, Read_H, NewSolv;

Const
  k_Boltz = 1.38066e-23;    {Boltzmann's constant}
  me = 9.1095e-31;          {Mass of an electron}
```

```
  mAr = 6.6817e-26;         {Mass of an Argon atom}
  mH = mAr/40;              {Mass of a hydrogen atom}
  q_el = 1.6021892e-19;     {Elementary charge}
  eps_dielec = 8.8542e-12;  {Dielectrical constant}
  el_factor = 1.44e-9;      {e/(4\pi\epsilon_0)}
  Sahaconst = 2.414721e+21; {Numerical constant in Saha relation}
  gammaH  = 5/3;            {Cp/Cv atomic hydrogen}
  gammaH2 = 7/5;            {Cp/Cv molecular hydrogen}
  a1 = 1/(gammaH-1);
  a2 = 1/(gammaH2-1);
  orde_RKn = 7;             {Number of flow equations}
  n_norm = 1e20;            {Normalized density=1e20/m3}
  {necessary in order to obtain stable LU decomposition}

Var
  ax_pos, p, ne, nH, nHplus, nH2, u, Th, Te, Tvib, straal,
  nHmin, nH2plus, nH3plus, nu            : float;
  pi,start_ne, start_nH, start_nHplus, start_nH2, start_p, start_Te,
  start_Th, start_u, r_start, tan_alfa, p_back, flow, part_s,
  D_ambip, x_eind                        : real;
  k, l, m                                : integer;
  y, v, s                                : TNvector;
  A, B                                   : TNmatrix;
  error                                  : byte;
  x, d, h, dummy                         : float;
  data_out, data_in, data_control        : text;
  H_dat                                  : atomic_data;
  SH,Se,SHplus,SH2,Qe,Qh                 : float;
  pop                                    : float_level_arr;
  Aantal                                 : array[1..2,1..11] of float;
  Diff                                   : array[1..11] of float;
  Test_result: byte; { Used in Turbo Pascal 7.0 to detect }
                     { a 386 or 486 and use 32 bits code. }

Function Coulomb_log(ne,Te: float): float; {ne in /m^3, Te in eV}
begin
Coulomb_log:=ln((12*pi*(eps_dielec*q_el*Te)*sqrt(eps_dielec*q_el*Te))/
               (q_el*q_el*q_el*sqrt(ne)));
end;

Procedure CRmodel(Var pop: float_level_arr);
Var exponent,Tvib,alfa_CR,S_CR,nHmin,nH3plus,
    gamma0,gamma1,gamma2,gamma3,deelv   : float;
    n_plus,n_1,n_H2,K_rate3             : float_level_arr;
    Total_Matrix,A_mat,K_rate           : float_level_arr_2dim;
    K_mol,K_mol_rev                     : K_arr;

Procedure Calculation(Var pop: float_level_arr);
begin
  Tvib:=0.3;
  nHmin:=1e17;
  nH3plus:=1e17;
  exponent:=6;
  with H_dat do
```

```
  begin
    Calc_Matrix(H_dat,ne,nHplus,nH,nH2,Te,Th,Tvib,deelv,Total_Matrix,
                K_rate,K_rate3,A_mat,K_mol,K_mol_rev,exponent,nHmin,
                nH3plus,gamma1,gamma2,gamma3);
    Calc_stat(n,m,plus,Total_Matrix,pop,n_plus,n_1,n_H2,alfa_CR,S_CR,
              nH2,nH,nHplus,ne);
  end;
end; {Calculation}

Procedure Iteration;
Var relax                   : float;
    test                    : float;
    dummyplus,dummyH,dummye: float;
    nu_ei,nu_eH,nu_eH2      : float;
    i,j                     : integer;
begin
  with H_dat do
  begin
    relax:=1;
    test:=relax*(ne+pop[plus+3]-pop[plus+1]-pop[plus+2])+(1-relax)*nHplus;
    while test < 1e3 do
    begin
      test:=relax*(ne+pop[plus+3]-pop[plus+1]-pop[plus+2])+(1-relax)*nHplus;
      relax:=relax/2;
      gotoXY(50,12);
      writeln('Decreasing relaxation factor; relax = ',relax);
    end;
    gotoXY(10,14);
    write('Relaxatiefactor = ',relax:2:6,'   ');
    i:=0;
    repeat
      writeln;
      i:=i+1;
      gotoXY(10,12);
      writeln(i,'th iteration step. ');
      nHmin:=pop[plus+3];
      nH3plus:=pop[plus+2];
      nHplus:=relax*(ne+pop[plus+3]-pop[plus+1]-pop[plus+2])
              +(1-relax)*nHplus;
      Calculation(ne,nHplus,nH,nH2,pop);
    until (Abs(nHplus+pop[plus+1]+pop[plus+2]-ne-pop[plus+3])<1e5) and
   (Abs(nHmin-pop[plus+3])<1e4) and (Abs(nH3plus-pop[plus+2])<1e4) or (i>10);
  for j:=1 to (plus+3) do if pop[j]<0 then pop[j]:=0;

  Aantal[1, 1] := deelv*pop[plus+m]*pop[plus]*K_mol[1];
  Aantal[2, 1] := pop[plus+1]*nH*K_mol_rev[1];
  Aantal[1, 2] := deelv*pop[plus+m]*ne*K_mol[2];
  Aantal[2, 2] := pop[plus+3]*nH*K_mol_rev[2];
  Aantal[1, 3] := pop[plus+1]*pop[plus+m]*K_mol[3];
  Aantal[2, 3] := nH*pop[plus+2]*K_mol_rev[3];
  Aantal[1, 4] := pop[plus+1]*ne*K_mol[4];
  Aantal[2, 4] := pop[2]*nH*K_mol_rev[4];
  Aantal[1, 5] := pop[plus+2]*ne*K_mol[5];
  Aantal[2, 5] := deelv*pop[plus+m]*pop[2]*K_mol_rev[5];
```

```
  Aantal[1, 6] := pop[plus+2]*ne*K_mol[6];
  Aantal[2, 6] := nH*nH*nH*K_mol_rev[6];
  Aantal[1, 7] := pop[plus]*pop[plus+3]*K_mol[7];
  Aantal[2, 7] := nH*pop[2]*K_mol_rev[7];
  Aantal[1, 8] := pop[plus+3]*ne*K_mol[8];
  Aantal[2, 8] := nH*ne*ne*K_mol_rev[8];
  Aantal[1, 9] := pop[plus]*pop[plus+3]*K_mol[9];
  Aantal[2, 9] := nH*pop[3]*K_mol_rev[9];
  Aantal[1,10] := pop[plus+3]*nH*K_mol[10];
  Aantal[2,10] := nH*nH*ne*K_mol_rev[10];
  Aantal[1,11] := pop[plus+3]*pop[plus+2]*K_mol[11];
  Aantal[2,11] := pop[plus+m]*pop[plus+m]*K_mol_rev[11];
  for j:=1 to 11 do Diff[j]:=Aantal[1,j]-Aantal[2,j];

{SHplus}
dummyplus:=0; {Atomic mass terms for Hydrogen atoms}
for j:=1 to (plus-1) do dummyplus:=dummyplus+
                        ne*pop[j]*K_rate[j,plus]-ne*ne*nHplus*K_rate3[j]+
                        ne*nHplus*(K_rate[plus,j]-K_rate3[j]);
SHplus:=-Diff[7]-Diff[9]+dummyplus;

{SH}
dummyH:=-dummyplus; {Atomic mass terms for protons}
SH:=Diff[1]+Diff[2]+Diff[3]+Diff[4]+3*Diff[6]+Diff[7]+Diff[8]+Diff[9]+
    2*Diff[10]+dummyH;

{SH2}
SH2:=2*Diff[11];

{Se}
dummye:=dummyplus; {Atomic mass terms for electrons}
Se:=-Diff[4]-Diff[5]-Diff[6]+Diff[8]+Diff[10]+dummye;

{Qh}
nu_ei:=(4/3)*sqrt(2*pi)*sqr(q_el*el_factor/me)*power(me/(q_el*Te),3/2)*
       nHplus*Coulomb_log(ne,Te);          {Proefschr. D.A. Benoy, p 85}
nu_eH:=1e-18*nH*power(3*q_el*Te/me,0.3);   {Inleiding plasmafysica H.2}
nu_eH2:=1e-18*nH2*power(3*q_el*Te/me,0.3); {Inleiding plasmafysica H.2}
Qh:=1.5*ne*q_el*(Te-Th)*(2*me/mH)*(nu_ei+nu_eH+0.5*nu_eH2);

{Qe}
Qe:=-Qh;
end; {with H_dat do}
gotoXY(10,16);
writeln(i,' iteration steps used.');
end; {Iteration}

begin {CRmodel}
  Qe:=0; QH:=0; SH:=0; SHplus:=0; SH2:=0; Se:=0;
  ne:=n_norm*ne; nHplus:=n_norm*nHplus;
  nH:=n_norm*nH; nH2:=n_norm*nH2;
  Calculation(pop);
  Iteration;
  ne:=ne/n_norm; nHplus:=nHplus/n_norm;
```

```
  nH:=nH/n_norm; nH2:=nH2/n_norm;
end;  {CRmodel}


Function Rechterlid(x: float; Var y: TNvector; i: integer):float;

{ rechterlid van het stelsel d.v.'s }
{ betekenis parameters: y[1]=nHplus }
{                       y[2]=nH     }
{                       y[3]=nH2    }
{                       y[4]=ne     }
{                       y[5]=u      }
{                       y[6]=Th     }
{                       y[7]=Te     }

Var pp,nee,nHH,nHHplus,nHH2,uu,Thh,Tee,
    MM_2,A_factor: float;
    ii,jj,kk: integer;

begin
  nHHplus:=y[1];
  nHH:=y[2];
  nHH2:=y[3];
  nee:=y[4];
  uu:=y[5];
  Thh:=y[6];
  Tee:=y[7];
  A_factor:=2.0*tan_alfa/straal;
  with H_dat do
  begin

  {Uitrekenen matrix A en bronvector S}
  for ii:=1 to orde_RKn do
  begin
    s[ii]:=0;
    v[ii]:=0;
    for jj:=1 to orde_RKn do
    begin
      A[ii,jj]:=0;
      B[ii,jj]:=0;
    end;
  end;

  A[1,1]:=uu; A[1,5]:=nHHplus;
  A[2,2]:=uu; A[2,5]:=nHH;
  A[3,3]:=uu; A[3,5]:=nHH2;
  A[4,4]:=uu; A[4,5]:=nee;
  A[5,1]:=k_Boltz*Thh; A[5,2]:=k_Boltz*Thh; A[5,3]:=k_Boltz*Thh;
   A[5,4]:=k_Boltz*Tee; A[5,5]:=mh*uu*(2*nHH2+nHH+nHHplus)*k_Boltz;
   A[5,6]:=(nHH+nHH2+nHHplus)*k_Boltz; A[5,7]:=nee*k_Boltz;
  A[6,1]:=k_Boltz*Thh*uu*a1; A[6,2]:=k_Boltz*Thh*uu*a1;
   A[6,3]:=k_Boltz*Thh*uu*a2;
   A[6,5]:=((1+a1)*(nHH+nHHplus)+(1+a2)*nHH2)*uu*k_Boltz;
   A[6,6]:=(a1*(nHH+nHHplus)+a2*nHH2)*uu*k_Boltz;
```

```
  A[7,4]:=k_Boltz*Tee*uu*a1;
   A[7,5]:=(1+a1)*nee*k_Boltz*Tee;
   A[7,7]:=a1*nee*uu*k_Boltz;

  S[1]:=SHplus-nHHplus*uu*A_factor;
  S[2]:=SH-nHH*uu*A_factor;
  S[3]:=SH2-nHH2*uu*A_factor;
  S[4]:=Se-nee*uu*A_factor;
  S[5]:=0;
  S[6]:=Qh-((1+a1)*(nHH+nHHplus)+(1+a2)*nHH2)*k_Boltz*Thh*uu*A_factor;
  S[7]:=Qe-(1+a1)*nee*k_Boltz*Tee*uu*A_factor;
  {Matrix A en bronvector S zijn bekend, nu door invertering rechterlid}

  Inverse(orde_Rkn,A,B,error); {berekening inverse A}
  if error=2 then writeln('Inverse matrix error.')
  else if error=1 then writeln('Matrix dimension error.');

  for ii:=1 to orde_RKn do
  begin
    v[ii]:=0.0;
    for jj:=1 to orde_RKn do
    begin
      v[ii]:=v[ii]+B[ii,jj]*S[jj];
    end;
  end;

  {v =M^(-1)*s te berekenen}
  {inverse_A;  v=inverse_A*s;}
  case i of 1: rechterlid:=v[1];
            2: rechterlid:=v[2];
            3: rechterlid:=v[3];
            4: rechterlid:=v[4];
            5: rechterlid:=v[5];
            6: rechterlid:=v[6];
            7: rechterlid:=v[7];
  end;
  end; {H_dat}
end; {rechterlid}

{$I RK4_N.INC}


begin {Main program}
CheckSnow:=false;
TextColor(LightGreen);
TextBackGround(Black);
ClrScr;

Test_result:=Test8086;
case test_result of
  0: writeln('8086 processor detected.');
  1: writeln('80286 processor detected.');
  2: writeln('80386, 80486 or Pentium processor detected.');
end;
```

```
assign(data_out,'HFLOW.DAT');
rewrite(data_out);
write(data_out,'#ax_pos   nHplus       nH    nH2    ');
write(data_out,' ne       flux         u (m/s)      ');
writeln(data_out,'Th (eV)  Te (eV) nH2+     nH3+      nH-');

{ x_eind  : eindpositie                                  }
{ d       : de stapgrootte                               }
{ p_back  : achtergronddruk (Pa)                         }
{ flow    : spreekt voor zich  (l/min)                   }
{ r_start : de beginwaarde van de straal van het plasma  }
{ tan_alfa: de tangens van de expansie hoek              }
{ de rest : spreekt voor zich                            }

pi:=4*arctan(1);
x_eind:=0.005;
d:=5e-4; {External stepsize of Runge-Kutta}
h:=d/20; {Internal stepsize of Runge-Kutta}
p_back:=40;
flow:=3500;
r_start:=5e-2;

start_ne:=1e19/n_norm;
start_nHplus:=1e19/n_norm;
start_nH:=1e20/n_norm;
start_nH2:=7e20/n_norm;
start_u:=1000;
start_Te:=0.3; {eV}
start_Th:=0.3; {eV}

nHplus:=start_nHplus;
nH:=start_nH;
nH2:=start_nH2;
ne:=start_ne;
u:=start_u;
Th:=start_Th;
Te:=start_Te;

y[1]:=start_nHplus;
y[2]:=start_nH;
y[3]:=start_nH2;
y[4]:=start_ne;
y[5]:=start_u;
y[6]:=start_Th;
y[7]:=start_Te;

p:=k_Boltz*((start_nHplus+start_nh+start_nH2)*start_Th+start_ne*start_Te)
   *N_Norm*k_Boltz/q_el;
x:=0.002;
ax_pos:=x;

straal:=r_start;
nu:=(4/3)*sqrt(2*pi)*sqr(q_el*el_factor)*power(me/(q_el*Te),3/2)*
```

```
     nHplus*Coulomb_log(ne,Te)/(me*mH);
D_ambip:=q_el*(Te+Th)/(mH*nu);
tan_alfa:=2*D_ambip/(u*straal);

Read_atomic_data(H_dat);
with H_dat do
begin

CRmodel(pop);
write(data_out,ax_pos:1:5,'  ',nHplus:12,'  ',nH:12,'  ',nH2:12,' ');
write(data_out,ne:12,'  ',u*pi*sqr(straal)*(nHplus+ne+2*nH2):12,' ');
write(data_out,u:12,'  ',Th:0:3,'    ',Te:0:3,'  ');
writeln(data_out,pop[plus+1]:12,' ',pop[plus+2]:12,' ',pop[plus+3]:12);

  while x < x_eind do
  begin
    gotoXY(15,10);
    TextBackGround(LightGray);
    TextColor(Red);
    writeln('  x = ',x:1:5,'  ');
    TextBackGround(Black);
    TextColor(LightGreen);
    nu:=(4/3)*sqrt(2*pi)*sqr(q_el*el_factor)*power(me/(q_el*Te),3/2)*
        nHplus*Coulomb_log(ne,Te)/(me*mH);
    D_ambip:=q_el*(Te+Th)/(mH*nu);
    tan_alfa:=2*D_ambip/(u*straal);
    straal:=straal+d*tan_alfa;
    gotoXY(1,18); ClrEol;
    RK4_N(orde_RKn,x,y,d,h);
    CRmodel(pop);
    ax_pos:=x;
    nHplus:=y[1];
    nH:=y[2];
    nH2:=y[3];
    ne:=y[4];
    u:=y[5];
    Th:=y[6];
    Te:=y[7];
    p:=k_Boltz*((pop[plus+1]+pop[plus+2]+pop[plus+3]+nHplus+nH+nH2)
                *Th+ne*Te)*N_Norm*k_Boltz/q_el;

    write(data_out,ax_pos:1:5,'  ',nHplus:12,'  ',nH:12,'  ',nH2:12,'  ');
    write(data_out,ne:12,'  ',u*pi*sqr(straal)*(nHplus+ne+2*nH2):12,'  ');
    write(data_out,u:12,'  ',Th:0:3,'    ',Te:0:3,'  ');
    writeln(data_out,pop[plus+1]:12,' ',pop[plus+2]:12,' ',pop[plus+3]:12);
  end;
end;
close(data_out);
close(data_control);
gotoXY(1,20);
end.
```

Appendix D

The positioning system

D.1 Basic setup of the positioning system

The positioning of the optical system with respect to the window of the vacuum vessel is adjusted with a platform which can move over 2 translation rails. The movement is achieved by pressured air. The pressured air can escape via 6 switches, of which 2 are used for the horizontal movement, 2 for the vertical movement and 2 brakes to maintain a position. When, for example, the left horizontal switch is open en the right one is closed, the pressered air will push the platform from the right to the left. When the switches are open they use an electrical current of 24 V and 0.3 A. This current is regulated with 6 solid state relais, which on their turn are controlled by a computer generating TTL pulses. The numbering and meaning of the switches is given in figure D.1.

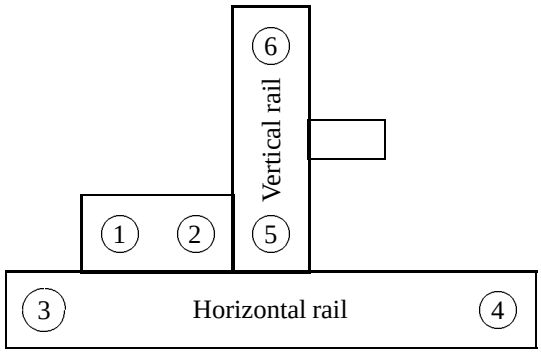

1	Vertical brake	4	Movement left
2	Horizontal brake	5	Movement up
3	Movement right	6	Movement down

Figure D.1: The placement and numbering of the switches on the positioning system.

D.2 Electrical diagram of the pressured air control

The positioning system is made up for by the electronic scheme which is given in figure D.2. The transistors are needed to convert the TTL pulses generated by the computer into pulses which can be used by the OPTO 22 solid state relais. If they were not used, the solid state relais would demand too much current from the PC-lab card, which could get damaged.

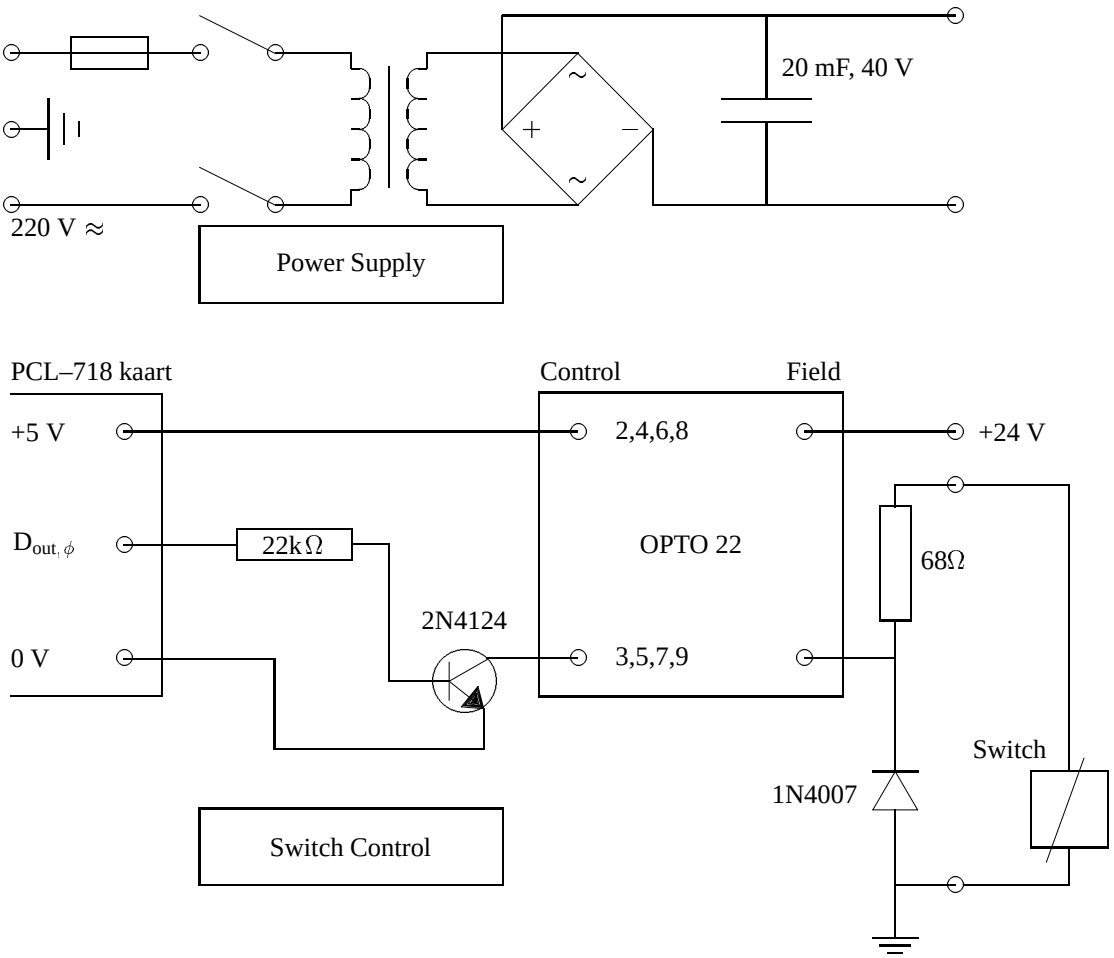

Figure D.2: The electrical control for the pressured-air switches.

There are 6 OPTO 22 switches used, so also 6 D_{out} lines from the PCL-718 card are needed. They are connected on connector CN(3) (Digital out) on pin 0 to 5.

D.3 Electrical diagram of the position measurement

For the measurement of the position, the electronic setup given in figure D.3 was used. To simplify the setup, one (double) cable is laid from the reference voltage supply to the positioning system, and one from the reference voltage supply to the computer. To achieve this, the plugs are internally cross-linked:

Con 1			Con 2		Computer
1	+ ref		1	nc	
2	0 V	↔	2	↔	0 V
3	nc		3	nc	
4	S1	↔	4	↔	S1
5	S2	↔	5	↔	S2

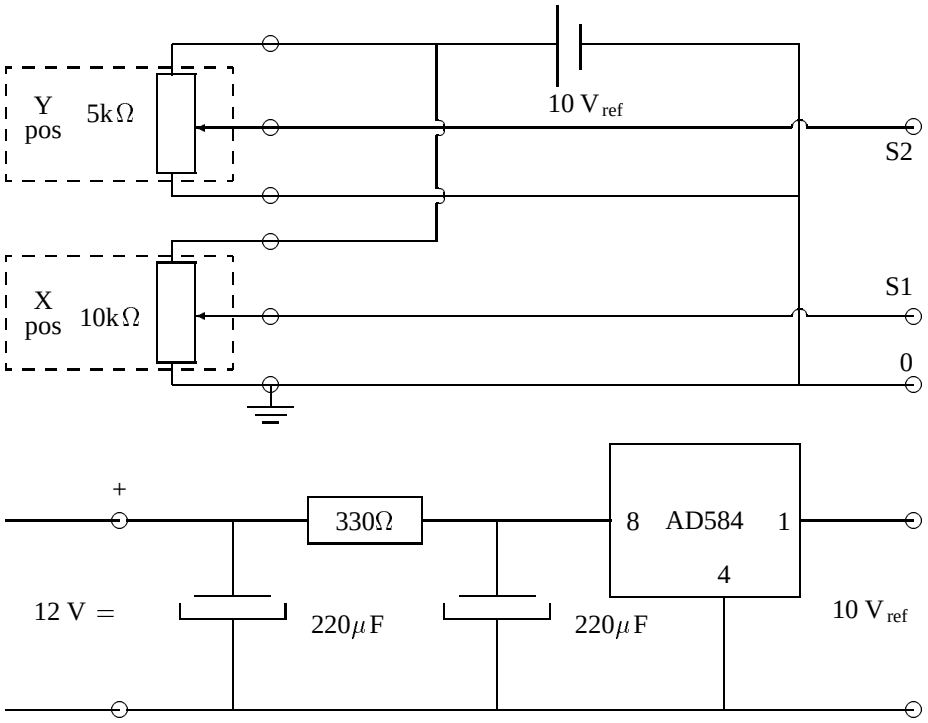

Figure D.3: The electrical setup for the position measurement.

D.4 Position install program

The positioning is regulated with a program from which the basic setup is given below. Unit `Move` contains the procedures and functions to measure the position and to control the pressured air. The main program is an example of how to use unit `MOVE`. The procedures in unit `MOVE` are integrated into a program that also controls the step engine of the monochromator and the readout of the photomultiplier.

Unit Move

```
Unit Move;

Interface

Type  coord_array = array[0..1] of real;
Var   coordinate: coord_array;

Procedure Read_position(Var coordinate:coord_array);
Procedure Set_position(posX,posY:real);

Implementation

Uses Crt;
```

```
Const
  Base           = $300;     {Base adress of the PCL-718 card}
  X_scale_factor = 0.02488;  {Factors to convert the A/D readout to cm}
  Y_scale_factor = 0.01246;
  Y_brake_up     = 0.43;     {Factors to compensate for the brake time}
  Y_brake_down   = 0.25;
  X_brake_right  = 0.33;
  X_brake_left   = 0.20;
  Error          = 0.25;     {Maximal allowed error in the position in cm}
Var
  sw1,sw2,sw3,sw4,sw5,sw6: boolean;
  posX,posY              : integer;

Procedure Init_ADC;
var
   test     : byte;
   msb, lsb : byte;
   uitlezing: integer;
begin
   port[base+9]:=$70;
   test:=port[base+9];
   if test <> $70
   then
   begin
     writeln ('PCL-718 Hardware verification failed!');
     readln;
     exit
   end;
   port[base+8]:=$1;   { clear interrupt request }
   port[base+2]:=$10;  { set MUX-range: channel 0 to 1}
   test:=port[base+2];
   if test <> $10
   then
   begin
     writeln('Set scan channel failed!');
     readln;
     exit
   end
end;   { end initialization }

Function ad_conversion: word;
Var msb, lsb: word;
begin
   port[base]:=$0;
     repeat until ((port[Base + 8] AND (1 SHL 7)) = $0);
          { A/D status register, end of conversion }
   lsb:=port[base];
   msb:=port[base+1];
   ad_conversion:=msb*16+lsb div 16;
end;

Procedure read_position(Var coordinate:coord_array);
Const average = 25;
Var i    : integer;
```

```
    dummy: longint;
begin
  dummy:=0;
  port[base+2]:=$55;          { Select X-input channel: CN3-5 }
  for i:=1 to average do dummy:=dummy+4095-ad_conversion;
  coordinate[0]:=(dummy/average)*X_scale_factor;
  dummy:=0;
  port[base+2]:=$66;          { Select Y-input channel: CN3-6 }
  for i:=1 to average do dummy:=dummy+ad_conversion;
  coordinate[1]:=(dummy/average)*Y_scale_factor;
end;

Procedure set_switches(sw1,sw2,sw3,sw4,sw5,sw6: boolean);
Var teller: byte;
begin
{ Switches 1 to 6 are connected with pin 0 to 6 from CN3 (D_out) }
  teller:=0;
  if sw1=true then teller:=teller+1;
  if sw2=true then teller:=teller+2;
  if sw3=true then teller:=teller+4;
  if sw4=true then teller:=teller+8;
  if sw5=true then teller:=teller+16;
  if sw6=true then teller:=teller+32;
  port[base+3]:=teller;
end;

Procedure Right;
begin
  sw1:=true; sw2:=false; sw3:=false;
  sw4:=true; sw5:=false; sw6:=false;
  set_switches(sw1,sw2,sw3,sw4,sw5,sw6); {Brake X OFF, Y ON, move X}
end;

Procedure Left;
begin
  sw1:=true; sw2:=false; sw3:=true;
  sw4:=false; sw5:=false; sw6:=false;
  set_switches(sw1,sw2,sw3,sw4,sw5,sw6); {Brake X OFF, Y ON, move X}
end;

Procedure Up;
begin
  sw1:=false; sw2:=true; sw3:=false;
  sw4:=false; sw5:=false; sw6:=true;
  set_switches(sw1,sw2,sw3,sw4,sw5,sw6); {Brake Y OFF, X ON, move Y}
end;

Procedure Down;
begin
  sw1:=false; sw2:=true; sw3:=false;
  sw4:=false; sw5:=true; sw6:=false;
  set_switches(sw1,sw2,sw3,sw4,sw5,sw6); {Brake Y OFF, X ON, move Y}
end;
```

```
Procedure Brake;
begin
  sw1:=true; sw2:=true; sw3:=false;
  sw4:=false; sw5:=false; sw6:=false;
  set_switches(sw1,sw2,sw3,sw4,sw5,sw6); { All brakes on }
end;

Procedure Set_hor_position(posX:real);
Begin
  Init_ADC;
  Read_position(coordinate);

  if (posX - coordinate[0] > 0) then
  begin
    Right;
    repeat
      Read_position(coordinate);
    until ((posX-coordinate[0]) <= X_brake_right);
    Brake;
  end
  else if (posX - coordinate[0] < 0) then
  begin
    Left;
    repeat
      Read_position(coordinate);
    until ((posX-coordinate[0]) >= -X_brake_left);
    Brake;
  end;
end;

Procedure Set_ver_position(posY:real);
Begin
  if (posY - coordinate[1] < 0) then
  begin
    Down;
    repeat
      Read_position(coordinate);
    until ((posY-coordinate[1]) >= Y_brake_down);
    Brake;
  end
  else if (posY - coordinate[1] > 0) then
  begin
    Up;
    repeat
      Read_position(coordinate);
    until ((posY-coordinate[1]) <= Y_brake_up);
    Brake;
  end;
  delay(200);
end;

Procedure Set_position(posX,posY:real);
begin
  Read_position(coordinate);
```

```
  { Achieve a defined distance of the wanted    }
  { distance to receive a constant brake length }

  if (Abs(posX - coordinate[0]) > Error) then
  begin
    Set_hor_position(posX-1);
    Set_hor_position(posX);
  end;
  if (Abs(posY - coordinate[1]) > Error) then
  begin
    Set_ver_position(posY-1);
    Set_ver_position(posY);
  end;
end;

end.
```

Program SetPos

```
Program Setpos(input,output);
Uses Crt, Move;
Label 10, 20;

Var i         : integer;
    posX,posY : real;
    coordinate: coord_array;
    key       : char;

begin
10:
begin
  Clrscr;
  Read_Position(coordinate);
  writeln('Current position:');
  writeln('X =',coordinate[0]:4:2,' cm, Y =',coordinate[1]:4:2,' cm');
  write('Which position do you want? X-coordinate: ');
  readln(posX);
  write('                            Y-coordinate: ');
  readln(posY);
  Set_Position(posX,posY);
  Read_position(coordinate);
  writeln('The current position is:');
  writeln('X =',coordinate[0]:4:2,' cm, Y =',coordinate[1]:4:2,' cm');
end;

20:
begin
  writeln('Do you want another position? (y/n)');
  key:=upcase(readkey);
  if key = 'Y' then goto 10 else
```

```
  begin
    if key <> 'N' then writeln('Incorrect choise !') else exit;
    goto 20;
  end;
end;

end.
```

References

[1] B. van der Sijde, *Inleiding plasmafysica*, lecture thesis, TUE 1989.

[2] D.A. Benoy, J.A.M. van der Mullen, B. van der Sijde, D.C. Schram. J. Quant. Spectrosc. Radiat. Transfer Vol 46, p. 195, 1991.

[3] L. Vriens, A.H. Smeets, Phys. Rev. A, Vol 22, 1980.

[4] W.L. Wiese, M.W. Smith, B.M. Glennon, *Atomic Transition Probabilities*, Volume I, NSDRS-NBS 4, Washinton DC, 1966.

[5] H.C.W. Beijerinck, *Thermische Verschijnselen*, lecture theses, TUE 1989.

[6] M.C.M. van de Sanden, *The expanding plasma jet: experiments and model*, Ph.D. thesis, TUE 1991.

[7] M.J. de Graaf, R.P. Dahiya, J.L. Jauberteau, F.J. de Hoog, M.J.F. van de Sande and D.C. Schram, Colloque de Physique C5, 1990, 387-392.

[8] Jeroen Nijs, *Spectroscopy setup for an expanding cascaded arc plasma*, TUE report VDF/NT 91-14, TUE 1991.

[9] G. Herzberg, *Molecular Spectra and Molecular Structure*, p.122-124, New York, 1950.

[10] R.K. Janev, W.D. Langer, K. Evans, D.E. Post, *Elementary Processes in Hydrogen-Helium Plasmas*, Springer-Verlag Berlin-Heidelberg, 1987.

[11] F.T.H. den Hartog, *Dichtheden van negatieve waterstofionen in een RF-plasma*, graduate thesis, TUE 1992.

[12] J.A.M. van der Mullen, Physics Reports, Vol 191 Nrs. 2 & 3, 1991.

[13] D.A. Benoy, *Modelling of Thermal Argon Plasmas*, Ph.D. thesis, TUE 1993.

[14] V.M. Lelevkin, D.K. Otorbaev, D.C. Schram, *Physics of Non-Equilibrium plasmas*, Elsevier Science Publishers B.V., 1992.

[15] R. van den Bercken & J. van Broekhoven, *Abelinversie door middel van filtered backprojection.* Internal report VDF/NT 91-06.

[16] J.A.M. van der Mullen, private communication, Juli 1993.

[17] M.Alonso, E.J. Finn, *Statistische fysica*, Elsevier 1979.

[18] H.A.J.M. Seelen, *Invloed niet lineaire effecten op de Lamb-golf*, internal report of the group theoretical physics, TUE 1988.

[19] J.J. Bleize, C.J. Timmermans, *Het juiste gebruik van bandlampen*, internal report VDF/NT 88-16, TUE 1988.

[20] A.T.M. Wilbers, *A wall stabilized arc as a source for spectroscopic techniques*, Ph.D. thesis, TUE 1991.

[21] J.B. Hasted, *Physics of Atomic Collisions*, Butterworth & Co Ltd., 1972.

[22] F.H.A.G Fey, *Exitation Balances and Transport in an inductively coupled Plasma*, Ph.D. theses, TUE 1993.

Acknowledgement

Here, I wish to thank all people who made it possible for me to succesfully finish this graduation study. First, I wish to thank my supervisors: Mark de Graaf, who contributed with a lot of interesting discussions, not always dealing with physics, to a pleasant working sphere, and Richard van de Sanden, my “only true graduation supervisor”: from his disagreements with other people in the group I have learnt a lot. Further I need to name Joost van der Mullen, whose common-sense approach of physics was sometimes very enlighting. Djoomart Otorbaev deserves thanks for his continuing emphasize on the greatest accuracy in the work. And of course Daan Schram. It took me some time before I could somewhat understand his complex way of thinking, but after that his deep insight in physics was often indispensable for the continuing of the work.

Further, I need to thank Frank Fey and Dany Benoy. From them I received the basis of the numerical model which is described in this report, and they have often helped me when I was stuck on numerical problems. The technicians of the department need also to be named: Bertus Hüsken, whose help was indispensable for finishing the electronic part of the positioning system, Herman de Jong, whose help on optics was of great value, and Ries van de Sande, whose work on the vacuum system and the pressured air system was nessecary.

Of course I also have to thank the other students who worked at Na. 1.73 and created a pretty climate: Edgar, René, Roger, Jeroen, Judith and Katrijn. Especially Judith had a very positive influence on the climate.

I also need to recommend Eberhart Mattes. Without his `emx` packet, TEX386 would not have been possible and neither this report in this shape.

Finally, I need to thank Mirjam and my mother. Without their moral support, finishing this work would have been much less easy.